2013

Advancing the field of polypeptoids through the synthesis of novel architectures and thermoresponsive polymers

Samuel Henry Lahasky
Louisiana State University and Agricultural and Mechanical College

ADVANCING THE FIELD OF POLYPEPTOIDS THROUGH THE SYNTHESIS OF NOVEL ARCHITECTURES AND THERMORESPONSIVE POLYMERS

A Dissertation

Submitted to the Graduate Faculty of the
Louisiana State University and
Agricultural and Mechanical College
in partial fulfillment of the
requirements for the degree of
Doctor of Philosophy

in

The Department of Chemistry

by
Samuel H. Lahasky
B.S., Tulane University, 2007
May 2013

Acknowledgments

My wife deserves many thanks for her unwavering support and patience during this adventure. For her care and encouragement, I am truly grateful.

My parents have instilled many of the great qualities in me that are necessary to achieve great things. For their resolute kindness and unyielding love, I am very thankful.

My advisors and mentors in the department have been extraordinary examples of how a scientist should approach his profession. For the unrelenting pursuit of academic perfection, I thank you.

Table of Contents

List of Acronyms

AcCl……...……...Acetylchloride

AFM……..…..Atomic force microscopy

ATRP……...Atom transfer radical polymerization

Boc_2O……..……Di-tert-butyl dicarbonate

BS…….....……..Brush star

CHCA……..……...α-cyano-4-hydrocinnamic acid

c-P(NEG-r-NBG) ……..…..……cyclic poly (N-ethyl glycine-random-N-butyl glycine)

c-PNPG-r-PNBG…….....….cyclic-poly (N-propargyl glycine-random-N-butyl glycine)

CuAAC……..…...Copper mediated alkyne/azide cycloaddition

DLS……...……Dynamic light scattering

DMF……..……..Dimethylformamide

DMSO……..……..Dimethylsulfoxide

DP……...…..……Degrees of polymerization

ESI-MS……..…..……..Electrospray ionization mass spectroscopy

FTIR……Fourier transform infrared radiation

GPC-DRI……...…..……...Gel permeation chromatography differential refractive index

l P(NEG-r-NBG) ……..……linear poly (N-ethyl glycine-random-N-butyl glycine)

LCST……..……Lower critical solution temperature

l-PNPG-r-PNBG……...linear-poly (N-propargyl glycine-random-N-butyl glycine)

MALDI-TOF……..…...Matrix assisted laser deabsorption ionization time-of-flight

MALS……..…….Multi angle light scattering

mDSC……Micro differential scanning calorimetry

MM……..……...Macromonomer

M_n……..……...Number average molecular weight

NaN(TMS)$_2$……..……Sodium bis(trimethylsilyl)amide

NEt$_3$……..……Triethylamine

NHC……..……N-hetercyclic carbene

NMP…….……..…..Nitroxide mediated polymerization

NMR……Nuclear magnetic resonance

Nor-P(NEG-r-NBG)……..Norborene poly (N-ethyl glycine-random-N-butyl glycine)

P(NEG-r-NBG) ……..……poly (N-ethyl glycine-random-N-butyl glycine)

PDI……..……Polydispersity index

PEG……..……Polyethylene glycol

PI……..……..……..……...Polyisoprene

PNAG……..……..poly (N-allyl glycine)

PNBG……..…….poly (N-butyl glycine)

PNEG……..…….……...…….poly (N-ethyl glycine)

PNIPAAm…….……..…poly N-isopropylacrylamide

PNMG……..…….poly (N-methyl glycine)

PNor-P(NEG-r-NBG)……Poly-norborene poly (N-ethyl glycine-random-N-butyl glycine)

PNPG……..……..poly (N-propargyl glycine)

PS ……..……...Polystyrene

RAFT……...Reversible addition-fragmentation chain-transfer polymerization

R-NCA……..……N-alkyl-carboxy anhydride

ROMP……..…...Ring opening metathesis polymerization

ROP……..……Ring opening polymerization

SEC-DRI……..….Size exclusion chromatography differential refractive index

T_{cp}……..……..Cloud point temperature

THF……..……..Tetrahydrafuran

TW……..……...Transition window

UCST……...……Upper critical solution temperature

UV-vis……...……...Ultraviolet visible spectrum

Abstract

Peptidomimetic polymers are an emerging class of polymers that are structurally related to polypeptides. Due to their structural similarities, these polymers can be used to study some of the physical aspects of polypeptides (for example, protein folding). They are also increasingly being used in the fields of biology and drug-delivery. Some members of peptidomimetic polymers include polyacrylamides, polyoxazolines and polypeptoids. Polymer synthesis and characterization has been performed for both polyacrylamides and polyoxazolines, with research dating back to the 1950s and 1980s respectively. Research in the field of polypeptoids has not been as extensive; however, emerging synthetic strategies are allowing for this class of peptidomimetics to be studied in greater detail and are revealing some interesting aspects of proteins. Current studies involving polypeptoids are expanding the limits of peptidomimetic polymers by developing their potential in materials science. The research presented in this dissertation is aimed at the synthesis of novel polypeptoid based architectures and stimuli responsive polypeptoid systems.

The synthesis of macrocyclic brush copolymers using a polypeptoid backbone has been achieved. The method selected for the synthesis this architecture circumvents many of the difficulties associated with prior attempts to make this structure, including high dilution for macrocyclization and linear contaminants in the final product. Typical polymer characterization of this novel architecture suggested that these structures were cyclic and contained poly-ethylene glycol side chains.

Polypeptoids that respond to changes in temperature (stimuli responsive polymers) have also been synthesized. The temperature at which the polymer responds can be controlled during the copolymerization of two different monomers. It has also been shown that the architecture of

the polypeptoid affects the stimuli response of the system. Several different architectures, including linear, cyclic and brush copolymers, are compared and show distinct stimuli responses from one another.

The ability to synthesize novel architectures allows for properties to closely studied and eventually exploited. Being a peptidomimetic polymer, polypeptoids have also been shown to biocompatible, making them a possible candidate for a bio-inspired therapeutic system.

Chapter 1. Introduction to Polypeptoid Research

1.1 Historical Development of Polypeptoid Research

In efforts to mimic biologically active systems, polypeptoids were first synthesized in the pharmaceutical industry to further the drug-discovery process.[1] Though peptoids have a brief history in the laboratory (developed in the late 1980s), their impact can be seen within areas such as drug-discovery, diagnostics, materials science and our fundamental understanding of protein folding.[2] Their similarity to proteins makes them ideal candidates for protein studies and overall replacement of peptides in some bio-pharmalogical applications. Being a peptidomimetic polymer (mimic of a peptide), polypeptoids are biocompatible and, in many cases, easy to synthesize. It is the goal of this dissertation to describe the relevance of peptoids in today's chemistry and illustrate some of the new advances and applications of peptoids in materials science.

First developed in the late 1980's by the Protos Corporation, peptoids (or more formally N-substituted glycines) had their origins in small-molecule drug-discovery program.[1] Large pharmaceutical companies needed a rapid and cheap method to access and screen for small peptide-like molecules, and a team of synthetic, computational and analytical chemists from Protos developed a combinatorial method of synthesizing polypeptoids that was quick and inexpensive. Peptidomimetic peptoids were used in many of these studies because of the difficulties of synthesizing short peptides with a defined sequence. By simply changing the attachment of the side-chain from the α-carbon to the nitrogen of the peptide backbone, chemists at Protos were able to successfully develop a peptidomimetic polymer that was similar in

structure to proteins, but still have the ability to retain diversity in the placement of different side-chains.

As polypeptoids have become more prevalent within materials science and biopharmakinetic studies, advances in the field have increased rapidly as more scientists find uses for these peptidomimetic polymers. Under the supervision of Dr. Ronald Zuckerman, peptoids have garnered enough attention over the past decade to warrant an entire conference dedicated to their research (*Peptoid Summit* hosted by the Molecular Foundry at the Lawernce Berkeley National Lab). This summit hosts the most recent advancements in the field of peptoid research and allows the academic field to understand how these peptidomimetic polymers can be used in drug-discovery and drug-delivery applications. Some of the research in this publication has been formally presented at this conference.

1.2 Polypeptoid Structure

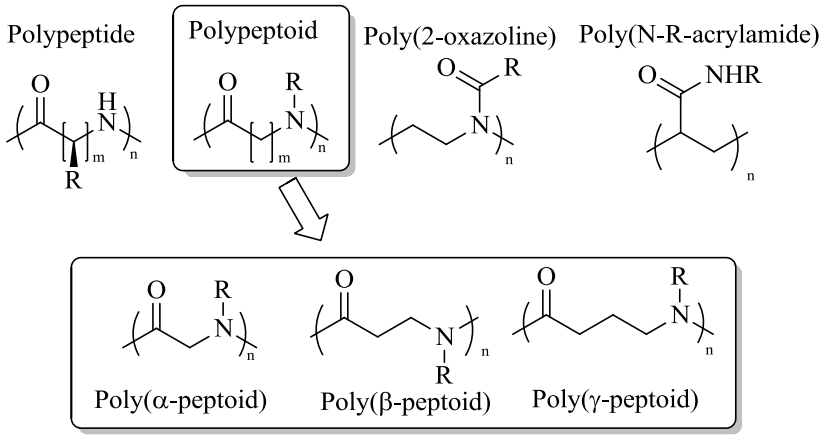

Figure 1.1. Examples of peptidomimetic polymers and polypeptoid structure.

Structurally, peptoids are a regioisomer of a peptide, where the backbone and the side-chain structures of the polymer have been retained, but the position of the side-chain differs.[3] Several peptidomimetic polymers are illustrated in **Figure 1.1**, with an emphasis on showing the

difference between the different peptoids, which differ only by the number of $-CH_2-$ carbons in the backbone (α, β and γ). For the purposes of the research presented in this publication, the term polypeptoids will refer solely to α-polypeptoids, unless otherwise stated.

The most notable structural difference between a peptide and a peptoid is the immediate loss of the amide proton (-NH-), which acts as a hydrogen-donor in hydrogen bonding. In addition to the lack of hydrogen bonding, peptoids lack stereogenic centers on the backbone (the –CH- carbon of the peptide backbone is a stereocenter, with the exception of glycine). Resulting from these two exceptions to peptides, peptoid conformations are governed by the properties of the side chain (i.e. sterics and electronics),[4-6] which can produce a random coil[7] or helical conformations.[8-10] Though lacking hydrogen donors, the hydrogen-bond acceptors along the backbone allow some polypeptoids to be soluble in water (depending on the side chain of the peptoid), while most polypeptoids are soluble in common organic solvents.

The bioactivity of polypeptides can be attributed to their ability to adopt a certain secondary structure in aqueous media.[11] For many years, it was considered that the hydrogen-bonding capabilities of the backbone were the reason for this protein folding. Due to the structural similarities of peptidomimetic polymers, peptoids are now revealing some interesting aspects of how proteins fold in solution. Peptoids have been found to fold into helical[12, 13] and non-helical[14] structures in different media though these polymers lack the N-H functionality on the backbone. These secondary structures can be attributed to the steric bulk of the tertiary amide N-alkyl substituents. Bulkier substituents can favor *cis* amide bonds, though this energetic preference is modest.[15] Blackwell demonstrated that the secondary structures of 9-mer oligo-peptoids (N-[1-pentafluorophenylethyl]glycines) were strongly affected by alterations of the hydrophobic residues within the neighboring side chains.[16] The ^{1}H NMR data of N-alkoxy

oligo-peptoids has trans amide bonds, allowing for a stable conformation that has a strong propensity to adopt a polyproline II type secondary structure.[17] Computational modeling of these N-alkoxy oligo-peptoids was used to confirm this energetic state.[17]

Due to the similarities in the backbone of these polypeptoids to polyamides, the potential for biodegradability and biocompatibility can be realized. Under controlled conditions, polypeptoids have been shown to be mostly stable in acidic conditions.[18] However, like most polyamides, they are degradable by alkaline solutions. Studies have shown that oligomeric peptoids are biodegradabe relative to similar α-peptides, though a conclusive study has yet to be performed on larger polymeric analogues.[19, 20] The similarities shared between peptides and peptoids, including biocompatibility, degradability and processability, can be potentially useful in the biotechnological fields.

1.3 Synthesis of Poly(α-peptoids)

Oligomeric or polymeric α-peptoids can be synthesized through several different routes. These synthetic methods can be summarized into three distinct categories: the solid-phase submonomer synthesis, ring-opening polymerization and metal-mediated synthetic route. Each method makes use of a different monomeric system and has its own distinct set of advantages and disadvantages. Of the listed synthetic routes towards polypeptoids, each has unique benefits for the desired application of the peptoid.

1.3.1 Solid-Phase Submonomer Synthetic Route Towards α-Oligo-Peptoids

The solid-phase submonomer approach to the synthesis of oligo-peptoids was first developed by Dr. Ronald Zuckerman and grew from earlier efforts to synthesize peptoids from the established Merrifield method of solid-phase peptide synthesis (SPPS).[21] The submonomer method towards to the synthesis of polypeptoids entails two chemical steps (**Scheme 1.1**). The

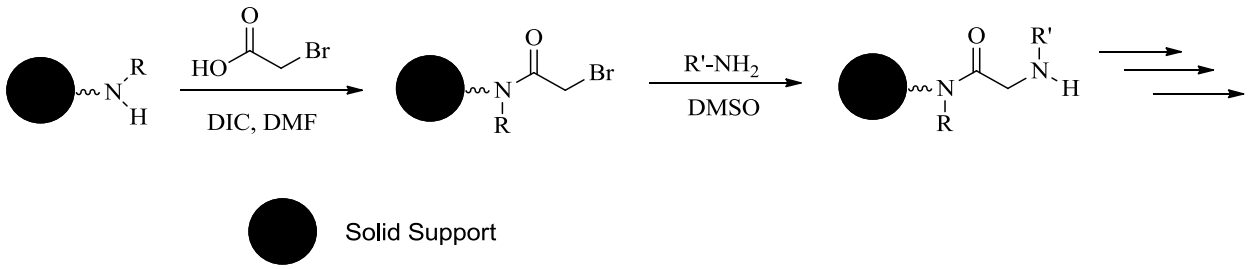

Scheme 1.1. Solid-Phase Submonomer synthetic scheme

first step is an acylation which involves the reaction of a resin-bound amine with a haloacetic acid (usually bromoacetic acid). This step is performed in the presence of N,N'-diisopropylcarodiimide (DIC), which is an activating agent for the haloacetic acid to form isourea. This is necessary because unlike the synthesis of the peptide through this method (which uses a primary amine attached to a resin), a secondary amine is needed for the synthesis of the peptoid. The reaction of secondary amines with haloacetic acids is slow, so the use of an activating agent, in this case DIC, helps to speed up the reaction. The second reaction of this synthetic route is an S_N2 displacement of the bromine with a primary amine, resulting in a new secondary amine bound to a resin. The synthetic cycle is then repeated until the desired repeat units have been attached to the peptoid.

A variety of primary amines are available through commercial sources, which makes this synthetic method appealing. Also, due to the development of automated systems, this route is efficient and cost effective, whereas earlier solid-phase methods used large excess of submonomers. The reactions in the submonomer method are not air sensitive (as is the case with other polypeptoid synthesis), having no need for an inert atmosphere. Precisely defined structures can be synthesized in this manner, allowing the chemist to place a particular side chain within the peptide at any n-mer he or she desires. The precise control of the polymer structure has allowed scientist to understand the relationship between polymer sequence and overall

polymer conformation, which is important in protein folding.[22] Advances in peptoid therapeutics and diagnostics have been aided by this microstructure control.[23]

The efficiency of the two chemical reactions in this synthetic route limits the peptoids to small fragments called oligomers (usually n-mers of less than 30). For example, Zuckerman states that to make a 5-mer, ten chemical reactions are needed, and these reactions must have a yield of 99% to make an oligomer with 90% purity.[1] The longest peptoid synthesized in this manner are only 50-mers.[24] Another slight disadvantage to this synthetic method is the time needed to make the peptoid. In some cases the S_N2 reaction can be as long as 2 hours, thus only allowing for several monomer additions per day, which differs from other synthetic routes where the polymerization kinetics are much faster.

1.3.2 Metal-Mediated Polymerization towards Polypeptoids

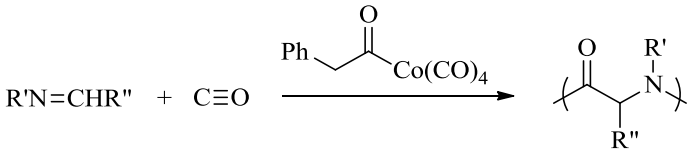

Scheme 1.2. Synthesis of polypeptoids via the metal-mediated route

In efforts to circumvent the tedious procedures in synthesizing polypeptides while using amino acid derivities, Sun et al reported a method the utilizes imines and carbon monoxide as monomers in a metal-mediated alternating copolymerization (**Scheme 1.2**).[18] To synthesize the peptoid, the R" in **Scheme 1.2** would be a hydrogen. Changing the side group that is attached to the imine allows for variations of polypeptoid structures.[18] Acylcobalt efficiently catalyzes the reaction of imine and carbon monoxide to produce high molecular weight polymers with low polydispersity indices. The cobalt was chosen over other metals, such as palladium, because of its frequent use as a catalyst in carbonylation reactions.[25] Evidences shows that the active

species in the metal-mediated carbonylation reaction is the acylcobalt.[26] The acylcobalt catalyst's reaction with the monomers resembles the characteristics of a controlled polymerization, though efforts to synthesize block copolymers were unsuccessful. It is assumed that the catalyst is considered to be unstable after all monomers have been consumed.[18]

The ability to produce large-scale quantities of polypeptoids (and peptides) can be made using the metal-mediated copolymerization of imines and carbon dioxide. The low cost and availability of the starting materials further encourages large scale production. In addition, bulky side chains that are difficult to incorporate using other methods of peptoid synthesis can be integrated into the polymer using this method. Nevertheless, the use of a metal as a catalyst can create issues with biocompatibility, as cobalt has been shown to be cytotoxic in some cases.[27]

1.3.3 Ring-Opening Polymerization Method towards Polypeptoids

Polypeptoids can by synthesized via a ring-opening polymerization (ROP) of a heterocyclic monomer. Like the two previous methods, this synthetic route has its origin in polypeptide synthesis.[28] The heterocyclic monomer used in these efforts is an N-substituted N-carboxyanhydride (R-NCA) (**Figure 1.2**).

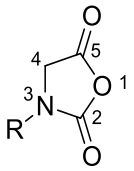

Figure 1.2. Illustration of N-substituted N-carboxyanhydride (R-NCA) heterocyclic monomer

There are many examples of ring-opening polymerizations throughout polymer chemistry. The polymerization of the lactide and cyclooctadiene monomers through ROP has been well documented and considered to adopt the characteristics of a controlled living

polymerization (i.e. a chain-growth process for which there are no irreversible termination or chain transfer reactions).[29] Most controlled polymerizations lead to narrow molecular weight distributions and provide a simple platform for the synthesis of block copolymers and end-group functionalized polymers (telechelic polymers). The ROP of NCA monomers is considered to have characteristics of a controlled polymerization, though some chain transfer reactions are unavoidable. There are two main synthetic ROP methods to make polypeptoids, each of which has a unique mechanism: primary amine-initiated and N-heterocyclic carbene (NHC) mediated polymerizations. Though polypeptoids are the product from both systems, their unique mechanisms yield polymers of different architectures (linear and cyclic for the primary amine-initiated and NHC-mediated polymerizations respectively).[7, 30] The two ROP methods have allowed chemists to study the physical differences between linear and cyclic polypeptoids.

As with all controlled polymerizations, both ROP synthetic routes towards polypeptoids can provide methods to make low-to-moderate molecular weight polymers with narrow polydispersities. The ROP method also allows for facile synthesis of block copolymers and for end-group functionalization. As compared to the solid-phase submonomer method, the ROP method can produce polypeptoids of longer length, though control of the microstructure sequence is greatly diminished, meaning that precise placement of the repeat units along the polymer backbone cannot be achieved.

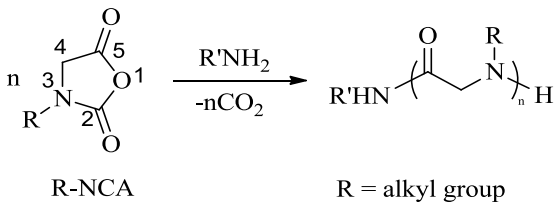

Scheme 1.3. Polymerization of NCA monomer with primary amine initiator

The primary amine-initiated system is a nucleophilic ring-opening polymerization of an R-NCA that produces poly(α-peptoids). In the most studied and well-understood cases, the nucleophile in this polymerization is a primary amine. After insertion into the non-amide carbonyl carbon (5-carbonyl position in **Scheme 1.3**), carbon dioxide (1-oxygen and 2-carbonyl positions in **Scheme 1.3**) is emitted from the system, leaving a neutral secondary amino chain end as the propagating species.[31-34] As a result, the steric effect of the substituents on the nitrogen can strongly influence the reaction, resulting in polymerization rates that differ by orders of magnitudes.[35-37] Studies by Luxenhofer and co-workers have shown that primary amine-initiated polymerizations of R-NCAs bearing different alkyl side chains (R = Me, Et, Pr, Bu, iBu) proceed through a controlled manner, where high molecular weights and narrow polydispersity indices were obtained.[38] Furthermore, the ability to synthesize sequential block copolymers was demonstrated using this method, which eventually afforded well-defined amphiphilic block co-polypeptoids that encapsulated Reichardt's dye.[38]

As **Scheme 1.3** depicts, the primary amine is incorporated as an end-group in to the polypeptoids. End-group characterization of polypeptoids can be conducted using ^{1}H NMR and MALDI-TOF.[38, 39] The ability to change the end-group from simple alkyl primary amines to more complex and reactive primary amines enables the chemist to perform post-polymerization modifications to the polypeptoids (an aspect that was exploited in this research, see Chapters 3 and 4).

Unlike the primary amine-initiated polymerization of NCA monomers, which extends the chain through a neutral propagating center, the N-heterocyclic carbene (NHC) mediated polymerization propagates through a proposed zwitterionic intermediate.[7] Waymouth and coworkers discovered that the NHC-mediated polymerizations of lactide (also a heterocyclic

monomer) produced mainly cyclic polymers, a fact they attributed to a zwitterionic propagating species.[40-42] The zwitterionic polymerization mechanism to make macrocycles was proposed in a 1960 study of anionic polymerizations performed by Swarg.[43]

Waymouth's report of NHC as an initiator in heterocyclic monomer systems inspired their use towards the synthesis of polypeptoids. Guo et al were the first to attempt a NHC-mediated polymerization of NCA monomers, and cyclic poly(α-peptoids) were the major product.[7] In an exhaustive effort, the Zhang group proposed that the NHC-mediated polymerization of NCA monomer proceeded through a zwitterionic propagating species.[44] The zwitterionic mechanism proposes that each chain end of the growing polymer has a different charge associated with it, and through Coulombic interactions, the chain ends are in close contact with one another (**Scheme 1.4**).

In the efforts to understand the mechanism of the NHC-mediated polymerization, Guo varied the solvent dielectric constant and the structure of the NHC initiator (steric and electronic properties), both of which proved to affect the polymer architecture, the kinetics of the polymerization and the molecular weight control.[44] It was shown that polymerizations in low dielectric solvents (i.e. toluene and THF) produced cyclic polymers, while polymerizations in higher dielectric solvents (i.e. DMSO) produced a mixture of both cyclic and linear species. It is assumed that the higher dielectric solvents facilitates the separation of the charges on the chain ends of the propagating polymer. Low dielectric solvents help to reduce the occurrence of side reactions due to the reduced basicity and nucleophilicity of the negatively charged chain ends of the zwitterions, resulting in a controlled polymerization. In low dielectric solvents, the structure of the NHC was also proven to not only have an effect on the initiation, but the propagation as well, further supporting the claim that the NHC-mediated polymerization of NCA monomers

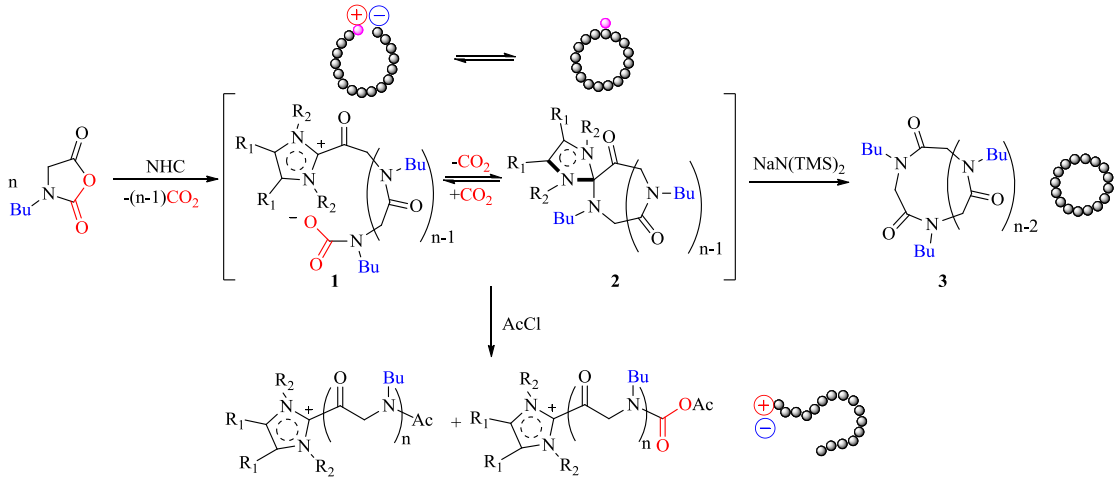

Scheme 1.4. NHC mediated ROP of NCA monomers and subsequent cyclization ($NaN(TMS)_2$) and macrocyclic opening (AcCl)

propagates through a zwitterionic species. As the steric bulk of the NHC initiator (defined as the percentage of buried volume V_{Bur}) was increased, the observed rate constants (k_{obs}) decreased, suggesting that bulkier NHC's slow down the addition of the next monomeric unit in the polymer. Proposed by Nolan and Cavallo, the V_{Bur} can be defined as the percent of the total volume of a sphere occupied by a ligand.[45] This indicates that propagation is also controlled by the initiator via an intra-molecular counter-ion effect, and furthermore, no such trend was observed in high dielectric solvents, indicating that propagation is determined by some other means in those solvents (i.e. anionic, linear propagating species). Similar studies involving the anionic polymerization of methacrylate in dioxane showed that increasing the size of the counter-cation from lithium to cesium drastically increased the polymerization rate.[46, 47] Through further investigation, two proposed pathways are possible for the initiation of the cyclic polymeric species, the regioselective insertion of the NCA and a proposed second pathway which travels through the formation of a possible Munchnone inititiating species, which forms from the reaction of the deprotonated Bu-NCA with another Bu-NCA (**Scheme 1.5**).[18, 48, 49]

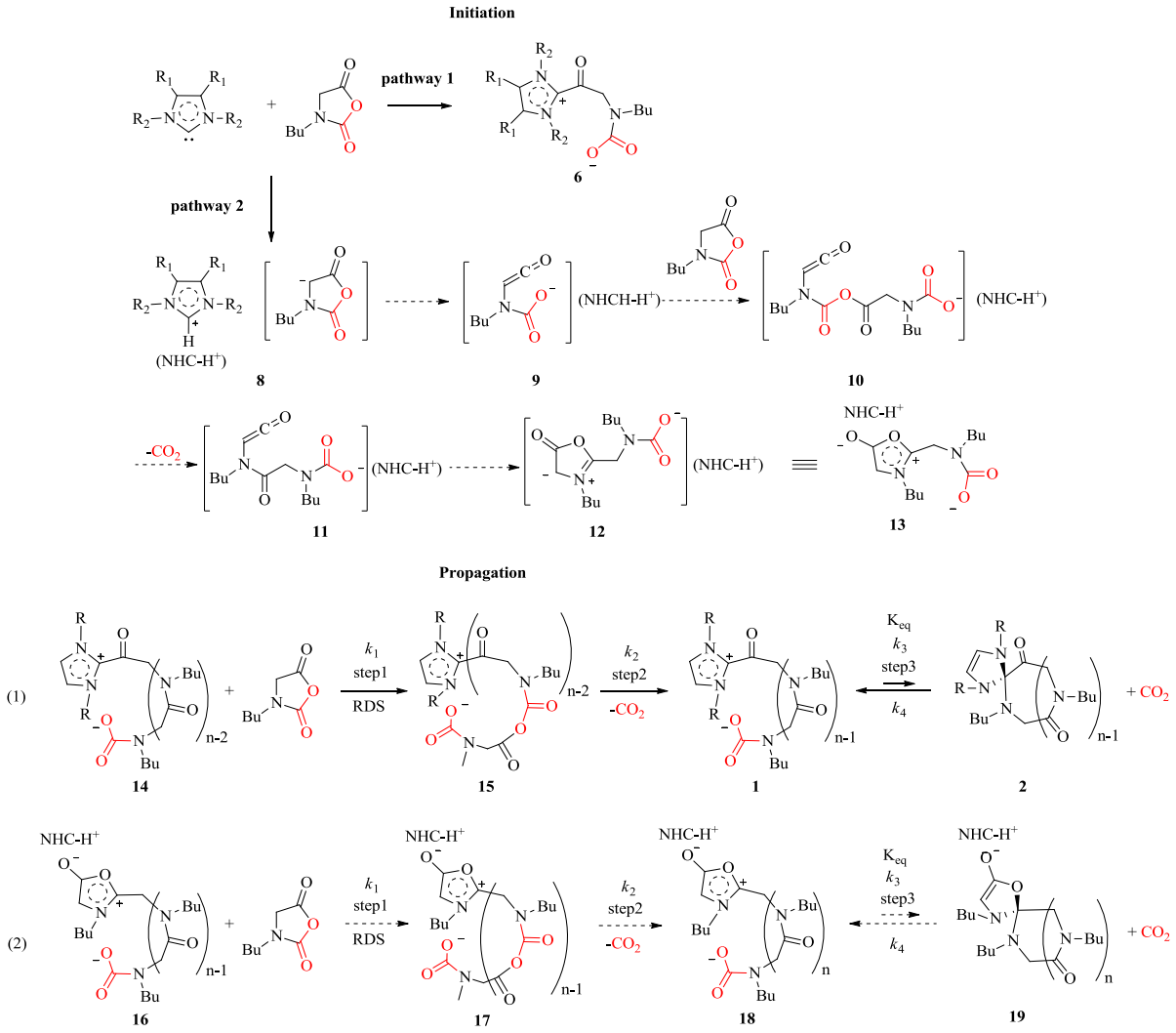

Scheme 1.5. Proposed mechanism for zwitterionic polymerization of the NHC meditiated ROP of NCA monomers.

After proposing two mechanisms for the NHC-mediated ROP of NCA monomers, conversions of the cyclic zwitterionic species (1 and 2 in **Scheme 1.4**) into linear species were achieved via the reaction of acetyl-chloride (AcCl) with, the zwitterionic propagating intermediates (1/2). The polymer was shown to be linear by ^{1}H NMR characterization and end-group analysis with MALDI-TOF MS technique. In a similar manner, the cyclic zwitterionic species can be converted to a neutral cyclic polymer via reaction with 5 equivalents of

$NaN(TMS)_2$ (3 in **Scheme 1.4**). Along with MALDI-TOF MS, size exclusion chromatography (SEC) traces provided further evidence that the hydrodynamic radius of the linear species was larger than the two cyclic species, confirming the successful architectural transformation.

Throughout this presented research, the preferred method of the synthesis of poly-(N substituted glycines) is the ROP of R-NCAs using either the primary amine or the NHC initiators. Each ROP method was used in the synthesis of linear or cyclic polymers. Several of the studies presented will focus on the physical differences between cyclic and linear polypeptoids, so a discussion on the synthesis of cyclic polymers and the physical differences between the two topologies is necessary to understand the following research.

1.4 Cyclic and Linear Polymers

Cyclic polymers are known to exist in nature, as the DNA of the Lambda bacteriophage reversibly cyclizes and uncyclizes during gene expressions.[50] Research on cyclic polymers is still in its infancy because of the limitations associated with the lack of efficient synthetic tools to access this unique architecture. Synthesis of cyclic polymers in an academic labs is currently limited to three options: ring-chain equilibrium, ring-closure, and ring-expansion techniques (**Figure 1.3**).[51]

Ring-chain equilibrium involves a competition between the propagation of a linear polymer and chain cyclization through back-biting of the chain ends into the growing chain. The ring-chain equilibrium cyclization is usually limited to ROP and thermodynamically controlled step-growth polymerizations.[52] While the total percentage of cyclic species can be increased by high dilution, smaller rings are still thermodynamically favored.[53] Kricheldorf and Schwarz demonstrated that in kinetically controlled step-growth polymerizations, cyclic polymers are the

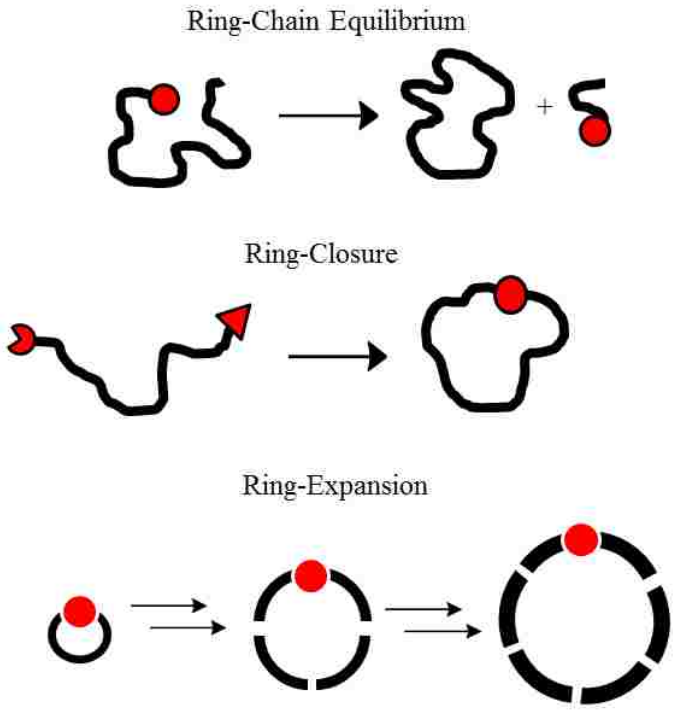

Figure 1.3. Methods of synthesizing cyclic polymers.

stable end-products.[54] However, the polymers tend to exhibit bimodal mass distribution where small rings are inevitably present.

The ring-closure technique involves the synthesis of a linear polymer with functional end groups that can either react with one another (unimolecular coupling) or react with a linker molecule (bimolecular coupling). For instance, bimolecular coupling was used to synthesize cyclic polystyrene. The anionic polymerization of styrene using a bis-anionic initiator allowed for the anionic end groups to react with a linker molecule, in this case a,a'-dihalo-p-xylene, to close the ring.[55-57] Alternatively, cyclic polystyrene has been synthesized via the unimolecular coupling technique. Grayson *et al.* crafted the end groups of the polystyrene so that one end group (alkyne functionalized) would react with the other (azide-functionalized) to close the ring by a 1,3-Huisgen dipolar cycloaddition reaction.[58] The ring-closure techniques require a high

degree of stoichiometric accuracy and high dilution to produce cyclic polymers of uniform ring size. Product yields using the ring-closure technique are typically low, due to competing linear coupling reactions, though new techniques are currently being developed to increase cyclization efficiency and product yields.[59, 60]

Nearly any polymer that is amenable to end-group functionalization can potentially undergo a ring-closure technique to form its cyclic analogue if the correct conditions are met. In contrast, the ring-expansion method towards cyclic polymers occurs only through a precise monomer-to-initiator pairing. The monomer, typically a cyclic monomer, inserts itself into a relatively labile bond formed by the initiator at the propagation site (e.g. organometallic or electrostatic). Propagation by insertion of the next monomer unit into the labile bond is usually favored thermodynamically, typically by ring strain in the monomer.[61] Bielawski et al demonstrated that a ruthenium catalyst can polymerize the cyclic monomer, cyclooctadiene, in a ring-opening metathesis polymerization to yield cyclic polymers.[62, 63] As previously shown in earlier sections of this chapter, the NCA (monomer) and NHC (initiator) pairing can produce cyclic polypeptoids.[7] Once the monomer-to-initiator combination has been discovered, high yielding cyclic polymers can be synthesized at relatively high concentrations. Coupling competition is not a limiting factor in this method, so linear polymers are not usually produced, though back biting or intramolecular chain transfer can be an issue with some systems.[64-66] In combination with the primary amine-initiated ROP of R-NCA monomers, the NHC-mediate route allows for the physical properties of linear and cyclic poly(N-substituted glycines) to be researched easily with regards to the synthesis of cyclic polymer.

Cyclic and linear polymers that have identical microstructures have measurable physical differences due to their architectures. Cyclic polymers offer different physical characteristics

than their linear counterparts because they have a more compact conformation a limited chain mobility in solution.[67] This difference in size is measured by the radius of gyration (R_g), which is the mass-weighted average distance of all monomers from the center of mass.[29] Linear and cyclic polymers of identical repeat units will have different sizes in solution, and this size difference affects some physical properties, such as lower solution and bulk viscosities,[68] higher SEC elution volumes,[69, 70] higher critical solution temperatures[71] and higher glass transition temperatures[72] than their linear counterparts. Coupled with typical characterization methods, these physical properties can be exploited to distinguish cyclic from linear and ultimately utilized in materials applications.

These differences in physical properties between cyclic and linear polymers are measurable and typically are used to distinguish between the two polymers. The SEC-DRI traces are indicative a change in size of the polymer (cyclic polymers have smaller R_g in solution), as cyclic polymers have longer elution volumes than their linear counterparts with identical molecular weight.[63, 73, 74] To determine if the two polymers have identical molecular weights, matrix assisted laser deabsorption ionization time of flight mass spectrometry (MALDI-TOF-MS) can be used. This method not only allows the chemist to determine the molecular weights and polydispersities of polymers, it allows for the end-group analysis of lower molecular weight polymers (< 10 kDa).[75] If a polymer lacks end groups (a cyclic polymer), there should be evidence in the MALDI-TOF spectra, and it has been shown through MALDI-TOF that peptoids that were prepared via the NHC-mediated polymerization of NCA monomers lack end groups, and thus are considered to be cyclic.[7, 13, 39, 76] Utilizing differences between solution intrinsic viscosities also allows the chemist to distinguish between cyclic and linear analogues of the same polymer.[77, 78] Waymouth and Guo have both illustrated the differences in intrinsic viscocities of

the NHC-mediated polymerizations of lactide and NCA monomers respectively.[7, 40] These methods have proved to be vital in the determination of linear and cyclic species and are used throughout the course of this research (Chapters 2 and 3).

1.5 Advancing the Field of Polypeptoids

Within the past five years, advances in the field of polypeptoids have come from many aspects of polymer chemistry, including polymer physics, synthesis and applications. Peptoids have been regarded as the next emerging class of peptidomimetic polymers, behind the more often researched poly(2-oxazoline)s or poly(N-R-acrylamide)s.[2] Though peptoids are similar in structure to other peptidomimetics, they offer appreciable differences in their physical properties along with a unique set of synthetic challenges. Understanding the fundamental structure-property relationship of peptoids will undoubtedly provide new insights into their physical behaviors.

The folding capabilities of these polypeptoids are of much interest to the scientist due to the similarity in structure of these polymers to proteins. To understand how these polymers interact with one another, it is important to understand their packing or 'crystalline' structure in the solid state. Studies performed by Rosales et al have shown that the thermal and crystallization behavior of poly(N-substituted glycines) is tunable by varying the alkyl side chain length and introducing defects at precise residues into the oligo-peptoid via solid-phase submonomer synthetic method.[79] These studies have shown that the side chain of the peptoid strongly influences the packing structure of the polymer. Lee and co-workers separately illustrated that the degree of crystallinity is highly dependent on the length of an alkyl side chain.[76] It was also shown that amphiphilic cyclic and linear block copolypeptoids (cyclic/linear-poly(N-methyl-glycine)-block-poly(N-decyl-glycine)) form micrometer long

cylindrical micelles with uniform diameter in methanol, a phenomenon that is driven by the crystallization of the *N*-decyl block.[76]

The side chain of the polypeptoids has been shown to affect many of the solution and thermal characteristics of the polymer, such as solubility, crystallinity and secondary structures. It was first noted that poly(N-methyl glycine), commonly referred to as polysarcosine, is water soluble.[32] Polysarcosine has been used in many cases as microcapsules that exhibit long circulation and non-specific organ uptake.[80, 81] Recently, more complex ethylene oxide side chains have been introduced into the peptoid that enable the polymer to exhibit unique metal coordinating sites and glass transition temperatures.[82] Having side chains that are amenable to post-polymerization modification allows the synthetic polymer chemist to create novel bio-related architectures. Robinson and co-workers were the first to publish the synthesis of a poly(N-allyl glycine) (PNAG) that was amenable to post polymerization modifications, most notably the thiol/ene 'click' reaction.[83] This group was also able to show that PNAG demonstrated a thermal stimuli-responsive behavior in water.[83]

The research presented in the subsequent chapters is aimed at further expanding the realm of potential uses for peptoids through the synthesis of novel peptoid architectures and their use as stimuli responsive polymers. While this research is rooted in the synthesis of novel polypeptoids, it relates to aspects such as polymer physics and biology. The majority of the research that will be presented has already been accepted by noteworthy peer-reviewed polymer journals.

Novel polypeptoid architectures will be presented in chapter 2. This chapter's focus is on the synthesis of a macrocyclic brush polymer, whose synthetic route combines several interesting

methods. The zwitterionic NHC-mediated polymerization of functional-NCAs (the novel N-alkyne carboxyanhydride) was combined with 'click' chemistry to develop these ring-like peptoidal structures (**Figure 1.4**). Along with the standard polymer characterizations (such as NMR, GPC etc.), these rings were characterized by atomic force microscopy (AFM), which allowed the macrocyclic brushes to be visualized.

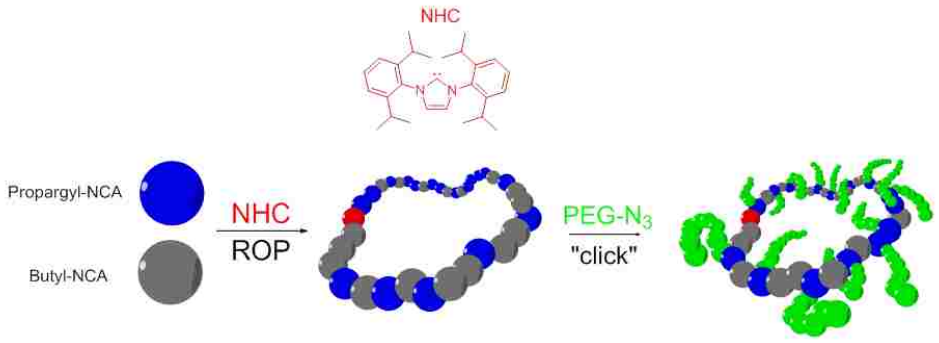

Figure 1.4. Synthesis of macrocyclic brush copolymer (Chapter 2)

Chapter 3 combines aspects of stimilu-responsive systems, polymer physics and biology. While copolypeptoids that exhibit thermoresponsive solution properties is the main focus of this peer-reviewed research, a deeper subject is connected with this investigation. Physical differences between linear and cyclic polymers are investigated by comparing the cloud point temperatures (T_{cp}) of polypeptoids with varying topologies (**Figure 1.5**). Cyclic copolypeptoids were found to systematically have lower cloud point temperatures than their linear counterparts, a proposal that had been much debated in other cyclic/linear thermoresponsive systems.[59, 84, 85] The biocompatibility of these polymers is also investigated in this chapter.

Chapter 4 will comment on the synthesis and thermoresponsive solution properties of the stimuli-responsive brush polypeptoids. Thermoresponsive copolypeptoids were combined with the grafting-through method of brush polymer synthesis to produce interesting stimuli responsive

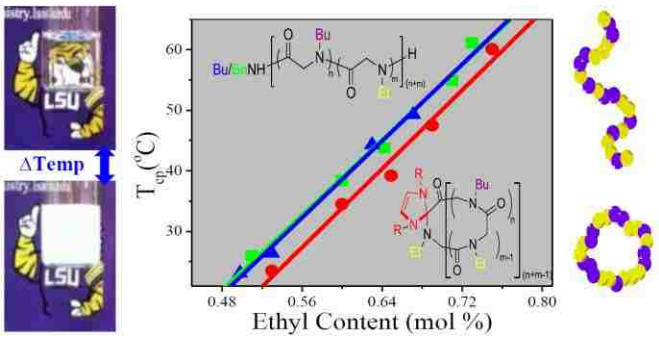

Figure 1.5. Comparison of cyclic and linear thermoresponsive copolypeptoids (Chapter 3)

systems (**Figure 1.6**). Named brush-stars due to their method of synthesis and shape respectively, these densely grafted copolymers are distinctions in their thermoresponsive behaviors than their linear components. These brush-stars exhibit no T_{cp} in water but are highly sensitive towards the addition of salt. Differences between the thermoresponsive polymer and its brush analogue are discussed and potential mechanistic differences are proposed.

The concluding chapter (Chapter 5) will encompass the broader impacts of this research in the field of polypeptoids. It will comment on the emergence of polypeptoids as useful and innovative peptidomimetic material. The chapter will demonstrate that the research presented in this dissertation has helped to advance the field of not just polypeptoids, but also peptidomimetic materials. Research in these fields are ongoing and continue to provide insight into areas such as protein chemistry, enzymology and biomedical fields.

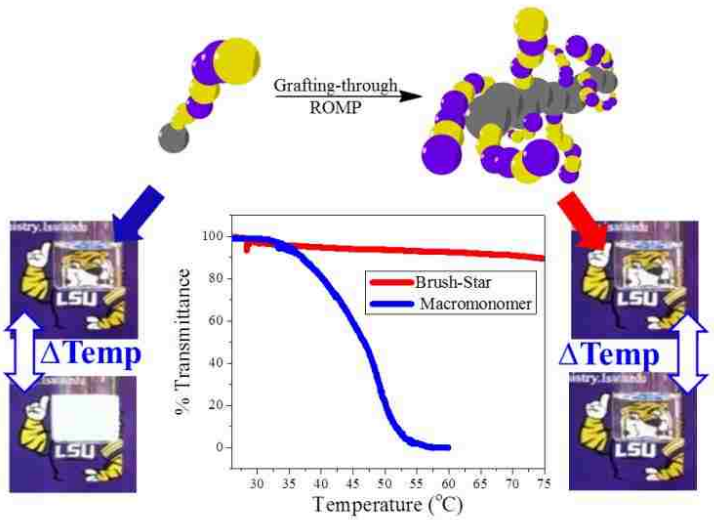

Figure 1.6. Comparison of linear and brush-star thermoresponsive copolypeptoids (Chapter 4).

Chapter 2. Synthesis of a Macrocyclic Brush Copolymer

2.1 Objectives and First Observations

The NHC-mediated polymerization of R-NCAs avoids many of the problems associated with other synthetic methods towards cyclic polymers, such as high dilution and linear contaminants. Once this relatively facile synthesis of cyclic polymers was discovered, interesting architectures could be more easily explored. Interesting architectures can be described as polymeric architectures that are not commonly synthesized or studied. Examples of interesting polymeric architectures are star-, dendritic-, cyclic- and brush-polymers. Brush polymers are used throughout biology, chemistry and materials science; though a polypeptoid molecular brush has yet to be synthesized. Combining cyclic and brush polymers was rather interesting due to many potential applications, most notably their use as a compatibilizers in duel polymer melt systems. Once the zwitterionic NHC-mediated polymerization of R-NCA monomers was discovered, a new strategy towards interesting molecular architectures (i.e. cyclic brush polymers) can be more easily accessed. By synthesizing R-NCA monomers with functionality (propargyl groups), cyclic polymers that have functional repeat units can be subjected to post polymerization modifications. These post-polymerization modifications include the attachment of an azide-terminated poly-ethylene glycol (PEG). Exploiting the ring-expansion of the NCA monomers to synthesize macrocyclic brush polymers is the objective of this project and of this chapter.

2.2 Introduction to Brush Polymers

Brush-like polymers, which consist of a backbone and a bristle, represent an interesting polymeric architecture (**Figure 2.2.1**).[86] Molecular brushes are a special type of graft copolymers in which multiple polymer chains are grafted to a backbone polymer. If the

backbone polymer is much longer than that of the bristle, then the molecular brush adopts a cylindrical shape with the backbone at the core.[87-89] Conversely, if the backbone is on same order of length as the bristles, the brush adopts a more compact, spherical shape, commonly referred to as a star polymer.[90] The conformation of these molecular brushes is determined by a multitude of congested sterics which are associated with an entropically unfavorable extention of the backbone and the bristle. Attachment or growth of the bristles increases the conformational strain of the backbone,[91] and accordingly increases the persistence length and reduces the chain entanglement.[92, 93] As a result, brush-like polymers have been investigated as precursors of shape-persistent organic nanotubes,[94] lubricants,[95] or self-assembled one dimensional photonic crystals.[96, 97] Proteoglycans, which are found readily in the body, have been shown to have a molecular brush architecture, and studying such structures and their effect on their biological properties could potentially lead to advances in biomedical applications.

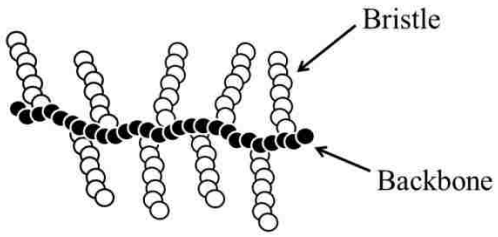

Figure 2.1. Depiction of brush polymer.

2.2.1 Synthetic Strategies towards Brush Polymers

Brush-like polymers can be synthesized by several synthetic strategies including the grafting-through, [98] the grafting-from,[99] and the grafting-to approaches.[100] Each synthetic strategy offers a different set of advantages and disadvantages towards the synthesis of the brush copolymer. In each method the end product will consist of bristles and a backbone; however the ability to structurally or chemically tailor the backbone or bristles may vary depending on the synthetic

strategy chosen. The desired application of the molecular brush typically dictates which synthetic route to be used. Typically, molecular brushes have a backbone that is a linear polymer with linear bristles as the side chains, though more interesting and complex structures are being made. The three synthetic strategies vary with respects to their versatility to provide access to more complex molecular brushes.

The grafting-from approach towards molecular brushes typically involves the use of macroinitiators.[101] A macroinitiator is a polymer which has initiation sites along its backbone which can initiate the polymerization of a second monomer. This synthetic route allows for a degree of control over the length of the backbone and the chain density of the bristles, where chain density (or grafting density) refers to the number of repeat units along the backbone that have an attached bristle. Atom transfer radical polymerization (ATRP) is an often used polymerization for the growth of the bristles, as pendant bromoester groups on polymethacrylates can be uses as initiators for ATRP.[99] The grafting-from approach does not allow a high degree of control over the length and type of bristles that can be grown from the backbone.

Molecular brushes can also by synthesized using the grafting-through method, which makes use of a macromonomer. A macromonomer is a polymer with a chain end that can be polymerized. These macromonomers are prepared and then the chain ends are polymerized to form the backbone of the molecular brush (where the polymer portion of the macromonomer is the bristle). This method allows for precise control over the length and type of bristle. The grafting-through method also allows for a 100% grafting density because each monomer of the backbone has a bristle attached before the backbone monomers are polymerized. For instance, ring-opening metathesis polymerizations (ROMP) of norbornene were used on terminally

functionalized polyacrylates.[102] Interesting worm-like polymeric structures were obtained using this grafting-through method. The set-backs of the grafting-through methods are the control of the backbone polymerization, where a high degree of polymerization (DP) are typically difficult to achieve. This is attributed to a low concentration of the polymerizable group (chain end of the bristle) and the steric hindrance of the bristle.

The grafting-to approach is particularly versatile regarding the chemistry of brush-like polymers. As the backbone and side chains are independently prepared prior to coupling, their composition can be precisely characterized. The drawback of this method is that the grafting density is often limited by the steric congestion of the polymeric side chains. The grafting efficiency (the conversion of the coupling reaction) is also significantly impacted by the method used to couple the side chains to the polymer backbone.[103] In this regard, click chemistry, particularly the copper-mediated alkyne/azide cycloaddition reaction (CuAAC),[104] has become increasingly employed in the synthesis of brush-like polymers[105-107] due to its high efficiency and stoichiometric bond formation under mild conditions.[108-112] Though the grafting efficiency is hindered, the ability to indepently control both aspects of the molecular brush (i.e. the bristle and backbone) makes the grafting-to approach rather appealing to the synthetic chemist.

2.2.2. Macrocyclic Brushes

Most synthetic brush-like polymers feature a linear polymer backbone. Molecular architectures such as cyclic or star-shapes have received less attention.[113] Schappacher *et al* reported the synthesis of cyclic polymer brushes bearing randomly grafted polystyrene (PS) and polyisoprene (PI) side chains. The cyclic polymer backbone was prepared by the ring-closure of an α-ω heterofunctional linear precursor and the PS/PI side chains were statistically grafted to the backbone in one step.[114] While the majority of the polymer brushes are linear, cyclic, tadpole and ∞-shape backbones have been evidenced by atomic force microscopy (AFM).[115, 116] These

architectural contaminants arise from the limitations of synthetic methods used to prepare the cyclic polymer backbone. Cyclic brush-like polymers can be synthesized by a grafting-from approach, where PS brushes are grown from a cyclic polyethylene glycol backbone via nitroxide-mediated radical polymerization (NMP), as shown by Jia *et al*.[117] Coulembier *et al* reported the synthesis of jellyfish macromolecular architectures by a grafting-through approach where a macromonomer (i.e. modified polymethylmethacrylate L-lactide) was copolymerized with L-lactide in the presence of *in-situ* generated *N*-heterocyclic carbene.[118] Macrocyclic brushes have been synthesized by ring expansion metathesis polymerization of functionalized norbornenes.[119, 120] In the former report, the side chains were installed prior to polymerization as part of the macromonomers, whereas in the latter case the side chains were attached by CuAAC post polymerization. While the cyclic polymer backbone itself has random coil conformations, the grafting of polymeric side chains rigidifies the backbone, resulting in shape-persistent ring-like nanostructures. Many of these polymers exhibit intriguing solution and self-assembly behaviors and have potential uses in nanotechnology and biomedical sciences. Before these applications can be realized, it is important to develop robust and efficient synthetic routes towards these materials. Special attention needs to be paid to the main challenge in cyclic brush-like polymer synthesis: the construction of the cyclic backbone architecture.[51, 74, 78, 121]

2.3 Results and Discussion

2.3.1 Synthesis and Characterization of Cyclic and Linear Poly(*N*-propargyl glycine) (*c*/*l*-PNPG)

The monomer *N*-Propargyl NCA (M_1) was successfully synthesized on a multi-gram scale by the Füch method, i.e., PCl_3-mediated cyclization of the corresponding *N*-Boc-*N*-propargyl glycine precursor **2** (**Scheme 2.1**).[7] The molecular structure of M_1 was unambiguously verified

by ^{1}H and ^{13}C $^{1}\{H\}$ NMR spectroscopy (**Figure 2.2**). The monomer is a white solid at room temperature and can be readily purified by sublimation prior to polymerization.

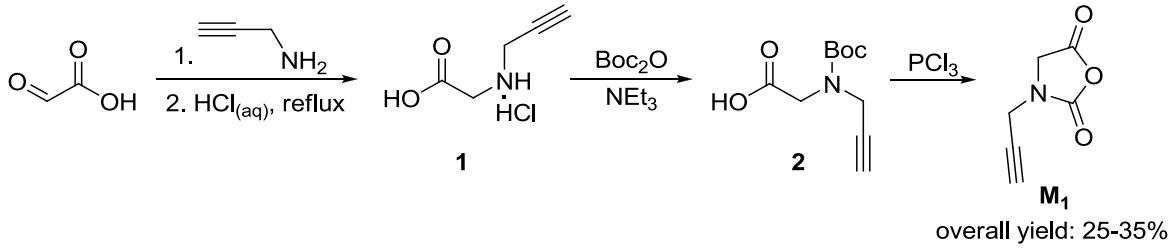

Scheme 2.1 Synthesis of N-Propargyl-NCA (M_1).

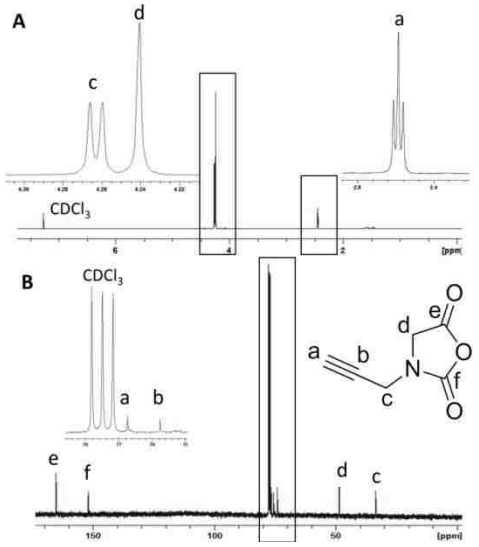

Figure 2.2. (A) ^{1}H NMR and (B) ^{13}C $^{1}\{H\}$ NMR spectra of *N*-propargyl NCA (M_1) in $CDCl_3$.

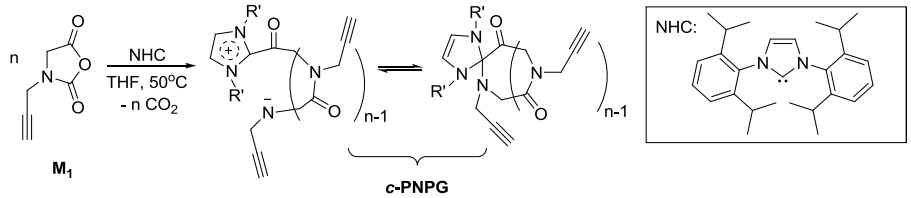

Scheme 2.2. Synthestic scheme of poly-(N-propargyl-glycine) PNPgG.

Polymerization of M_1 was achieved by heating different initial monomer to initiator ratios ($[M_1]_0$:$[NHC]_0$) in THF solution at 50°C for 18 h under a nitrogen atmosphere (**Scheme 2.2**).

Aliquots of the reaction mixtures were spectroscopically analyzed to monitor conversion of M_1 to the polymer. FTIR spectroscopy was used to determine monomer conversion because M_1 exhibits two characteristic $\nu_{C=O}$ stretching modes at 1859 and 1786 cm^{-1} (**Figure 2.3**). All reactions reached high or quantitative monomer conversion (95-100%) under these conditions (**Table 2.1**). In addition to polymer formation, ^{1}H NMR and ESI MS analysis of the reaction mixture also reveals the formation of 1,4-di(prop-2-ynyl)piperazine-2,5-dione (6MR) along with cyclic and linear oligomers in small quantities, presumably formed by an intramolecular "back-biting" mechanism (**Figure 2.4** and **2.5**).[13] The 6MR constitutes less than 15% of the reaction product (**Figure 2.6**). Heating of the isolated and purified polymers can cause further depolymerization to yield 6MR. This is in contrast to a previous study on NHC-mediated polymerization of *N*-alkyl NCA (alkyl: Me, Bu) where no "back-biting" products were observed.[7] The polymer products were precipitated by the addition of excess room temperature hexane. Further purification was achieved by extraction into warm hexane (50°C), which removes cyclic oligomers. The samples were dried under vacuum prior to further analysis.

The ^{1}H NMR analysis of a low M_n polymer reveals three broad resonances in the ^{1}H NMR spectrum (a,c,d **Figure 2.7(A)**), consistent with the targeted poly(*N*-propargyl glycine) backbone structure (*c*-PNPG) (**Scheme 2.2**). In addition, resonances due to NHC moieties are also evident in the ^{1}H NMR spectrum, in agreement with NHC initiator being affixed to the polymer chain ends as previously reported (**Scheme 2.2**).[7, 13] The $^{13}C^1${H} NMR spectrum (**Figure 2.7 (B)**) is also consistent with the PNPG backbone structure. The ESI MS analysis of a low M_n polymer reveals a major set of doubly charged mass ions whose mass equals to the sum of integer number of the desired repeating unit mass (95.10), one NHC mass (388.29) and two proton masses (1.01), in agreement with a cyclic PNPG polymeric species with one NHC moiety

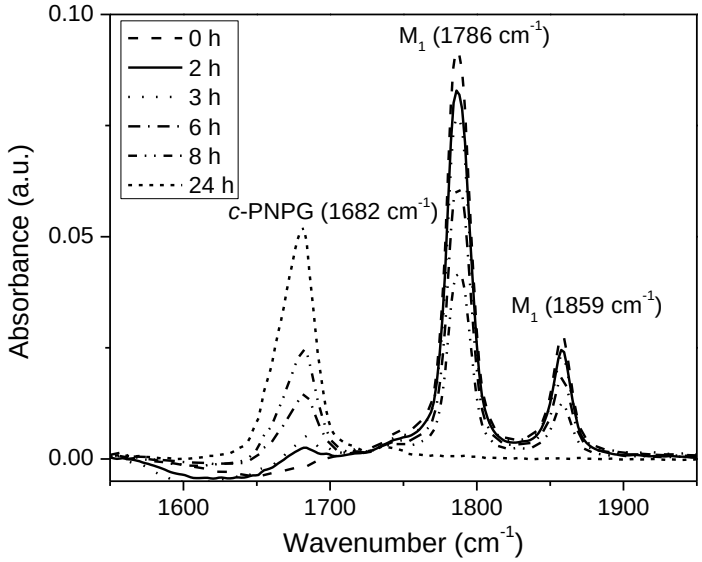

Figure 2.3. Time-dependent FTIR spectra of a representative NHC-mediated polymerization of M_1 ($[M_1]_0$= 0.4 M, $[M_1]_0$:$[NHC]_0$= 50:1, 50°C, THF).

attached (a, **Figure 2.8 (A-C)**). Apart from the major species, several minor sets of mass ions that are consistent with PNPG polymeric species with different end groups or co-ionized with solvent molecules are also present. For example, doubly charged mass ions indicated by *b* and *c* are due to the *c*-PNPGs with NHC attached that are co-ionized by Na^+ and a proton (*b*) or Na^+, a proton and a solvent molecule (*c*). The mass ions indicated by *d* are the singly charged linear PNPG bearing carboxyl and amino chain ends, presumably formed by the reaction between *c*-PNPG having NHC attached with adventitious moisture. The end groups for the PNPG polymeric mass ions indicated by *e* have yet to be determined. The MALDI-TOF MS analysis of the low M_n polymer sample also corroborates the ESI MS results (**Figure 2.9**). In the MALDI-TOF MS experiment, it is critical to use a soft matrix such as α-cyano-4-hydroxycinnamic acid (CHCA) so that the original polymers remain structurally intact upon desorption and ionization. We have previously shown that the NHC moieties that are attached to the polymers are

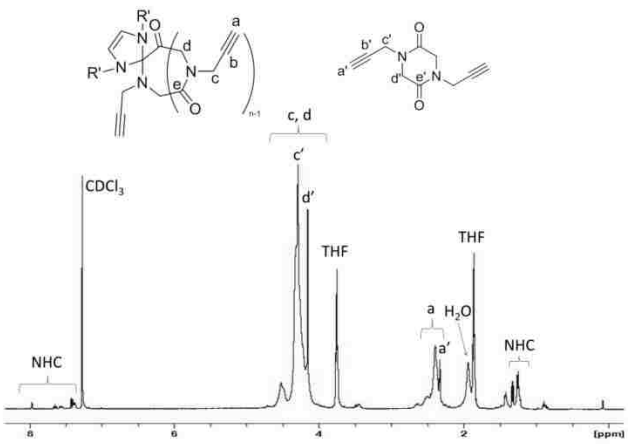

Figure 2.4. Representative ^{1}H NMR spectrum of a reaction mixture from NHC-mediated polymerization of M_1 in $CDCl_3$.

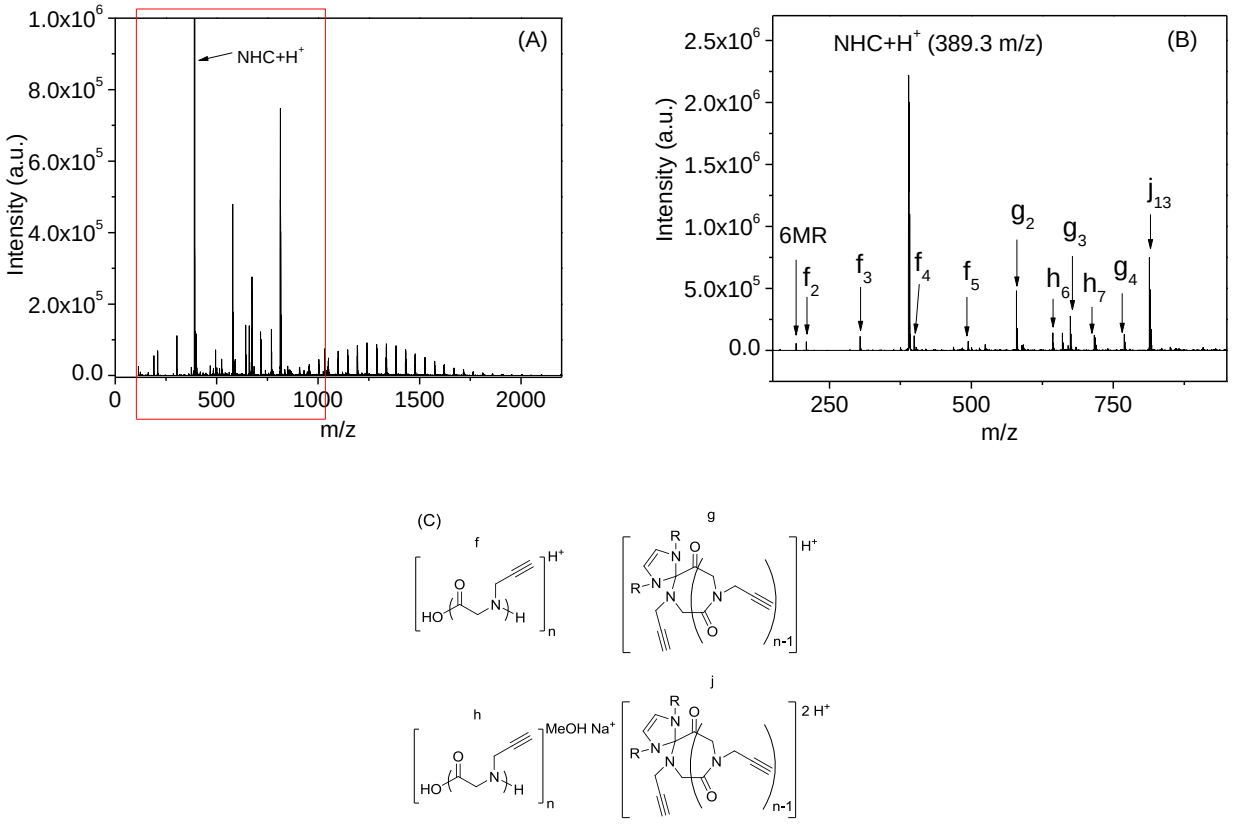

Figure 2.5. (A) Representative full and (B) expanded ESI MS spectrum of a reaction mixture from NHC-mediated polymerization of M_1 where cyclic oligomers are notably visible in addition to *c*-PNPG; (C) the molecular structures that correspond to the mass ions.

photolabile.[39] Strong laser power or a hard matrix such as dithranol causes the NHC to dissociate from the polymers.

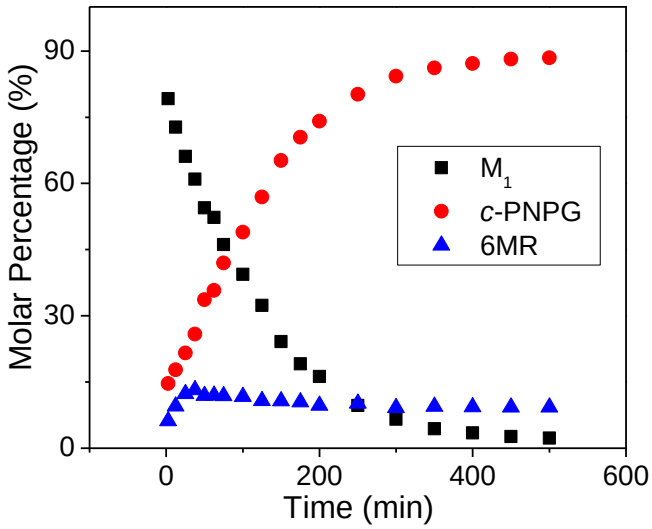

Figure 2.6. The molar percentage of M_1 (■), *c*-PNPG (●) and 6MR (▲) as a function of polymerization time ($[M_1]_0$= 0.22 M, $[M_1]_0$:$[NHC]_0$ =50:1, 50°C, THF).

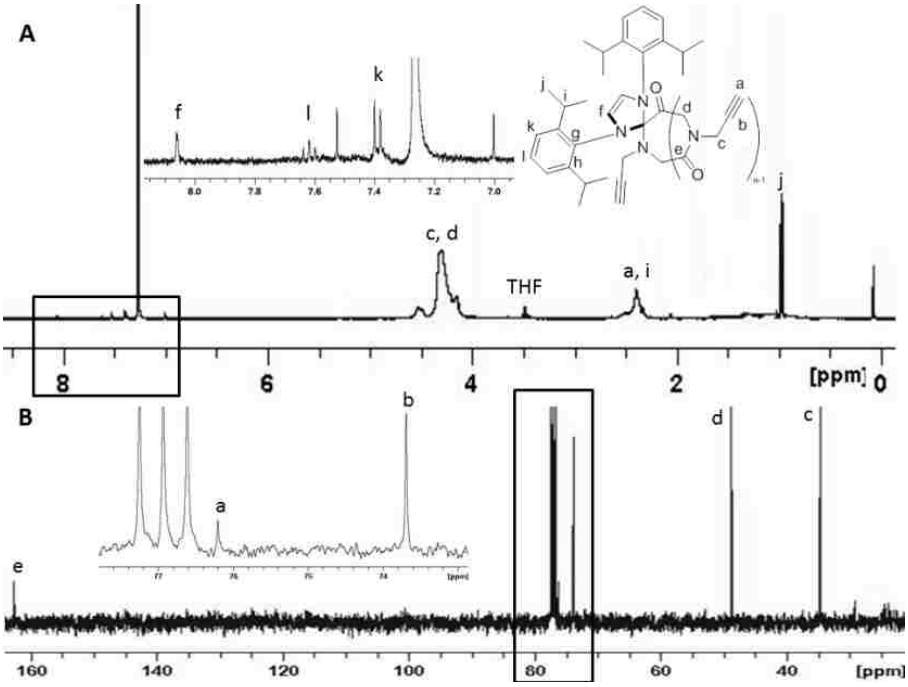

Figure 2.7. (A) ^{1}H NMR and (B) ^{13}C ^{1}{H} NMR spectra of *c*-PNPG (M_n=4.3 kg·mol^{-1}, PDI= 1.10) in $CDCl_3$.

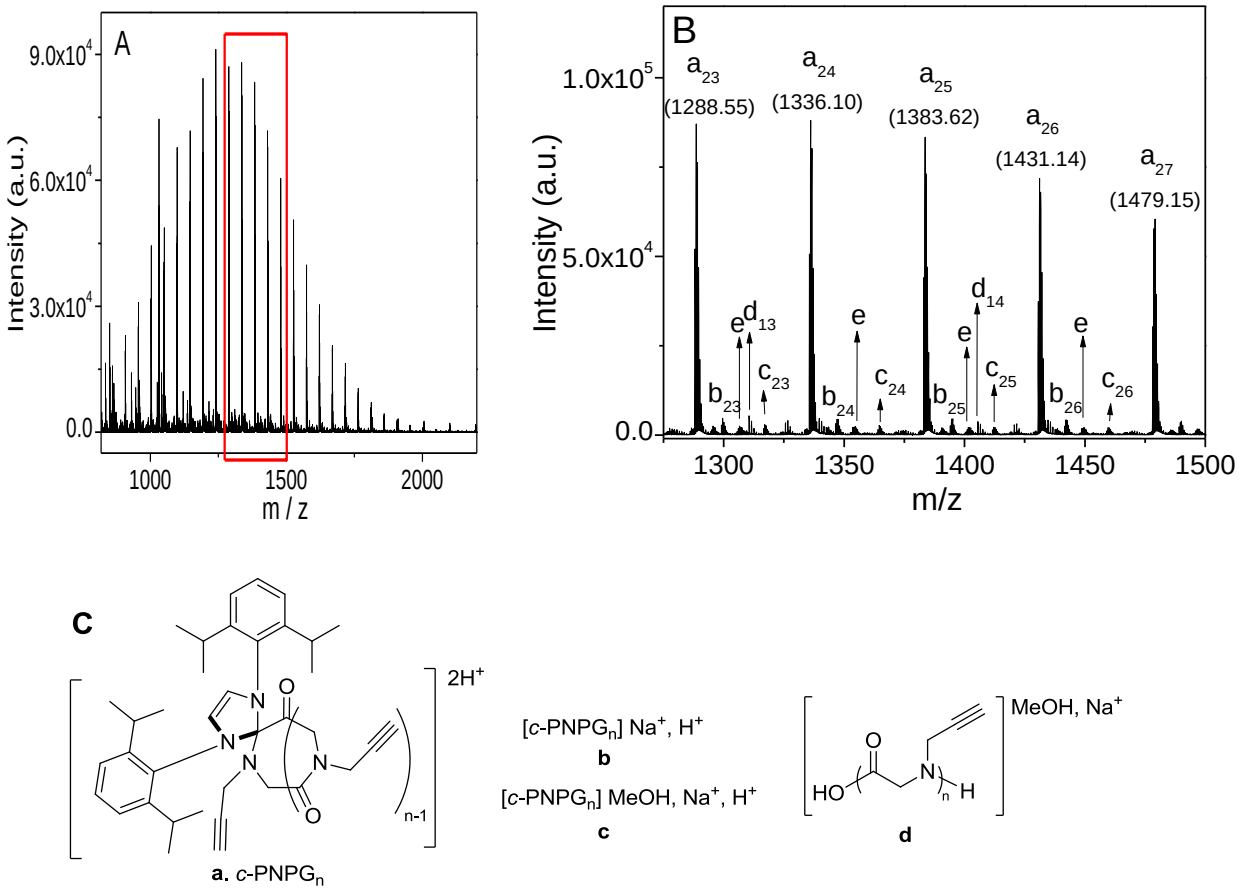

Figure 2.8. (A) Representative full and (B) expanded ESI MS spectra of a low M_n *c*-PNPG (M_n = 2.8 kg·mol^{-1}, PDI = 1.09) as well as (C) their assigned molecular structures.

The polymers were analyzed by ^{1}H NMR (**Figure 2.7**) and SEC-MALS-DRI (**Figure 2.12**) techniques for their molecular weight and molecular weight distribution. The polymer molecular weights (M_n) were determined by integrating the *c*-PNPG methine proton (a, **Figure 2.7** (**A**)) and the NHC phenyl protons (i, **Figure 7** (**A**)) to give the number average degree of polymerization (DP_n), assuming that each polymer chain has one NHC affixed to it. Polymerization of M_1 with increasing $[M_1]_0$:$[NHC]_0$ leads to the formation of *c*-PNPG with increasing polymer M_n (M_n= 2.2-15.6 kg·mol^{-1}) and relative narrow molecular weight

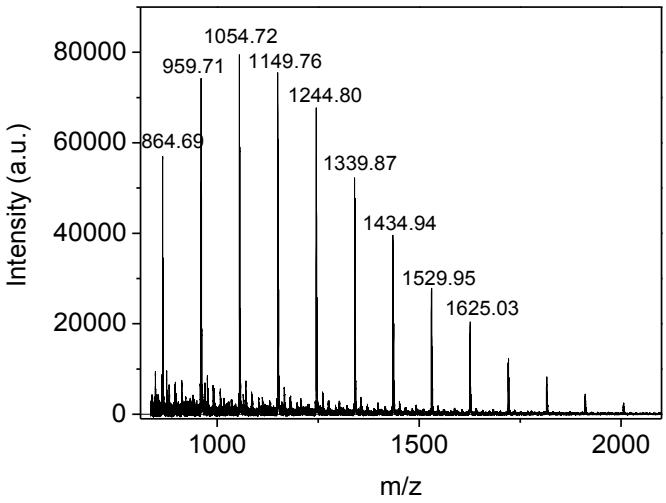

Figure 2.9. Representative MALDI-TOF MS spectrum of a purified low molecular weight *c*-PNPG [Matrix: α-cyano-4-hydroxycinnamic acid (CHCA)].

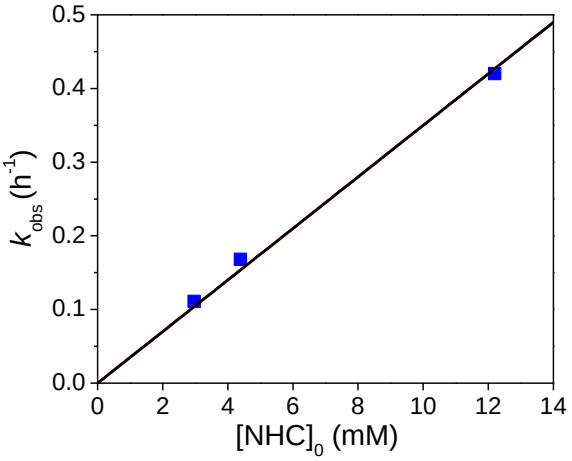

Figure 2.10. Plot of the observed rate constant (k_{obs}) versus the initial NHC concentration ($[NHC]_0$) (■) and the linearly fitted curve (black line) for the NHC-mediated polymerizations of M_1 ($[NHC]_0$ = 3.0, 4.4, 12.2 mM, $[M_1]_0$:$[NHC]_0$ =50:1, THF, 50°C).

distribution (PDI = 1.03-1.13) (entry 1-6, Table 1). The experimental molecular weight agrees reasonably well with the theoretical values based on single-site initiation and living polymerization. Furthermore, NHC-mediated polymerization of M_1 also exhibits a linear increase of molecular weight over conversion while the molecular weight distribution remains narrow (PDI=1.10-1.23) (**Figure 2.11** (**A**)), suggesting a constant concentration of propagating species throughout the reaction course, indicative of a living polymerization. Kinetic studies

reveal that the polymerization is first-order dependent on the monomer and NHC concentration (i.e., $d[M_1]/dt=k_p[NHC]_0[M_1]$, k_p= 35 $M^{-1}\cdot h^{-1}$) **(Figure 2.11** (**B**) and **Figure 2.10**). The plots of $\ln([M_1]_0/[M_1])$ versus time (**Figure 2.11** (**B**)) all pass through (0,0), consistent with an initiation that is fast or comparable to the propagation.[52]

Table 2.1. NHC-mediated polymerization of M_1 and copolymerization of M_1 and M_2.

Entry	Polymer	$[M_1]_0$:$[M_2]_0$: $[NHC]_0$ [a]	M_n(theor.) [b] (kg·mol^{-1})	M_n(SEC) [c,d] (kg·mol^{-1})	M_n(NMR) (kg·mol^{-1})	PDI	Conv.[e]
1	*c*-PNPG	25:0:1	2.4	-	2.2	-	100
2	*c*-PNPG	50:0:1	3.8	4.3 [c]	4.1	1.10 [c]	100
3	*c*-PNPG	75:0:1	5.5	5.7 [c]	5.8	1.03 [c]	100
4	*c*-PNPG	100:0:1	9.1	9.1 [c]	10.9	1.13 [c]	96
5	*c*-PNPG	122:0:1	11.6	13.3 [c]	11.5	1.12 [c]	100
6	*c*-PNPG	200:0:1	18.1	15.6 [c]	-	1.10 [c]	95
7	*c*-PNPG$_{159}$-*r*-PNBG$_{173}$	150:150:1	20.5	44.6 [d]	43.2	1.12 [d]	99
8	*c*-PNPG$_{150}$-*r*-PNBG$_{30}$	250:50:1	29.4	49.2 [d]	17.7	1.15 [d]	99
9	*c*-PNPG$_{102}$-*r*-PNBG$_{73}$	100:133:1	24.1	49.9 [d]	17.7	1.30 [d]	90
10	*c*-PNPG$_{103}$-*r*-PNBG$_{35}$	76:24:1	9.9	56.0 [d]	13.7	1.20 [d]	99
11	*c*-PNPG$_{62}$-*r*-PNBG$_{49}$	50:50:1	10.5	38.9 [d]	10.9	1.14 [d]	99
12	*c*-PNPG$_{39}$-*r*-PNBG$_{99}$	20:80:1	11.1	37.1 [d]	14.9	1.11 [d]	99

[a.] $[M_1]_0=[M_2]_0$= 0.4 M for all polymerizations; [b.] theoretical molecular weights were calculated from the $[M_1]_0$: $[M_2]_0$:$[NHC]_0$ ratio and the conversion of monomer to polymer (Note: the 6MR content is subtracted in the calculation); [c.] experimental molecular weight and polydispersity index were determined by a tandem SEC-MALS-DRI system in LiBr (0.1 M)/DMF solution at 50°C using a measured dn/dc of 0.1094(14) mL·g^{-1}; [d.] experimental molecular weight and polydispersity index were determined by a SEC-DRI system in LiBr

(0.1M)/DMF solution at 50°C using polystyrene standards; [e.] monomer conversions were determined by FTIR spectroscopy.

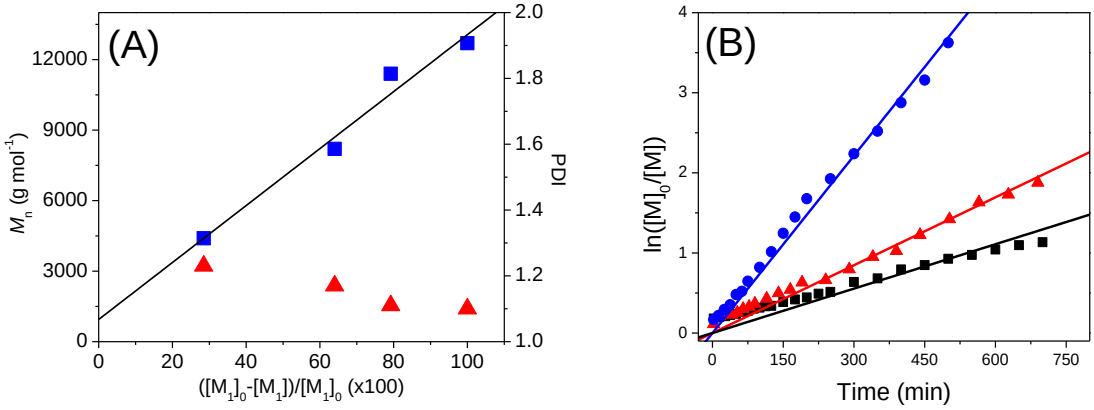

Figure 2.11. (A) Plot of M_n (■) and PDI (▲) versus conversion (i.e., $([M_1]_0-[M_1])/[M_1]_0$) for NHC-mediated polymerization of M_1 (THF, 50°C) and the linearly fitted curve for the M_n-vs-conversion data (black line). (Note: the monomer conversion was determined by FTIR spectroscopy while M_n and PDI were measured by SEC-MALS-DRI in LiBr (0.1 M)/DMF solution [dn/dc= 0.1094(14) mL·g^{-1}]); (B) plot of $\ln([M_1]_0/[M_1])$ versus time for the NHC-mediated polymerization of M_1 and their linearly fitted curves ($[NHC]_0$ = 3.0 (■), 4.4(▲), 12.2 mM (●), $[M_1]_0$:$[NHC]_0$ =50:1, THF, 50°C)

The SEC chromatograms of *c*-PNPGs exhibit a multi-modal distribution (**Figure 2.12**) in common organic solvents [e.g., THF, $CHCl_3$ and LiBr (0.1M)/DMF] regardless of the M_n range. This is in contrast to MS results where only a mono-modal distribution of mass ions was observed (**Figure 2.5(A) and 2.9**). The DLS analysis of *c*-PNPG reveals the presence of large particles having non-uniform size. The size of the particles increases from ~10 nm to several micron over 3 h in THF, strongly suggesting polymer aggregation (**Figure 2.13**). Aggregation in solution appears to be an innate property of the PNPG polymer rather than being induced by the zwitterionic chain ends, since the linear poly(*N*-propargyl glycine)s (*l*-PNPG) that are independently prepared by primary amine-initiated polymerization of M_1 (**Figure 2.14** and **Table 2.2**)[7] also exhibit multi-modal SEC chromatograms in spite of their neutral chain ends (**Figure 2.15**). This is in contrast to cyclic poly(*N*-Bu-glycine)s (*c*-PNBG) that do not appear to

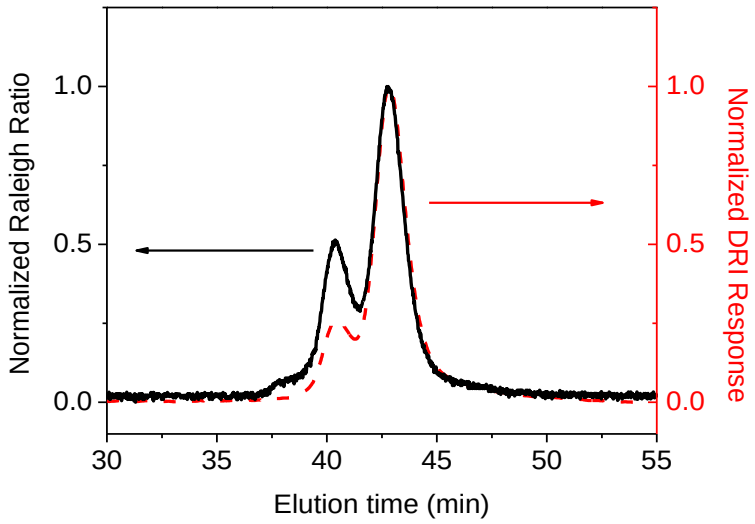

Figure 2.12. Representative SEC-MALS-DRI chromatograms [50°C, LiBr (0.1 M)/DMF] of *c*-PNPG prepared by NHC-mediated polymerization of M_1 [(-) MALS response; (---) DRI response].

substantially aggregate, as supported by mono-modal SEC chromatograms.[7] In view of this evidence, we attribute the high M_n components in the SEC chromatograms of PNPGs (i.e., at low elution time) to polymer aggregation. The polymer M_n s determined from the SEC mode at long elution times agree reasonably well with those determined by ^{1}H NMR analysis (Entry 1-6, Table 1).

Table 2.2. Primary amine ($BuNH_2$)-initiated polymerization of M_1

Entry	$[M_1]_0$:$[BuNH_2]_0$ [a]	M_n(theor.) [b] (kg·mol^{-1})	M_n(SEC) [c] (kg·mol^{-1})	M_n(NMR) [d] (kg·mol^{-1})	PDI [c]	Conv. [e]
1	25:1	2.4	4.9	2.2	-	100
2	50:1	4.8	6.6	4.1	1.10	100
3	75:1	5.5	5.7	5.8	1.03	100
4	100:1	9.5	9.0	-	1.03	99
5	200:1	19.0	14.9	-	1.04	99

[a.] $[M_1]_0$= 0.4 M for all polymerizations; [b.] theoretical molecular weights were calculated from the $[M_1]_0$:$[NHC]_0$ ratio and the conversion of monomer to polymer (Note: 6MR content is very low and neglected in the calculation); [c.] experimental molecular weight and

polydispersity index were determined by a tandem SEC-MALS-DRI system in LiBr (0.1 M)/DMF solution at 50°C using a measured dn/dc of 0.1012(7) $mL \cdot g^{-1}$; [d.] experimental molecular weights were determined by ^1H NMR analysis [e.] monomer conversion determined by FTIR spectroscopy.

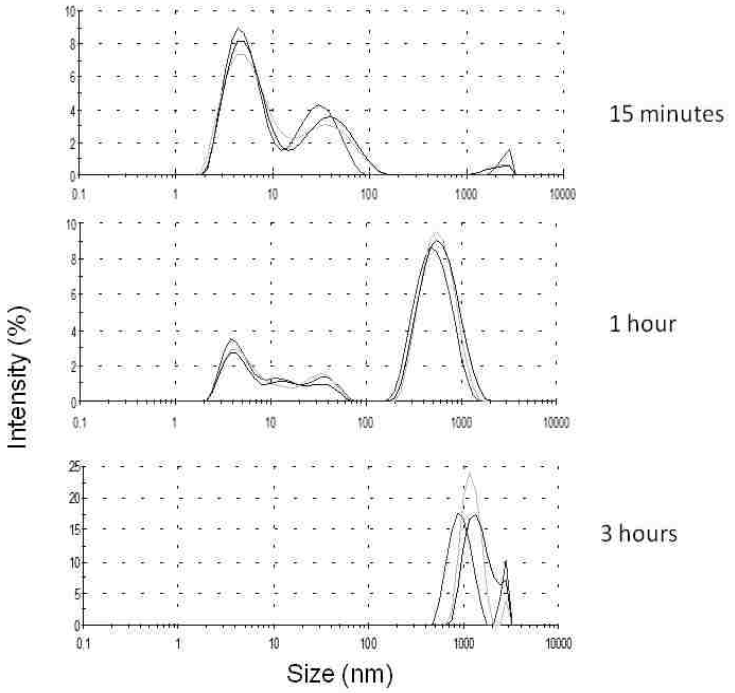

Figure 2.13. DLS analysis of *c*-PNPG in room temperature THF (*c*-PNPG concentration=5 $mg \cdot mL^{-1}$). An increase in aggregate size over a period of 3 h was observed by DLS, strongly suggesting polymer aggregation. (Note: DLS data was collected in triplicate).

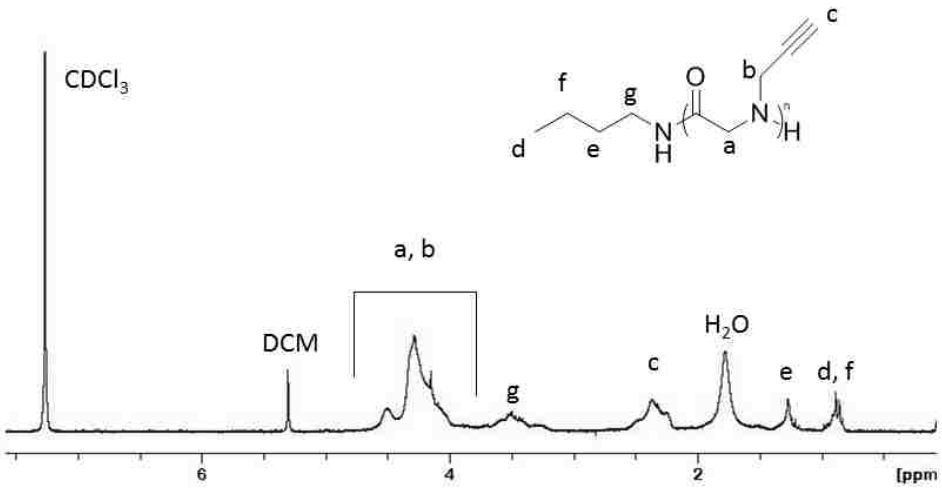

Figure 2.14. Representative ^1H NMR spectrum of *l*-PNPG in $CDCl_3$.

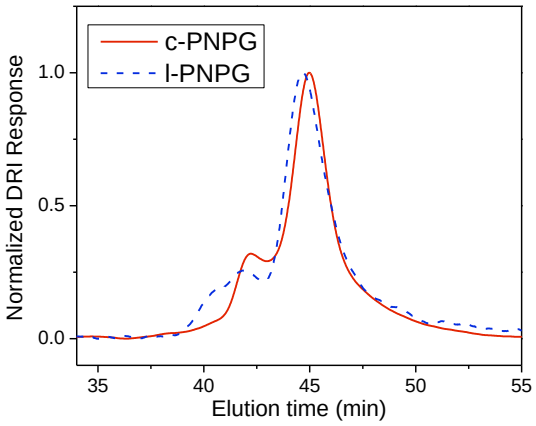

Figure 2.15. SEC chromatograms [LiBr(0.1)/DMF, 50°C] of *c*-PNPG (M_n=9.9 kg·mol^{-1}, PDI=1.05) (—) and *l*-PNPG (M_n=9.8 kg·mol^{-1}, PDI=1.06) (---) having identical polymer MW that are prepared by NHC or primary amine-initiated polymerization of M_1 respectively. The polymer MWs were determined using measured dn/dc of *c*-PNPG (0.1094 ± 0.0014 mL·g^{-1}) and *l*-PNPG (0.1012 ± 0.0007 mL·g^{-1}).

A comparison of SEC chromatograms of *l*-PNPG and *c*-PNPG having nearly identical polymer M_n reveals that the *l*-PNPG elutes at a shorter elution time than the *c*-PNPG (**Figure 2.15**), consistent with the cyclic polymers being hydrodynamically more compact than their linear analogues. Intrinsic viscosity measurement is often conducted to verify the polymer architecture.[7, 13, 41, 63] However, it was proven difficult for the analysis of *l*-PNPG and *c*-PNPG due to their strong tendency to aggregate in common organic solvents. As a result, the intrinsic viscosity difference observed for *l*-PNPG and *c*-PNPG of identical M_n cannot be unambiguously attributed to differences in their molecular architecture or their aggregation state (**Figure 2.16**).

2.3.2 Synthesis and Characterization of Cyclic Poly(*N*-propargyl glycine)-*ran*-poly(*N*-butyl glycine) Random Copolymers (*c*-PNPG-*r*-PNBG)

Cyclic poly(*N*-propargyl glycine)-*ran*-poly(*N*-butyl glycine) random copolymers (*c*-PNPG-*r*-PNBG) were prepared by NHC-mediated copolymerization of M_1 and *N*-Butyl *N*-carboxyanhydride (M_2) with different initial $[M_1]_0$:$[M_2]_0$:$[NHC]_0$ ratio. The *c*-PNPG-*r*-PNBG copolymer composition and polymer M_n (**Table 2.1**, entry 7-12) were determined by ^{1}H NMR

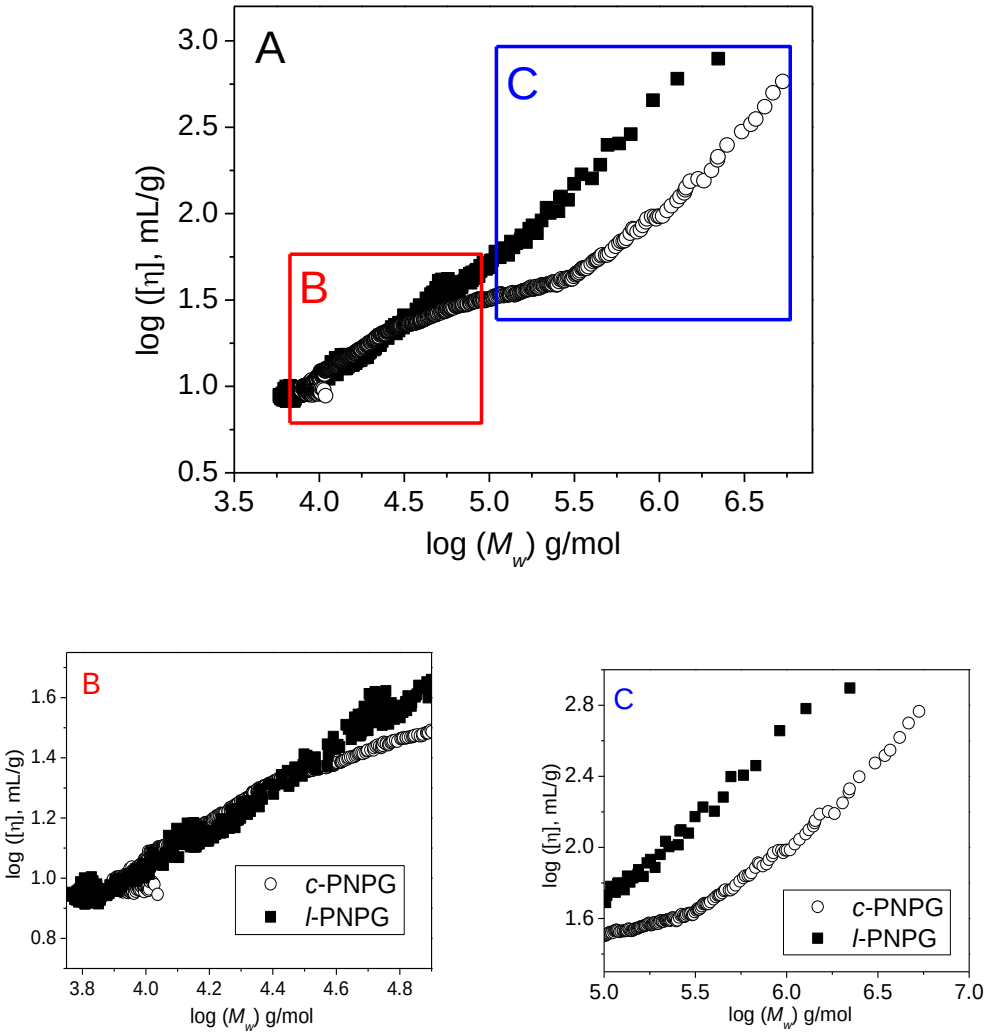

Figure 2.16. (A) Full and (B, C) expanded logarithmic plot of intrinsic viscosity versus polymer molecular weight (Mark-Houwink-Sakurada plot) of *c*-PNPG (○) and *l*-PNPG (■) prepared by the NHC-mediated or primary amine-initiated polymerization of M_1, respectively.

integration of the PNPG methylene protons (d) and the PNBG methine proton (g) relative to the phenyl proton (i) of the NHC moiety (**Figure 2.17**). Polymer M_ns and PDIs were also determined by SEC using a calibration curve constructed with mono-disperse polystyrene standards (**Table 2.1**, entry 7-12). As the amount of M_2 incorporated into the *c*-PNPG-*r*-PNBG copolymer increases, the bimodal character of the SEC chromatogram appears to decrease, suggesting reduced aggregation of the *c*-PNPG-*r*-PNBG copolymers in the solution (**Figure 2.18**).

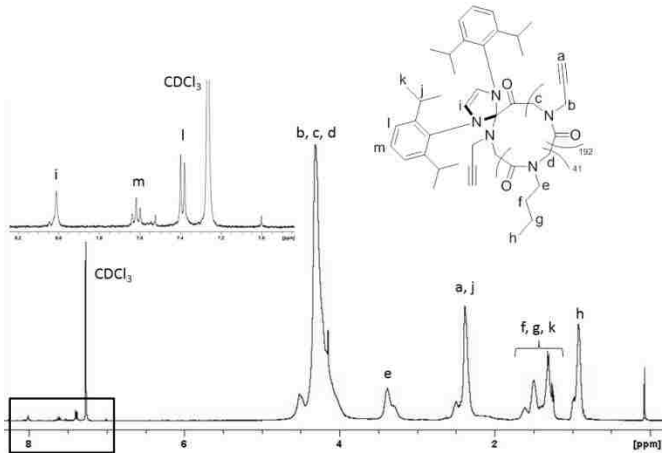

Figure 2.17. Representative ^{1}H NMR spectra of *c*-PNPG$_{193}$-*r*-PNBG$_{41}$ random copolymer in $CDCl_3$.

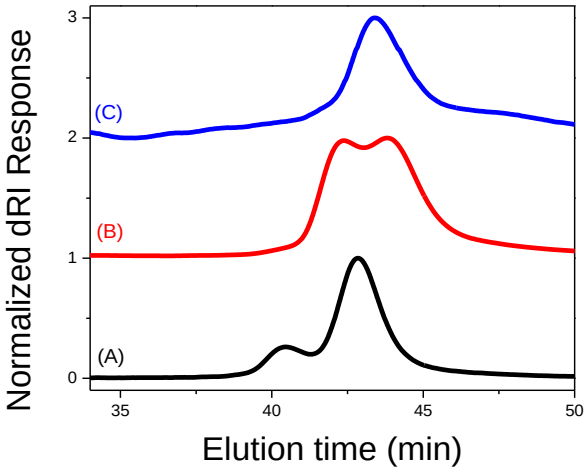

Figure 2.18. SEC chromatograms of (A) *c*-PNPG$_{200}$, (B) *c*-PNPG$_{166}$-*r*-PNBG$_{33}$ and (C) *c*-PNPG$_{116}$-*r*-PNBG$_{81}$ in LiBr (0.1M)/DMF solution.

2.3.3 Synthesis and Characterization of Cyclic and Linear Brush-Like Copolymers

Two azido-terminated poly(ethylene glycol) polymers (PEG-N_3) of different M_n (M_n=2 kg·mol-1, PDI=1.03; M_n=500 g·mol-1, PDI=1.05) were prepared by a previously reported procedure and their M_n were determined by MALDI TOF MS analysis.[122] Grafting of PEG-N_3 to PNPG and PNPG$_n$-*ran*-PNBG$_m$ proceeded at room temperature in CH_2Cl_2 in the presence of CuBr/PMDETA (1:1) (~20-30 mol % relative to propargyl content) over a period of 3 h under

nitrogen atmosphere (**Scheme 2.3.3.1**). The polymer product was purified by passing it through a neutral alumina column and precipitated by excess hexane.

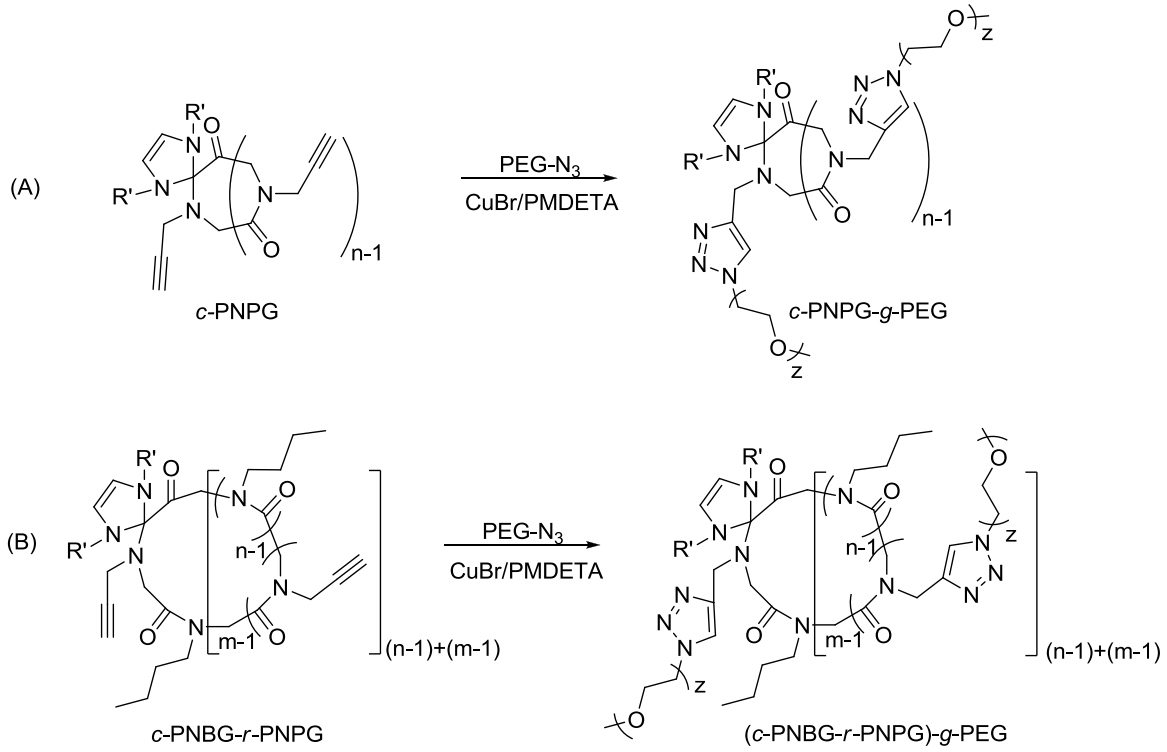

Scheme 2.3. Synthetic strategy towards cyclic brush copolymers (R'= 2,6-diisopropylphenyl)

Successful grafting of the polymeric side chains by CuAAC chemistry is evidenced by the appearance of characteristic triazolium protons at 8.0 ppm in the ^{1}H NMR spectrum of the polymer product (*c*-PNPG-*g*-PEG) (k, **Figure 2.20**). The SEC analysis of the polymer product also reveals an increase in the molecular weight relative to that of *c*-PNPG, confirming successful grafting of the PEG side chains to the *c*-PNPG backbone (**Figure 2.19**). However, the molecular weight distribution is fairly broad (PDI =1.68-2.28) (entry 1-2, **Table 2.3**). The integration ratio of the triazolium proton (k, **Figure 2.20**) relative to the propargyl methine proton (y, **Figure 2.20**) has been used to determine the grafting density ($Y_{GRAFTING}$). The maximum grafting density is ~20%, which is low relative to typical polymer brushes prepared by

the graft-to method (entry 1-2, **Table 2.3.3.**).[53, 100] Varying the ratio of $[N_3]_0$:$[propargyl]_0$ does not appear to have an appreciable effect in the grafting density. While steric crowding of the affixed polymeric side chains limits the grafting density, PNPG aggregation also contributes to the restricted access of propargyl groups by azido-ended PEG. As a result, we reason that random copolymers (*c*-PNPG-*r*-PNBG) will likely provide improved grafting efficiency due to the reduced aggregation tendency of these copolymers.

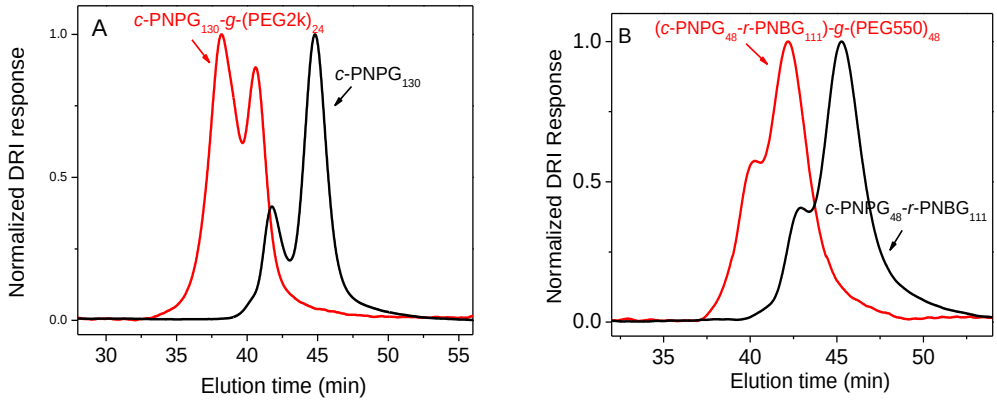

Figure 2.19. (A) Representative SEC chromatograms [LiBr (0.1M)/DMF, 50°C] of *c*-$PNPG_{130}$ and *c*-$PNPG_{130}$-*g*-$(PEG2k)_{24}$ obtained after grafting of PEG by CuAAC chemistry; (B) representative SEC chromatograms [LiBr (0.1M)/DMF, 50°C] of *c*-$PNPG_{48}$-*r*-$PNBG_{111}$ and (*c*-$PNPG_{48}$-*r*-$PNBG_{111}$)-*g*-$(PEG550)_{48}$ obtained after grafting of PEG by CuAAC chemistry.

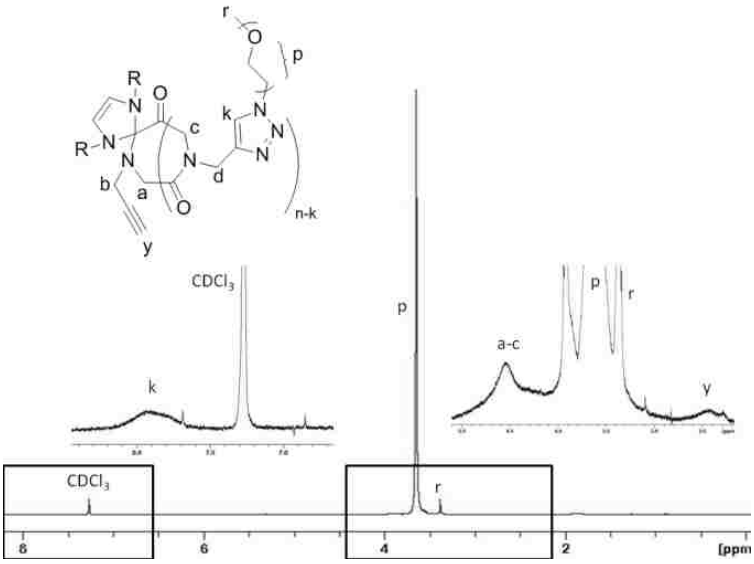

Figure 2.20. Representative ^1H NMR spectra of *c*-PNPG-*g*-PEG in $CDCl_3$.

Table 2.3 Cyclic brush-like polymers with poly(*N*-substituted glycine) backbone and PEG side chains.

Entry	Backbone Composition [a]	Backbone M_n [b] ($kg \cdot mol^{-1}$)	PEG M_n ($g \cdot mol^{-1}$)	$[N_3]_0$: $[propargyl]_0$	M_n [b] ($kg \cdot mol^{-1}$)	PDI [b]	Y_g [c] (%)	Y_g [d] (%)
1	*c*-$PNPG_{141}$	43.8	2k	0.5:1	121	1.68	19	-
2	*c*-$PNPG_{141}$	43.8	2k	0.8:1	174	2.28	19	-
3	*c*-$PNPG_{221}$-*r*-$PNBG_{196}$	44.6	2k	1.2:1	194	1.27	37	42
4	*c*-$PNPG_{221}$-*r*-$PNBG_{196}$	44.6	2k	1.5:1	204	1.23	47	45
5	*c*-$PNPG_{166}$-*r*-$PNBG_{33}$	49.2	550	0.75:1	142	1.82	45	-
6	*c*-$PNPG_{166}$-*r*-$PNBG_{33}$	49.2	550	2:1	175	1.73	62	-
7	*c*-$PNPG_{166}$-*r*-$PNBG_{33}$	49.2	550	3:1	145	1.78	77	-
8	*c*-$PNPG_{150}$-*r*-$PNBG_{30}$	49.2	550	1.6:1	155	1.71	52	-

[a.] All reactions were carried out in THF (entries 1 and 2) or CH_2Cl_2 (entries 3-8) and the polymer composition is determined by ^1H NMR analysis; [b.] all M_ns and PDIs were determined by SEC [LiBr(0.1M)/DMF, 50°C] using polystyrene standards; [c.] grafting density was determined by ^1H NMR analysis; [d.] grafting density was determined by the changes of PEG-N_3 concentration, i.e., percentage intensity change of their SEC-DRI response.

The side chain grafting density is substantially increased to 37-77% (entry 3-8, **Table 2.3**), corresponding to high CuAAC coupling efficiency (70-93%), when the random copolymers (*c*-PNPG-*r*-PNBG) are used. The molecular weight distributions are also narrower (PDI= 1.23-1.82) than those obtained when *c*-PNPGs are used in the PEG grafting experiments. The grafting density was determined by integrating the resonance for the single triazolium proton (k, **Figure 2.21**) relative to the three protons on the methyl group of the PNBG repeating unit (i, **Figure 2.21**), which is then multiplied by the molar percentage of PNBG repeating unit in the random copolymers. Grafting densities can also be enhanced by increasing the ratio of $[N_3]_0$:$[propargyl]_0$

(entries 5-7, **Table 2.3**). We have shown that increasing PNBG content results in reduced aggregation of the random copolymers *c*-PNPG-*r*-PNBG, as manifested in increasingly mono-modal SEC chromatograms (**Figure 2.18**). The molecular weight distribution (PDI) of the cyclic brush-like polymers [i.e., (*c*-PNPG-*r*-PNBG)-*g*-PEG] also appears to decrease with increasing PNBG backbone content, suggesting that perhaps the reduced aggregation facilitates the statistical grafting of the side chains, resulting in lowered PDIs (entry 3-8, **Table 2.3**).

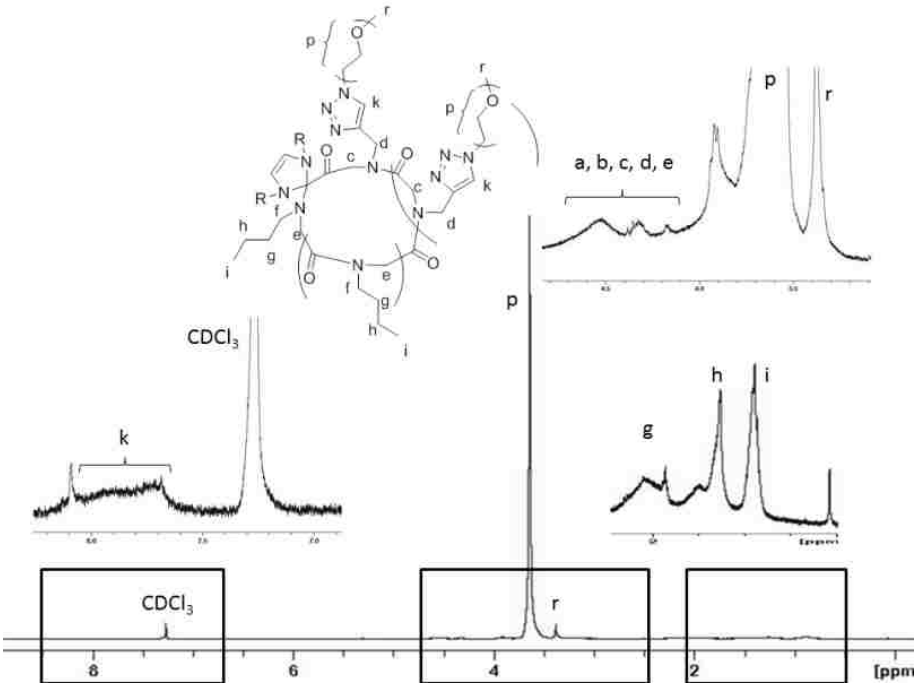

Figure 2.21. Representative ^{1}H NMR spectra of (*c*-PNPG$_{166}$-*r*-PNBG$_{33}$)-*g*-PEG, in $CDCl_3$. (Note: the small sharp peak overlapped with peak 'k' is the ^{13}C satellite resonance of $CDCl_3$).

To further validate the grafting density obtained by ^{1}H NMR analysis, we quantified the percentage decrease of PEG-N_3 content prior to and post CuAAC by the SEC-DRI method (**Figure 2.22**).[100] As the initial $[N_3]_0$:$[propargy]_0$ ratio is known, the grafting density can be deduced. The grafting densities obtained by ^{1}H NMR or SEC analysis are in good agreement (entry 3-4, **Table 2.3**).

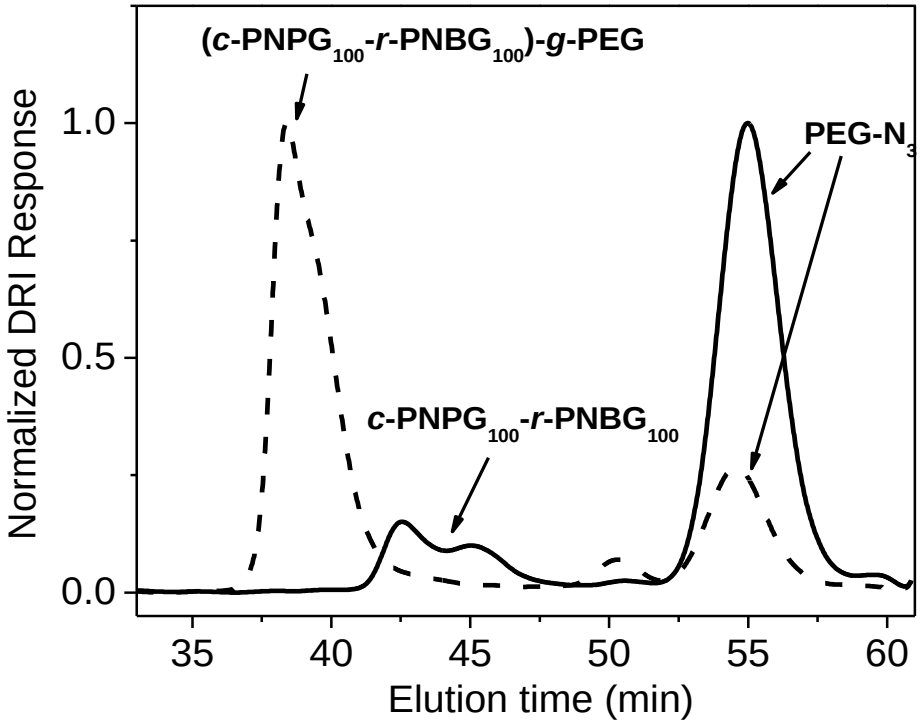

Figure 2.22. SEC chromatograms [LiBr(0.1M)/DMF, 50°C] of the reaction mixture prior to (-) and after the grafting of PEG-N_3 to *c*-$PNPG_{100}$-*r*-$PNBG_{100}$ by CuAAC chemistry (---).

2.3.4 AFM Analysis of Cyclic Brush-Like Copolymers

Atomic force microscopic (AFM) analysis of the cyclic brush-like polymers [i.e., *c*-$PNPG_{141}$-*g*-$(PEG2k)_{27}$ and (*c*-$PNPG_{166}$-*r*-$PNBG_{33}$)-*g*-$(PEG550)_{154}$] (entry 1 and 7, **Table 2.3**) is presented in **Figure 2.23**. Bright areas in the topography images (**Figure 2.23 A** and **E**) display ring-shaped nanostructures, which exhibit a narrow size distribution. The darker areas in these topographical figures are considered to be the mica background. The height profiles for all samples were relatively low (< 2.5 nm), consistent with a single layer of nanostructures lying flat on the mica surface (Figure 7C and 7G). Amplitude images constructed by mapping the cantilever oscillation as it is raster scanned across the surface also reveal ring-shaped

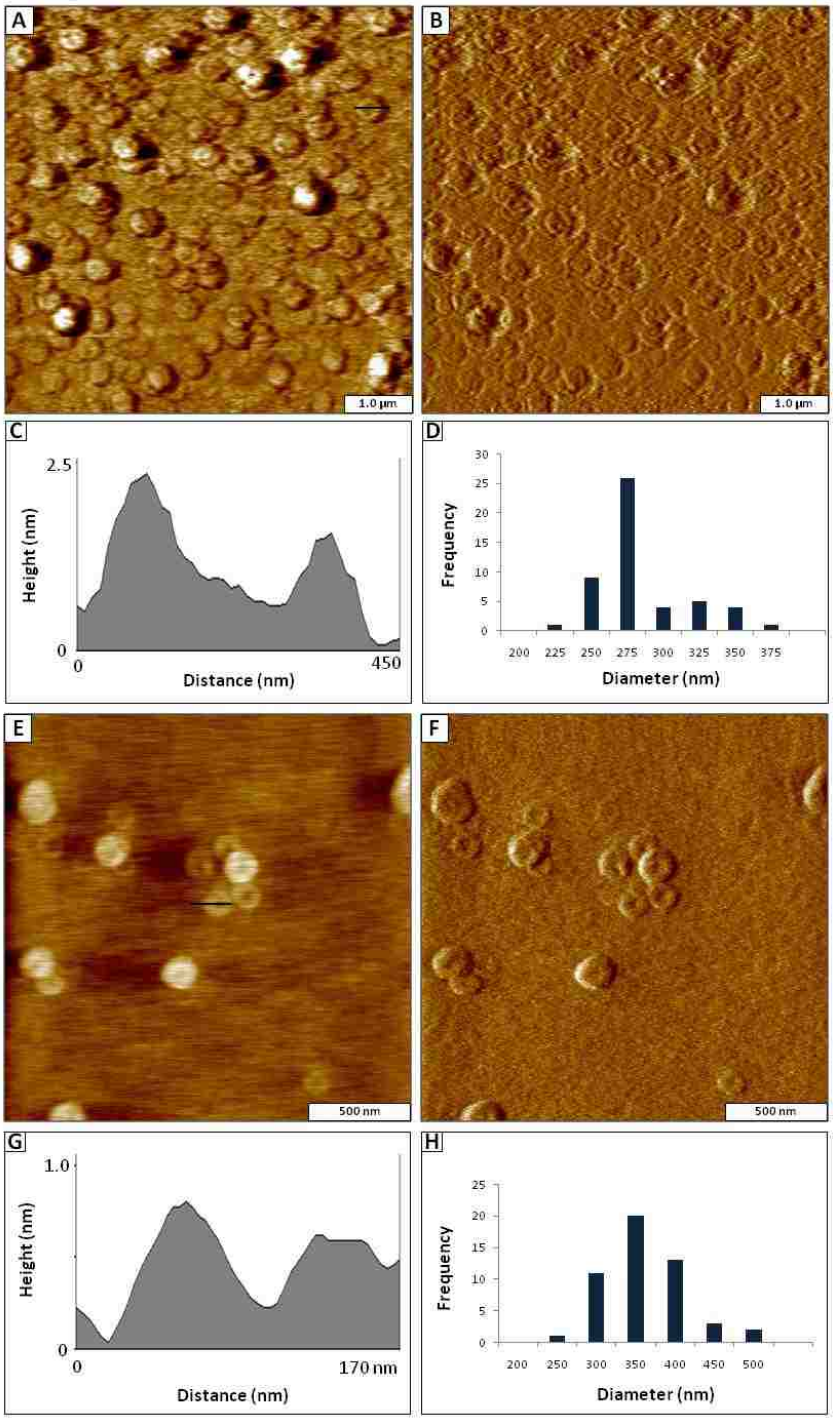

Figure 2.23. Representative AFM topographic (A, E) and amplitude (B, F) images of *c*-$PNPG_{141}$-*g*-$(PEG2k)_{27}$ and (*c*-$PNPG_{166}$-*r*-$PNBG_{33}$)-*g*-$(PEG550)_{154}$ (entry 1 and 7, Table 2) respectively on mica (0001) and the cross-section (C, G) and histogram analysis (D, H) of selected ring polymers within the respective sample. (Sampling size = 50) (Note: the black line in Figure A and E indicate the specific nanostructure whose cross-section analysis is shown in Figure C and G).

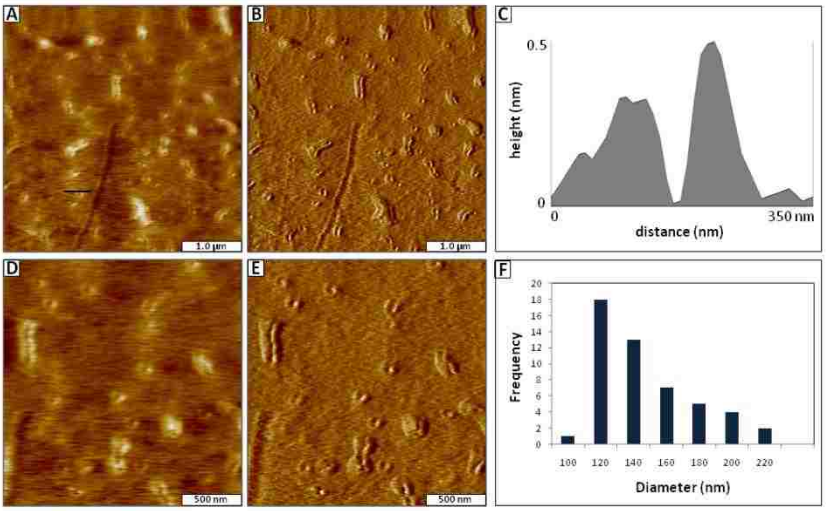

Figure 2.24. AFM topographic (A, D) and amplitude images (B, E) of (*c*-PNPG$_{150}$-*r*-PNBG$_{30}$)-*g*-(PEG550)$_{94}$ on mica(0001) where both ring-like nanostructures and larger aggregates are observed; (C) cross-section analysis of a selected ring-like nanostructure and (F) the histogram analysis of 50 ring-shaped nanostructures giving the average diameter (d=147 nm). (Note: the theoretical diameter of the nano-rings is estimated to be 40 nm, if the cyclic backbone and the side chains are assumed to adopt a fully extended zig-zag conformation).

nanostructures (**Figure 2.23 B** and **F**). Differences in the nanostructure size were observed for the cyclic brush-like polymers with variable composition. The cross-section and histogram analysis of the nanostructures reveals an average diameter of 283 and 362 nm for *c*-PNPG$_{141}$-*g*-(PEG2k)$_{27}$ and (*c*-PNPG$_{166}$-*r*-PNBG$_{33}$)-*g*-(PEG550)$_{154}$ respectively (**Figure 2.23 D** and **H**). The lateral dimensions are exaggerated when compared to the theoretical diameters based on the polymer composition (i.e., 49 and 32 nm). This is attributed to the tip effect in AFM imaging that displays a convolution of the geometry of the sample and tip, resulting in overestimation of the lateral features.[123]

While the 'donut-shape' is not as evident for *c*-PNPG$_{141}$-*g*-(PEG2k)$_{27}$ (**Figure 2.23 A** and **B**), it is clearly visible for (*c*-PNPG$_{166}$-*r*-PNBG$_{33}$)-*g*-(PEG550)$_{154}$ (**Figure 2.23 E** and **F**). This is likely to arise from the difference in side chain length relative to the diameter of the cyclic backbone. If the cyclic backbone and the side chains are assumed to adopt a fully extended zig-

zag conformation, the cyclic backbone diameter of *c*-$PNPG_{141}$-*g*-$(PEG2k)_{27}$ is estimated to be 17 nm and PEG chain length is 16 nm, resulting in a theoretical diameter of 49 nm for the nanostructure. In comparison, the theoretical diameter of the (*c*-$PNPG_{166}$-*r*-$PNBG_{33}$)-*g*-$(PEG550)_{154}$ nanostructure is estimated to be 32 nm, which is the sum of the cyclic backbone diameter (24 nm) and the twice the PEG side chain length (4 nm). As a result, one would expect to observe a "donut hole" in the AFM images of the former sample, but not necessarily the latter. Additionally, the cyclic brush-like polymers can also self-assemble into larger aggregates (**Figure 2.24**), but small ring nanostructures are still visible along with the aggregates.

2.4 Concluding Remarks

The monomer *N*-propargyl *N*-carboxyanhydrides were successfully polymerized using NHC initiators to yield cyclic poly(*N*-propargyl glycine) (*c*-PPNG) in a controlled manner. The propargyl groups enable further side chain derivation by CuAAC chemistry. This was demonstrated in the synthesis of brush-like polymers having poly(*N*-substituted glycine) backbone and PEG side chain. The grafting efficiency of polymer side chain is low when *c*-PPNG homopolymer is used, presumably due to polymer aggregation that hinders access to the propargyl groups. High-to-quantitative grafting efficiencies can be obtained by utilizing cyclic random block copolymers (i.e., PPNG-*r*-PBNG) where the reactive propargyl groups are spaced by inert butyl side chains. The increase in grafting density is attributed to either a decrease in cyclic backbone aggregation in the CuAAC reaction medium, or a decrease in steric crowding among the side chains on the cyclic backbones. The AFM analysis of the cyclic brush-like polymers reveals the formation of donut-shape nanostructures whose dimension correlates well with the molecular composition of the polymers. The successful development of NHC-mediated polymerization of NCA bearing side chains amendable to CuAAC chemistry will enable future

development of structurally and functionally diverse polymer materials with novel architectures. Future work will entail the ability to control the amount of and the direct placement of thermo- and pH-responsive polymers to the cyclic backbone to yield highly tailored responsive cyclic brush-like polymers. Control over such polymeric architectures allows for materials that can be tailored for specific needs, such as polymeric blend compatabilizers, temperature-induced breathable channels or 'smart' drug-delivery systems.

2.5 Experimental

2.5.1 Materials and Instrumentation

Materials. Glyoxylic acid monohydrate (98%), progargyl amine (98%), butyl amine (98%), di-*tert*-butyl dicarbonate (97%), triethylamine, copper bromide (I), PMDETA, and phosphorus trichloride were purchased from Sigma Aldrich and used as received. All solvents used in this study were purchased from Sigma-Aldrich and purified by passing through alumina columns under argon. The compounds 2,6-diisopropylphenylimidazol-2-ylidene (NHC)[124] and azido terminated polyethylene glycol (PEG-N_3) (M_n=2 kg·mol^{-1}, PDI=1.03; M_n=500 g·mol^{-1}, PDI=1.05) were synthesized by reported procedures.[125] The compounds of *N*-propargyl NCA (M_1) and *N*-butyl NCA (M_2) were synthesized by adapting a literature procedure.[7]

Instrumentation. The ^{1}H and ^{13}C {^{1}H} NMR spectra were recorded on a Bruker AV-400 spectrometer, and the chemical shifts were referenced in parts per million (ppm) relative to proton impurities or ^{13}C isotopes of $CDCl_3$ respectively. The FTIR spectra were collected on a Bruker Tensor 27 FTIR spectrometer. The ESI spectra were recorded on an Agilent 6710 TOF mass spectrometer in the positive ion mode. The SEC analyses were conducted using an Agilent 1200 system (Agilent 1200 series degasser, isocratic pump, auto sampler and column heater) equipped with three Phenomenex 5 μm, 300×7.8 mm columns [100 Å, 1000 Å and Linear(2)],

Wyatt DAWN EOS multi-angle light scattering (MALS) detector (GaAs 30 mW laser at λ=690 nm), Wyatt ViscoStar viscometry (VISC) detector and Wyatt Optilab rEX differential refractive index (DRI) detector with a 690 nm light source. DMF containing 0.1 M LiBr was used as the eluent at a flow rate of 0.5 $mL \cdot min^{-1}$. The column temperature was 50°C and the detector temperature was 25°C. All data analyses were performed using Wyatt Astra V 5.3 software. Polymer molecular weight (M_n) and molecular weight distribution (PDI) were obtained by two methods: (1) Zimm model fit of MALS-DRI data; (2) conventional SEC analysis with a calibration curve. The calibration curve was constructed from twenty three pauci-disperse polystyrene standards (M_n= 590 $g \cdot mol^{-1}$-1472 $kg \cdot mol^{-1}$, Polymer Laboratories, Inc.) using Astra's column calibration template. Relative M_n and PDI were then calculated using Astra's conventional calibration template. Dynamic light scattering (DLS) analysis was conducted on a Malvern Zetasizer Nano-ZS instrument while using the Zetasizer software version 6.12. The *c*-PNPG polymer solution was prepared by filtering through a 0.2 micron PTFE filter prior to DLS data collection.

Refractive index increment (dn/dc) measurement. The refractive index increment (dn/dc) of the synthesized polymers was measured using Wyatt's rEX DRI detector and Astra software dn/dc template. Six polymer/DMF/0.1M LiBr solutions with different concentrations of polymer were sequentially injected into the DRI detector. The measured refractive index values were plotted versus concentration. The slope from a linear fitting of the data is the dn/dc of the polymer. The measured dn/dc values of *c*-PNPG and *l*-PNPG in LiBr (0.1 M)/DMF at 25°C and 690 nm wavelength are 0.109(1) $mL \cdot g^{-1}$ and 0.101(1) $mL \cdot g^{-1}$ respectively.

Intrinsic viscosity measurement. Eight polydisperse cyclic or linear poly(*N*-propargyl-glycine) samples with different M_n were independently prepared from NHC or butylamine-mediated

polymerizations of M_1. Polydisperse cyclic (M_n=14.8 kg·mol^{-1}, PDI=1.70) and linear poly(*N*-propargyl-glycine) samples (M_n=9.3 kg·mol^{-1}, PDI=1.55) were prepared by mixing the four pauci-disperse polymers with different M_n in equal weight fractions. The polydisperse samples were then analyzed by SEC-MALS-VISC-DRI for their intrinsic viscosities ([η]) and the absolute M_n s.

Atomic force microscopy (AFM). Imaging of the cyclic brush-like polymers was accomplished using tapping mode AFM (Agilent 5500 AFM/SPM system) in ambient air with Picoscan v5.3.3 software with probes acquired from Vista probes. The driving frequency for the tip during the imaging of the polymers was 181 kHz. Polymer samples were dissolved in chloroform to make a final concentration of 0.02 mg·mL^{-1}. A volume of polymer solution (~ 15 μL) was drop-casted and dried on freshly cleaved mica (0001) in ambient conditions for 24 h before AFM imaging. Minimal processing of the images was done using Picoscan software from Agilent.

2.5.2 Monomer Synthesis

Synthesis of 2-(prop-2-yn-1-ylamino)acetic acid hydrochloric salt (1). Propargyl amine (5.0 g, 90.8 mmol) and glycoxylic acid (16.72 g, 225 mmol) were both dissolved in CH_2Cl_2 (230 mL) and allowed to react overnight at room temperature. The CH_2Cl_2 was removed under reduced pressure and aqueous HCl (137 mL, 137 mmol, 1.0 M) was added. The solution was heated at reflux for 24 h, after which the water was removed by rotary evaporation. The resulting solid was redissolved in methanol and precipitated by the addition of copious volumes of ether. The product was collected by filtration and dried under vacuum to yield a brown solid (8.55 g, 63% yield). ^{1}H NMR (400 MHz, D_2O) δ: 4.0 (d, -C*H*$_2$, 2H), 3.8 (t, -C*H*$_2$CH, 2H), 2.3 (t, -C*H*, 1H). ^{13}C {^{1}H} NMR (100 MHz, D_2O) δ: 173 (-*C*O-), 82 (-*C*≡), 73 (≡*C*H), 50 (NH*C*H$_2$CO), 40 (≡C*C*H$_2$NH-).

Synthesis of 2-((tert-butoxycarbonyl) (prop-2-yn-1-yl)amino)acetic acid (2). The compound **1** (6.0 g, 40.1 mmol) was dissolved in distilled water (135 mL), to which di-*tert*-butyl dicarbonate (29.3 g, 134 mmol) and triethylamine (37.4 mL, 268 mmol) were sequentially added. The reaction mixture was stirred overnight at room temperature and then washed with hexane to remove any unreacted di-*tert*-butyl dicarbonate. The aqueous phase was separated and made acidic (pH = 3) with 1N HCl (aq). The product was extracted into ethyl acetate (3 x 100mL) and the organic layer was combined and washed with a saturated aqueous NaCl solution, dried over anhydrous $MgSO_4$, and concentrated to afford a beige solid. The product was recrystallized from MeOH/diethyl ether to yield a brown solid (7.53 g, 70% yield). ^{1}H NMR (400 MHz, $CDCl_3$) δ: 4.1 (t, -CH_2-, 2H), 4.0 (s, -CH_2-, 2H), 2.3 (t, -CH, 1H), 1.4 (d, -(CH_3)$_3$, 9H). ^{13}C {^{1}H} NMR (100 MHz, $CDCl_3$) δ: 173 (-COOH), 154 (-NCOO-), 80 (-OC(CH$_3$)$_3$), 78 (≡C-), 73 (≡CH), 54 (-NCH$_2$COOH), 40 (≡CCH$_2$N-), 28 (-(CH$_3$)$_3$).

Synthesis of *N*-propargyl *N*-carboxyanhydride (M_1). The compound **2** (1.74 g, 6.5 mmol) was dissolved in anhydrous CH_2Cl_2 (230 mL) under a nitrogen atmosphere. PCl_3 (1.15 mL, 13.1 mmol) was added dropwise to the solution at 0°C. The reaction mixture was stirred for 3 h and the solvent was removed under vacuum. The solid residue was extracted with anhydrous CH_2Cl_2 (20 mL) and filtered. The filtrate was evaporated to afford a white solid. Further purification by recrystallization from anhydrous CH_2Cl_2/hexane and sublimation yielded white crystals (0.5 g, 55 % yield). ^{1}H NMR (400 MHz, $CDCl_3$) δ: 4.3 (-CH_2-, 2H), 4.2 (-CH_2-, 2H), 2.4 (≡CH, 1H). ^{13}C{^{1}H} NMR (100 MHz, $CDCl_3$) δ: 165 (-CH$_2$$C$(O)O-), 151 (-O$C$(O)N-), 77 ($C$H≡), 76 (≡$C$-), 49 (≡C$CH_2$N-), 32 (C(O)$CH_2$N-).

2.5.3 Polymer Synthesis

Representative synthetic procedure for the cyclic poly(*N*-propargyl-glycine) (*c*-PNPG). Inside a glovebox, M_1 (200 mg, 1.44 mmol) was dissolved in THF (2.5 mL) to which a THF

stock solution of NHC (267 μL, 14.4 μmol, 53.8 mM) was added at room temperature. The reaction was stirred and heated at 55°C for 18 h. An excess of hexane (10 mL) was added to the remaining reaction mixture. The suspension was stirred at 50°C for 8 h and filtered while still warm to remove low molecular weight oligomers. The yellow solid that was obtained was dried under vacuum (120 mg, 88% yield). ^{1}H NMR (400 MHz, $CDCl_3$) δ: 4.6-4.0 (bm, -COC*H*$_2$N-, -CC*H*$_2$N-, 4H), 2.4 (bm, -CC*H*, 1H). ^{13}C{^{1}H} NMR (100 MHz, $CDCl_3$) δ: 163 (*C*=O), 76 (H*C*≡), 74 (*C*≡), 49 (*C*H$_2$C=O), 35 (*C*H$_2$C≡).

Representative synthetic procedure for the linear poly(*N*-propargyl-glycine) (*l*-PNPG). Inside a glovebox, M_1 (91 mg, 0.654 mmol) was dissolved in THF (2.5 mL) to which a THF stock solution of butyl amine (143 μL, 7.69 μmol, 53.8 mM) was added at room temperature. The solution was degassed by freeze-pump-thaw cycle three times and left to react under reduced pressure in a sealed flask. The reaction was stirred and heated at 50°C for 48 h. An excess of hexane (10 mL) was added to the remaining reaction mixture. The suspension was stirred at 50°C for 8 h and filtered while still warm to remove low molecular weight oligomers. The white solid that was obtained was dried under vacuum (31 mg, 50% yield). ^{1}H NMR (400 MHz, $CDCl_3$) δ: 4.8-3.2 (bm, -COC*H*$_2$N-, -CC*H*$_2$N-, 4H), 2.4 (bm, -CC*H*, 1H). ^{13}C {^{1}H} NMR (100 MHz, $CDCl_3$) δ: ^{13}C {^{1}H} NMR (400 MHz, $CDCl_3$) δ: 163 (*C*=O), 76 (H*C*≡), 74 (*C*≡), 49 (*C*H$_2$C=O), 35 (*C*H$_2$C≡).

Representative synthetic procedure for the cyclic poly(*N*-propargyl-glycine)-*ran*-poly(*N*-butyl-glycine) random copolymers (*c*-PNPG$_n$-*r*-PNBG$_m$).
In a glovebox, M_1 (64 mg, 0.46 mmol) and *N*-butyl NCA (M_2) (72 mg, 0.46 mmol) were dissolved in anhydrous THF (4 mL). A stock solution of NHC in THF (91 uL, 2.83 μmol, 31.1 mM) was added to the reaction flask. The flask was sealed and stirred at 55°C for 2 d. The polymerization was terminated by adding cold hexane (20 mL). The precipitated polymer was

isolated by decantation and dried under vacuum (52 mg, 54% yield). ^{1}H NMR (400 MHz, $CDCl_3$) δ: 4.7-3.9 (bm, -CC*H*$_2$N-, -NC*H*$_2$CO-, -NC*H*$_2$CO, 6H), 3.4 (bm, -CH$_2$C*H*$_2$N-, 2H); 2.3 (bm, -CC*H*, 1H), 1.5 (bm, -CH$_2$C*H*$_2$CH$_2$-, 2H), 1.3 (bm, CH$_3$C*H*$_2$-, 2H), 1.0 (bm, C*H*$_3$CH$_2$-, 3H).

Brush Polymer Synthesis 2.5.4

Representative synthetic procedure for the cyclic PEG-grafted poly(*N*-propargyl-glycine) (*c*-PNPG-*g*-PEG). Inside a glovebox, *c*-PNPG$_{137}$ (85.5 mg, [propargyl]$_0$=0.87 mmol, M_n=13.4 kg·mol^{-1}, PDI=1.16) was dissolved in CH_2Cl_2 (3 mL) along with PEG-N_3 (288 mg, 0.14 mmol, M_n =2.0 kg·mol^{-1}, PDI=1.03, [N_3]$_0$:[propargyl]$_0$=1:6). A measured volume of CH_2Cl_2 stock solution containing CuBr/PMDETA (1.70 mL, 0.202 mmol, 119 mM, [CuBr]$_0$:[PMDETA]$_0$:[propargyl]$_0$=23:23:100) was added to the solution which was then stirred at room temperature for 3 h. The copper catalyst was removed by passing through an alumina column, and the grafted copolymer was precipitated by adding an excess of hexane and dried under vacuum at 25 °C (165 mg, 44% yield). ^{1}H NMR (400 MHz, $CDCl_3$) δ: 8.01 (bs, -NC=C*H*N-), 4.49 (bm, -NC*H*$_2$CO-, CC*H*$_2$N-), 3.61 (bm, -C*H*$_2$C*H*$_2$O-), 3.35 (bs, -CC*H*).

Representative synthetic procedure for the cyclic PEG-grafted poly(*N*-propargyl-glycine)-*ran*-poly(*N*-butyl-glycine) random copolymers [(*c*-PNPG-*r*-PNBG)-g-PEG]. Inside a glovebox, *c*-PNPG$_{166}$-*r*-PNBG$_{33}$ (72.8 mg, [propargyl]$_0$=0.62 mmol) and PEG-N_3 (465 mg, 0.85 mmol, M_n = 550 g·mol^{-1}, PDI=1.05, [N_3]$_0$:[propargyl]$_0$=1.4:1) were both dissolved in CH_2Cl_2 (5 mL). A measured volume of CH_2Cl_2 stock solution containing CuBr/PMDETA (1.70 mL, 0.202 mmol, 119 mM, [Cu]$_0$:[PMDETA]$_0$:[propargyl]$_0$=33:33:100) was added to the solution which was then stirred at 40°C for 3 h. The reaction mixture was then passed through a silica column. The filtrate was concentrated and cold hexane was added to precipitate the polymer (172 mg, 42% yield). ^{1}H NMR (400 MHz, $CDCl_3$) δ: 8.0 (bs, -NC=C*H*N-), 4.3 (bm, -NC*H*$_2$CO-, CC*H*$_2$N-,

-NCH_2CO-), 3.4 (bm, -CH_2CH_2O-, -CH$_2$CH_2N-), 2.3 (bm, -CCH), 1.4 (-CH$_2$CH_2CH$_2$-), 1.3 (bm, CH$_3$CH_2-), 1.0 (bm, CH_3CH$_2$-).

Representative synthetic procedure for linear PEG-grafted poly(*N*-propargyl-glycine)-*ran*-poly(*N*-butyl-glycine) random copolymers [(*l*-PNPG-*ran*-PNBG)-*g*-PEG]. Inside a glovebox, *l*-PNPG$_{250}$-*r*-PNBG$_{50}$ (17.0 mg, [propargyl]$_0$= 0.14 mmol) and PEG-N$_3$ (201 mg, 0.37 mmol, M_n = 550 g·mol^{-1}, PDI= 1.05, [N$_3$]$_0$:[propargyl]$_0$=2.6:1) were both dissolved in CH$_2$Cl$_2$ (1 mL). A measured volume of CH$_2$Cl$_2$ stock solution containing CuBr/PMDETA (388 μL, 46 mmol, 119 mM, [Cu]$_0$:[PMDETA]$_0$:[propargyl]$_0$=33:33:100) was added to the solution which was stirred at 40^{o}C for 3 h. The reaction mixture was passed through a silica column. The collected filtrate was concentrated and cold hexane was added to precipitate the polymer (54 mg, 57% yield). ^{1}H NMR (400MHz, CDCl$_3$) δ: 8.0 (bs, -NC=CHN-); 4.3 (bm, -NCH_2CO-, CCH_2N-, -NCH_2CO-), 3.4 (bm, -CH_2CH_2O-, -CH$_2$CH_2N-), 2.3 (bm, -CCH), 1.4 (-CH$_2$CH_2CH$_2$-), 1.3 (bm, CH$_3$CH_2-), 1.0 (bm, CH_3CH$_2$-).

Chapter 3. Comparison of Linear and Cyclic Thermoresponsive Copolypeptoids

3.1 Objectives and First Observations

The following chapter contains research related to water-soluble polypeptoids and their associated temperature induced phase changes. The observation that polysarcosine (PNMG) was soluble in water but the similar poly(butyl-glycine) lacked solubility in an aqueous solution was the basis for this research. The difference between these similar polypeptoids is the number of carbons attached to the side chain of each repeat unit, and as the number of carbons increased, it appeared the solubility of the polymer in water decreased. By incorporating water-soluble chains alongside longer water-insoluble chains (copolymerizations), the first thermoresponsive polypeptoids were envisioned. It was the objective of this research to exploit the potential for the thermoresponsive characteristics of water soluble polypeptoids. However, this research was not restricted to the synthesis of thermoresponsive polypeptoids. With the ability to change the topology of the polymer (from cyclic-to-linear) by the use of different initiators, it was also shown that the architecture of the polymer affects the thermoresponsive characteristics of the system.

This chapter will encompass all research performed in the area of thermoresponsive polypeptoids. The chapter will begin with a brief explanation of how some polymers can exhibit thermoresponsive characteristics, and then rationalize the usefulness of these polymers. Several common thermoresponsive polymers will then be highlighted, followed by a detailed description of the thermoresponsive polypeptoids, again starting from monomer synthesis and finishing with the end-polymeric product. Lastly, biological compatibility and cell imaging of these water-soluble polypeptoids will be presented.

3.2 Thermoresponsive Polymeric Systems

A stimuli-responsive polymer is any polymer that undergoes some sort of physical change in the presence of an external stimulus. By controlling the polymer structure, specific responses can be expected and creating smart materials.[126] Some of the common external stimuli that are used to trigger these responses are changes in pH[127], ionic strength[128], light[129] and temperature.[130] A typical response from a polymer to external stimuli is a coil-to-globule transformation.[131-133] For many biological applications of these smart materials, changes in pH and temperature are of often the triggers used to induce these physical changes in the polymer due to their prevalence within the human body (i.e. different organs and organelles have different pH's and temperatures). The ability to precisely control when the response happens in the smart material (at a certain temperature or pH) is important for these stimuli responsive materials' practical use.

Thermoresponsive polymers undergo a physical change when there is either a decrease or increase in temperature. For example, polymer solubility may change in a specific solvent at certain temperatures. These changes are mainly driven by unfavorable entropy of mixing.[29, 134] Though this phenomenon can be applied to polymers in any solvent, for the purpose of this research, water (which is most relevant to biological applications) will be the selected solvent.

Thermoresponsive polymers can be classified into two main categories, polymers that can either exhibit a lower critical solution temperature (LSCT) or exhibit an upper critical solution temperature (UCST). The LCST and USCT are the temperatures above and below at which the polymer is fully miscible with the solvent.[29] Some aqueous polymeric systems exhibit both LCSTs and UCSTs (See **Figure 3.1**). It is worth noting that the LCST is entropically[135] driven

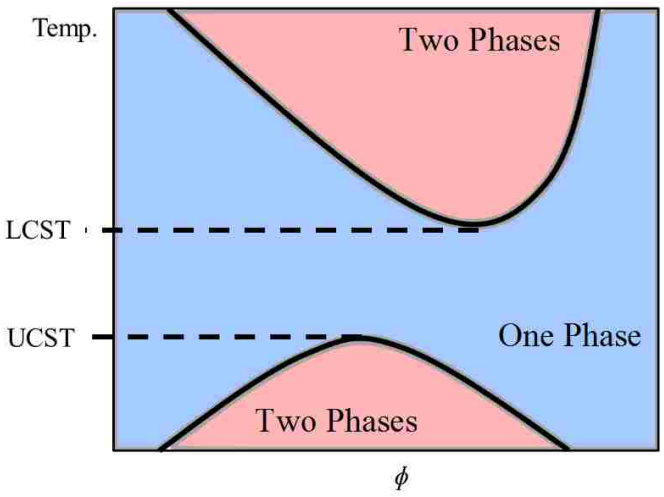

Figure 3.1. Plot of temperature against polymer volume fraction (ϕ). Theoretical phase diagram for a polymer solution that exhibits both UCST and LCST behavior.

while the UCST is enthalpically driven.[134] The research presented in this chapter will focus on the LCST behavior of thermoresponsive polymers.

For polymeric solutions that have an LCST, below the critical temperature the polymer is fully miscible with water and the sample is homogeneous; however, above the LCST, the polymer solution is heterogeneous and appears cloudy (See **Figure 3.2**). The driving force for this physical change is the entropy of the system. When the polymer is fully hydrated (below LSCT), the water molecules are 'locked' into position surrounding the larger polymer due to hydrogen bonding interactions, and the polymer adopts a random-coil conformation.[136] When there is enough energy to break apart the hydrogen bonds between the polymer and the water molecules (increasing the temperature), the entire systems adopts are more energetically favorable state.[136] This more energetically favorable system is entropically driven because the water molecules have increased translation motion in their unbound state (i.e. $\Delta S_{mix} > 0$).[135, 137] The Gibbs free energy equation, $\Delta G_{mix} = \Delta H_{mix} - T\Delta S_{mix}$, establishes the relationship between entropy and the energy of the system. Though the ΔH_{mix} can be measured during this phase

change,[84] the change in entropy (ΔS_{mix}) is considered to be the major contributor for LCST behavior. At temperatures below the LCST, the ΔG_{mix} of the solvent/polymer system is negative, resulting in the dissolution of the polymer.[138] Below the LCST, interactions between the solvent and polymer molecules (hydrogen bonding) are spontaneous and favored. Increasing the temperature above the LCST disrupts these interactions, resulting in the two component system. This heterogeneous solution is a consequence of having a positive ΔG_{mix}. The entire process of de-mixing is nonspontaneous and requires energy, in the form of heat. At a temperature above the LCST, the dehydrated polymer tends to collapse, adopting a globule conformation.

Figure 3.2. Solution of cyclic-poly(N-ethyl$_{55}$-ran-N-butyl$_{26}$ glycine) in water at 7 mg·mL^{-1} at temperatures below (a) and above (b) the cloud point temperature of polymeric sample.

The globular conformation adopted by the polymer at temperatures above the LCST tends to aggregate with other globules, eventually turning the solution cloudy or turbid and giving rise to the term cloud point temperature (T_{cp}).[139] There is a distinction between the LCST and T_{cp}. The difference between the two is that the LCST is the lowest temperature on the phase transition curve at which the polymer solution goes from single to bi-phase (**Figure 3.1**).[29] The T_{cp} is the temperature at which the system begins to have a phase change at any polymer volume

fraction. Thermoreponsive polymer have LCST-like behavior, but until all volume fractions of that polymer in solvent have been tested, the LCST is unknown. The T_{cp} is the response at an individual volume fraction while the LCST represents the entire system at all volume fractions.

There are several methods to experimentally determine T_{cp}'s and LCSTs. A common process measures of the turbidity of the solution as the temperature is increased. Either a turbidometer, or more commonly, either an optical microscope or a UV-vis detector can be used to measure the turbidity of the solution.[140] If equipped to record transmittance (for example a photomonitor), an optical microscope can be used directly to measure the cloud point transition of a polymeric solution. The UV-vis detector records the absorbance of the solution at a certain temperature and wavelength, which translates into transmittance. As the temperature is increased, the solution becomes cloudier and the light from the UV-vis is being scattered. The detector recognizes this scattering as absorbance, though it is not. The UV-vis method of measuring turbidity is a quick and simple method of determining when the polymeric solution begins to scatter (aggregate formation). When performing turbidity measurements with a UV-vis, it is important to know if the polymer or the solvent absorbs (or fluoresces) light, and if so, at which wavelengths. It is common to choose a wavelength large enough to avoid these polymeric or solvent absorbances, and this is why it is typical to use wavelengths at 450-500 nanometers.[141, 142] After collecting data at many temperatures, these 'absorbances' can be plotted as transmittance through the Beer-Lambert law (**Equation 3.1**),[143] where I_0 and I are the intensity of the incident and transmitted light respectively and A is absorbance.

Equation 3.1 $$A = -log_{10}(\frac{I}{I_0})$$

The ratio of transmitted light to the incident light is the transmittance. By multiplying the transmittance by 100, the percent transmittance can be obtained and plotted (**Figure 3.3**). The temperature at 50% transmittance is assumed to be the cloud point temperature (T_{cp}).[144, 145] When performing cloud point measurements for different polymer samples, the transmittances are normalized because different polymer volume fractions tend to vary in their scattering intensities. Since the UV-vis cannot measure the intensity of the scattered light, normalization is necessary to compare different samples.

Other methods of T_{cp} determination include multi angle static light scattering (MALS)[146] and microdifferential scanning calorimetry (mDSC).[147] Using MALS allows the determination

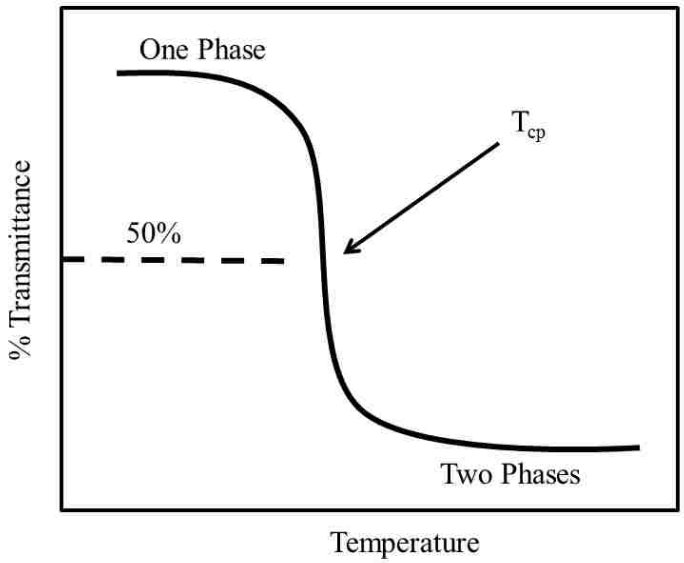

Figure 3.3. Plot of temperature against percent transmittance for a theoretical polymer that has LCST behavior. The temperature at 50 percent transmittance is considered to be the cloud point temperature (T_{cp}).

of the size of the globules and the aggregates being formed during these physical transitions.[85, 146] Before the T_{cp}, the particle size is small; however above the T_{cp}, these particles will aggregate and grow larger. Using MALS, the temperature at which particles begin to grow in size is the

T_{cp}.[146] Dilute samples can only be measured using MALS because the multiple scattering (scattering from more than one particle) becomes an issue. mDSC helps in the understanding of the enthalpic changes associated with the this conformational change.[147] These slight variations in the energies are determined using mDSC, and the temperature at the maximum endotherm (T_M) exhists is presumed to be closely related to the T_{cp}.[84] Unlike MALS, mDSC needs concentrated samples, as too dilute of a sample will not have a measurable change in enthalpy. Though these two methods (mDSC and MALS) describe interesting and important physical characteristics of the thermoresponsive system, UV-vis and optical miscroscopy are easier for T_{cp} determination due to simpler sample preparation.

3.3 Thermoresponsive Random Copolymers

There are several methods of influencing the thermally induced transition of polymers that include changing the polymer functionality, end-group, architecture and microstructure, but a common method is through the synthesis of a copolymer. There are several types of copolymers that exhibit thermally controlled responses which include star copolymers,[148] brush copolymers,[149] block copolymers[150] and random copolymers.[151] Random copolymers allow for control over the copolymer's physical transition. Using the one-pot method of copolymerization, two or more monomers that varying in their hydrophobicity, are co-initiated to make a random copolymer (depending on the reactivity ratios of the monomers determines whether the copolymer is considered to be random).[152] Many different polymerization techniques such as free-radical polymerization, atom transfer radical polymerization (ATRP) and reversible addition-fragmentation polymerization (RAFT) have been used to synthesize these thermoresponsive copolymers.[151]

3.3.1 Reactivity Ratios

Any discussion of random copolymers would be incomplete without reference to reactivity ratios of the monomer/initiator systems. During the course of any chain growth copolymerization, four distinctly different propagation mechanisms can take place when two monomers are in the reaction system (**Scheme 3.1**). Each of these distinct propagation reactions can be characterized by a propagation rate constant, k. The first subscript in this rate constant denotes the terminal repeat unit in the growing chain end while the second subscript identifies the next added monomer.

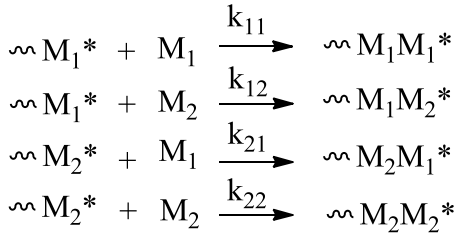

Scheme 3.1. Propagation mechansims of a two monomer system.

It is assumed that these rate constants are independent of the size of the propagating center, and thus the nature of the chain end (i.e., the terminal repeat unit) influences the rate constant of propagation. This phenomenon is commonly referred to as the *terminal control mechanism.*[29] The magnitudes of these rate constants help describe the various modes of addition that can take place during a copolymerization, and thus there are four different rate law equations to describe these modes of addition.

Assuming that the steady-state approximation is applicable to chain-growth copolymerizations, the total concentration of propagating chain ends is constant, meaning that the rate of crossover between the different types of terminal units is also equal throughout the copolymerization ($R_{p,12} = R_{p,21}$).[29] Though there are four different rate constants, *k*'s, there is an

$$R_{p,11} = k_{11}[M_1^*][M_1]$$
$$R_{p,12} = k_{12}[M_1^*][M_2]$$
$$R_{p,21} = k_{21}[M_2^*][M_1]$$
$$R_{p,22} = k_{22}[M_2^*][M_2]$$

Scheme 3.2. Propagation rates and rate constants for a two monomer copolymerization

equation which combines them, the copolymer composition equation or the Mayo-Lewis equation.[153]

Equation 3.2
$$\frac{d[M_1]/dt}{d[M_2]/dt} = \frac{[M_1]}{[M_2]} \frac{(k_{11}/k_{12})[M_1]+[M_2]}{(k_{22}/k_{21})[M_2]+[M_1]}$$

Equation 3.2 can be used to decipher the relative amounts of each monomer that has been incorporated into the polymer. The ratios of two of the rate constants within **Equation 3.2** can be further simplified to give more straightforward notations,

Equation 3.3
$$r_1 = \frac{k_{11}}{k_{12}} \qquad r_2 = \frac{k_{22}}{k_{21}}$$

r_1 and r_2 are known as the reactivity ratios of a copolymerization, and are the ratios of the rate constant for each growing polymer chain with a certain terminal repeat unit. These ratios help to define the probability of the ensuing monomeric unit to be added to the growing polymer chain. For many copolymerizations, several limiting cases can be distinctly described by these reactivity ratios:[29]

• $r_1 >> 1$, $r_2 >> 1$ neither of the growing polymer chains tend to add the opposite monomer and thus leading to a mixture of homopolymers

• $r_1 = r_2 > 1$ with both ratios larger than one, homopolymerization is favored; however crossover between terminal chain repeat units can happen which usually gives rise to block copolymers.

• $r_1 = r_2 \approx 1$ where both ratios are near one and the terminal repeat unit has equal reactivity to both monomers in the system giving rise to a random copolymer.

• $r_1 = r_2 \approx 0$ with both ratios near zero, the terminal repeat unit prefers to add the opposite monomer to growing chain end and thus giving rise to an alternating copolymer.

• $r_1 >> 1 >> r_2$ with the ratio of r_1 is much larger than one and the ratio of r_2 is much lower than one, the growing polymer chain will preferentially consume monomer 1 faster than monomer 2, giving rise to a gradient copolymer.

It is often convenient to describe the composition of the copolymer (F_i) and the feedstock (initial monomer ratios, f_i) in terms of the mole fraction of each monomer. Using these notations allows for determination of the reactivity ratios to be performed experimentally since the monomer feedstock can be controlled. The following equations numerically describe F and f.

Equation 3.4 $$F_1 = 1 - F_2 = \frac{d[M_1]/dt}{[M_1]/dt + [M_2]/dt}$$

Equation 3.5 $$f_1 = 1 - f_2 = \frac{[M_1]}{[M_1]+[M_2]}$$

To examine copolymerization rate constants (reactivity ratios), one must perform a number of copolymerization experiments while varying the ratios of the two monomers in solution (the monomer feedstock, f_i), and the copolymer composition, F_i, is measured at low monomer conversion. F_i needs to be measured at low conversion because as the conversion increases throughout the reaction, the composition of the solution is changing and the feedstock ratio is no longer a constant.[153] Usually the copolymer composition is measured at monomer

conversions less than 20%. Using the Mayo Lewis equation, it is common to plot the copolymer composition against the monomer feedstock, and the reactivity ratios can be obtained graphically from the initial and final slopes of this plot (See **Figure 3.4**).

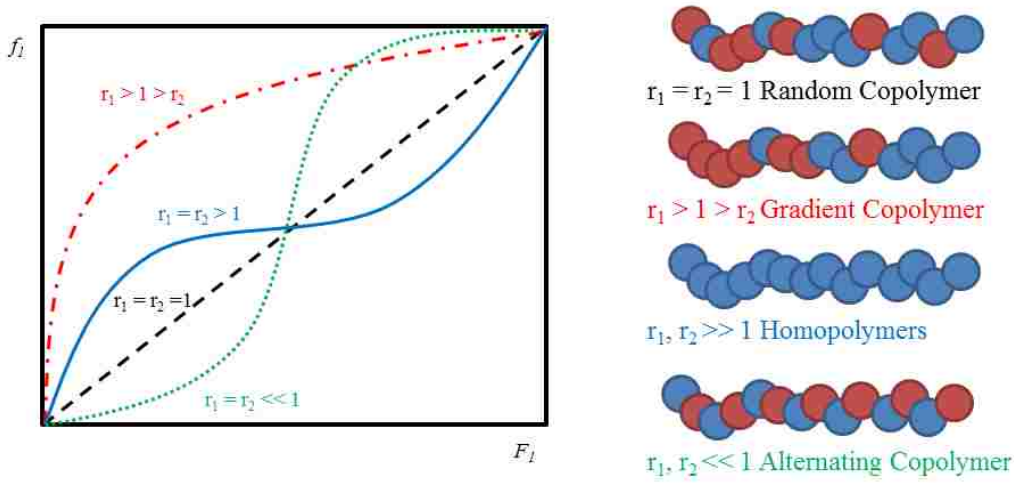

Figure 3.4. Plot of copolymer composition versus monomer feedstock with varying the reactivity ratios for theoretical monomers 1 and 2 (blue and red respectively).

In 1949, Fineman and Ross mathematically found a simpler technique for obtaining the reactivity ratios with the same experimentation needed for the Mayo Lewis method.[154] At low monomer conversions, Fineman and Ross found that,

Equation 3.6 $$F_1 = \frac{d[M_1]}{d[M_2]} \text{ and } f_1 = \frac{[M_1]}{[M_2]}$$

in doing so, they could rewrite the Mayo Lewis equation into

Equation 3.7 $$f = F\,\frac{r_1 F+1}{r_2+1}$$

which can be rearranged into the form most typically called the Fineman-Ross equation,

Equation 3.8 $$\frac{F}{f}(f-1) = r_1\frac{F^2}{f} - r_2$$

Once the copolymer composition has been determined through experimentation, the data can be plotted with (F_2/f) and (F/f)(f-1) as the x- and y-axis respectively, giving a straight line. The

slope of this line is r_1 and the intercept is r_2, which is a convenient graphical method of determining the reactivity ratios. The sequence structure (placement of the repeat units along the copolymer backbone) governs the thermoresponsive characteristics of the copolymer in solution.

3.3.2 Synthetic Strategies of Random Copolymers.

Several of the typical thermoresponive polymers such as PNIPAAm,[155] poly vinyl ethers[156] and polyethylene oxides[157] have been used in copolymerization techniques to tune their LCST/T_{cp} temperatures. It has been shown that as the hydrophilic monomer content within the copolymer is increased, the T_{cp} of the copolymer increases.[151, 156, 158] Chung et al were able to show that when poly(N-isopropylacrylamide) was copolymerized with a more hydrophilic monomer, such as acrylic acid or dimethyacrylamide, the LCST was raised nearly 20 ^{o}C.[155] Copoly (alkyl-2-oxazolines), which are structurally similar PNIPAAm, have been synthesized at certain monomer ratios that exhibit LCST behavior at temperatures between 9^{o}C to 46^{o}C.[159] Different types of methacrylates were copolymerized and showed that the size of the macromolecule (degrees of polymerization) did not affect the LCST of the copolymer.[160] This is different from homopolymer with LCST behavior, where increasing the molecular weight of the polymer usually decreases the LCST.[145, 160]

Savoji et al combined the idea of block and random copolymers to produce a system that exhibits two phase changes.[161] By copolymerizing N-n-propyl and N-ethl acrylamides via RAFT polymerization, they were able to tune the T_{cp} of random copolymers by controlling the amount of the more hydrophobic monomer in the polymeric chain. Since RAFT is considered to be a 'living' polymerization, block copolymers were synthesized where each block consisted of a random copolymer of certain hydrophobic content, and thus each block had its unique T_{cp}.[161]

DLS was used to show the stepwise aggregation properties of these random-block-copolymers in aqueous solution.

3.4 Applications for Thermoresponsive Polymers

The ability to tailor a certain material to have a physical change at particular temperatures is advantageous throughout fields such as materials science, biology and pharmokinetics.[127, 136, 162, 163] The following section will not only address specific cases where thermoresponsive polymers have played a contributing factor in the science, but put 'names to the faces' to some of the common polymers that are being used.

As the term suggests, drug delivery is the method of administering a molecule to a certain location within the body to achieve a therapeutic effect. There are many factors that contribute to this delivery mechanism: time and location of the drug's release, concentration and solubility of the drug being released, enzymatic degradability of the drug vehicle (usually a polymer), and many other obstacles.[127] Several smart polymers are being used to carry these drugs throughout the body, and one of the most common polymer is poly(N-isopropylacrylamide) (PNIPAAm). PNIPAAm has an LCST at 32^{o}C, which is a very useful temperature since it is close to body temperature (37^{o}C).

The literature is abundant with uses of PNIPAAm in a drug carrier system. PNIPAAm has been used in gene therapy during transfection.[164, 165] The ability to change the temperature during complexation and transfection is instrumental in enhancing the transfection efficiency.[166] Zhou et al used block star copolymers of PNIPAAm to complex the DNA to the polymer below LCST, but deposit the complex on the cell surface above the LCST.[167] This resulted in an increase in transfection to the cells. Another method of entrapping DNA, or any drug for that

matter, is micellization. The literature is vast with the use of PNIPAAm as a copolymer in the formation of micelles.[150]

PNIPAAm has also been used in hydrogel formulations. A hydrogel is a three-dimensional polymeric network that can be dispersed in water to form a semi solid state.[168] The amount of water the hydrogel can absorb depends on the type of hydrogel being synthesized (covalent or physical).[169] PNIPAAm's coil-to-globule transition at nearly body temperature makes this type of thermoresponsive hydrogel ideal for an *in situ* response to temperature as an implantation device within the body. It has been shown that when copolymerized with butyl methacrylate, a PNIPAAm thermoresponsive hydrogel can help control the rapid or a sustained release of an entrapped drug due to the temperature of the solution.[170] PNIPAAm has also been used in conjuction with poly(styrene sulfonic acid sodium salt) to make a semi-interpenetrating polymer network.[171] This interpenetrating polymeric system differs from some of other hydrogels in that it does not restore to its original volume when it reswells after shrinking, a phenomenon attributed to the charged polyelectrolyte fraction.

3.5 Thermoresponive Behavior of Polypeptoids

It has been well documented that poly(N-methyl glycine), or polysarcosine, is a water soluble polypeptoid.[2] It has been used to make hydrophobic systems water soluble.[172-174] Due to the small alkyl side chain ($-CH_3$), the nitrogen on the backbone can readily hydrogen bond with water molecules and thus add to the hydrophilicity. No known LCST behavior accompanies the polysarcosine homopolymer. It has also been reported that the poly(N-ethyl glycine)[38] and poly(N-allyl-glycine)[83] are both water soluble and the later was recently shown to exhibit LCST behavior. A study describing the ability to perform post polymerization modifications to the

poly(N-allyl glycine) through thiol/ene chemistry also reported the homopolymer's thermoresponsive behavior (though this report was published after this research).[83]

Though these homopolypeptoids are water soluble, there are no known studies reporting the LCST-like behavior for the methyl- and ethyl-substituted peptoids. By combining the water soluble NCA monomers (methyl- and ethyl-NCAs) with the water insoluble NCA monomer (butyl-NCA), the thermoresponsive behavior of the copolymers can be observed.

3.6 Results and Discussion

This section of the chapter will encompass monomer synthesis, copolymerization techniques, copolymerization kinetics, a review of the Hofmeister salt series and a comparison of thermal response of cyclic and linear copolypeptoids. All experimental procedures and selected characterization data is located in the last section of this chapter.

3.6.1 Monomer Synthesis

To synthesize a copolymer with a tunable T_{cp}, the amphiphlicity of the copolymer should be controlled. To control this, copolympeptoids were made by combining R-NCA monomers whose homopolymers varied in their solubility in water. Three different monomers were synthesized for this project, N-methly, –ethyl-NCA and -butyl-NCA. The homopolymers made from the N–methyl and N–ethyl NCA are water soluble, while the homopolymer from the N-butyl-NCA is not. Homopolymers of both N-methly- and N-ethyl-NCAs did not appear to have LCST behavior within the instrumental limits. However, copolymerizations with N-butyl-NCA, cloud point temperatures were observed and depended on the molar amount of the hydrophobic portion incorporated into the polymer.

The three R-NCA monomers were synthesized via the Füch method. This method allows for the synthesis of a variety of R-NCAs baring different side chains which govern the solubility of the polymerized product. The experimental procedures and characterizations of these monomers are at the end of this chapter, **3.7 Synthetic Procedures** (**Figures 3.31** and **3.32**).

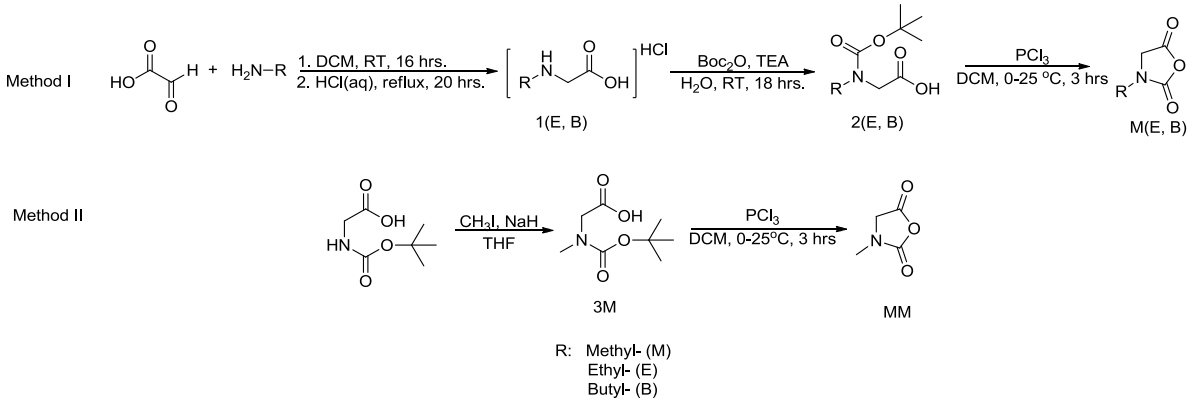

Scheme 3.3. Synthetic strategies for N-methyl (MM), -ethyl (ME) and –butyl (MB) NCA monomers.

3.6.2 Copolymerizations of MM/ME and MB

All of the copolymerizations were executed using the one-pot synthetic method. In this method, two or more monomers are dissolved in a common solvent (either THF or toluene) and an initiator is added which initiates the copolymerizaton of the monomers. The initiator used (primary amine or NHC) dictates the topology of the copolymer (i.e. linear or cyclic copolymer). The polymerization of R-NCAs using a primary amine produces linear polymers. The end group of these poly-N-substituted glycines is dictated by the type of primary amine used as the initiator. For example, a benzyl-amine initiated polymerization of NCA monomers will bear a benzyl end group of the linear polypeptoid (See Figure MALDI-TOF Benzylamine). As previously discussed (**Chapter 1.3.3**), the N-heterocyclic carbene (NHC) tends to produce cyclic polymers when an R-NCA is used as the monomer. The readily accessible topologies produced by these initiators enable the comparison of architecture effects on the T_{cp}.

The section that covers the experimental procedures is at the end of this chapter (**3.7 Synthetic Procedures**), the following sections will discuss the copolymerizations and the characterizations of the copolypeptoids. Afterwhich, the reactivity ratios of the monomers with different initiators will be discussed in detail.

3.6.2.1 Synthesis of P(NMG-r-NBG)

During the synthesis of these copolypeptoids, it was observed that the solubility of these copolymers greatly varied in different organic solvents. The butyl-glycine homopolymer has been shown to undergo a NHC-controlled polymerization in organic solvents such as toluene and tetrahydrofuran, solvents that are not amenable to methyl-NCA homopolymerizations (PNMG will precipitate from solution in these organics).[44] It was found that acetonitrile was the best solvent for both monomers. The high molecular weight PNMG (DPn > 50) was not soluble in acetonitrile. This made control over the copolymerizations of N-methyl- and -butyl-NCAs very difficult, and thus the ability to design and tailor the phase transition characteristics was compromised due to poor control of the copolymer composition. The SEC-DRI traces of different copolymers with the same M:I ratio indicates the lack of molecular weight control of these copolymers (**Figure 3.5**).

The lack of control of the copolymer composition of the P(NMG-r-NBG) copolymer was evident when recording differences in the T_{cp} of the linear and cyclic copolypeptoids (See **Figure 3.14**). The T_{cp}s of these copolymers and the differences between topologies were inconsistent. It was assumed that the problems associated with the copolymerizations arose from the solubility of the poly-N-methyl glycine portion of the copolypeptoid. To circumvent this problem, N-ethyl-NCA was used in place of the N-methyl-NCA.

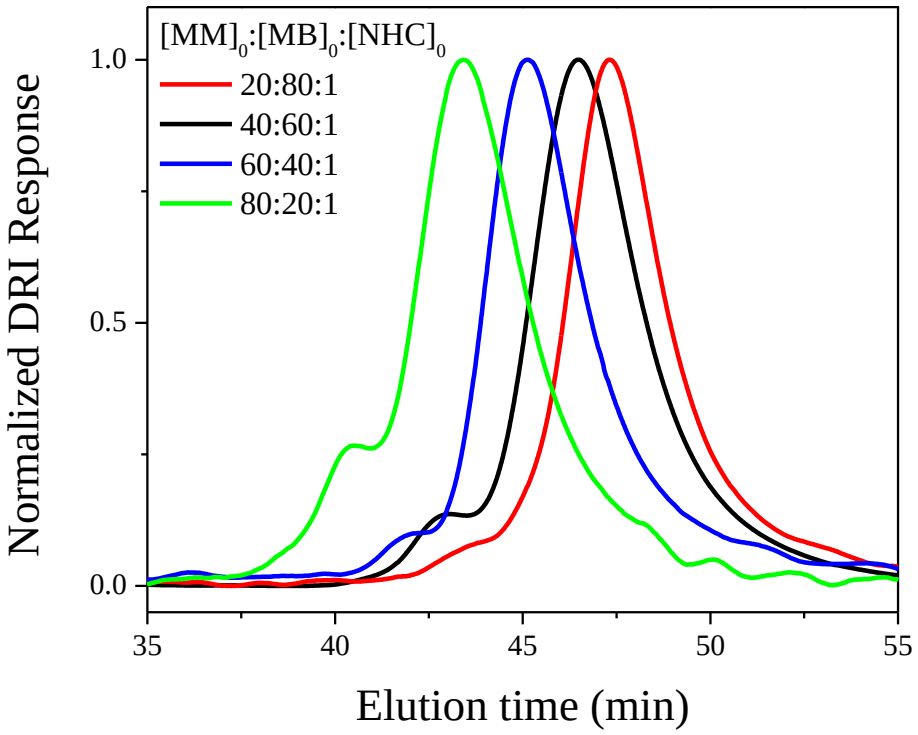

Figure 3.5. GPC-DRI traces of different initial NCA monomer to initiator loadings ($[MM]_0$:$[MB]_0$:$[NHC]_0$).

3.6.2.2 Synthesis of P(NEG-r-NBG)

N-ethyl-NCA was used as a replacement for the N-methyl-NCA in these copolymerizations because the homopolymer of N-ethyl-NCA is water soluble, and many of the problems associated solubility during the copolymerization of this monomer are alleviated. While high molecular weight poly-N-ethyl-glycine (PNEG) has low solubility in organic solvents such as toluene, when copolymerized with N-butyl-NCA, the copolymer remains soluble throughout the polymerization. This improvement allowed for a higher degree of control of the copolypeptoid composition, which is reflected in the ^{1}H NMR (**FIGURE 3.34** and **TABLE 3.1**) and the T_{cp} data. Comparing the architectural effects on the T_{cp} of the copolypeptoids was achieved by the use of different initiators (primary amine and NHC).

However, these initiators are known to propagate through different species, a consequence that effects the microstructure (repeat unit sequence) of the copolymer. To investigate the differences in the microstructures of each initiated system, reactivity ratios were measured using the conversions of each monomer as determined by ^{1}H NMR.

3.6.2.2 Determination of the reactivity ratios for NHC-mediated copolymerization of ME and MB.

Kinetic studies were conducted for the NHC-mediated copolymerization of ME and MB with different initial monomer feed ratios (i.e., $[ME]_0$:$[MB]_0$ = 80:20, 62:38, 40:60, 44:56, 21:79). Specifically, a predetermined amount of NHC/toluene-d_8 stock solution was added to a toluene-d_8 solution of ME and MB at room temperature. The reaction mixture was transferred into a resealable J. Young NMR tube. ^{1}H NMR spectra were collected automatically every 2.7 min at 50°C for two to four half-lives. The monomer conversion was calculated from the relative integration of the methyl proton resonances of each monomer, ME and MB, and its corresponding polymeric methyl proton resonance (**Figure 3.6**). At the time for the first spectrum collection, approximately 0.5-20% monomer has been converted to the polymer. The polymerization rate constants (k_{obs}) were determined from the $\ln([M]_0/[M])$ plots for both monomers, which were used to calculate the polymer composition at 25% monomer conversion (**Figure 3.7**). Determination of reactivity ratio at low conversions can be affected by the different reactivity of initiators towards a specific monomer.[175] As a result, we chose a slightly higher conversion to calculate the polymer composition. The reactivity ratios were determined by the Fineman-Ross method using these polymer compositions and the initial monomer feed ratios (**Figure3.8**).[154]

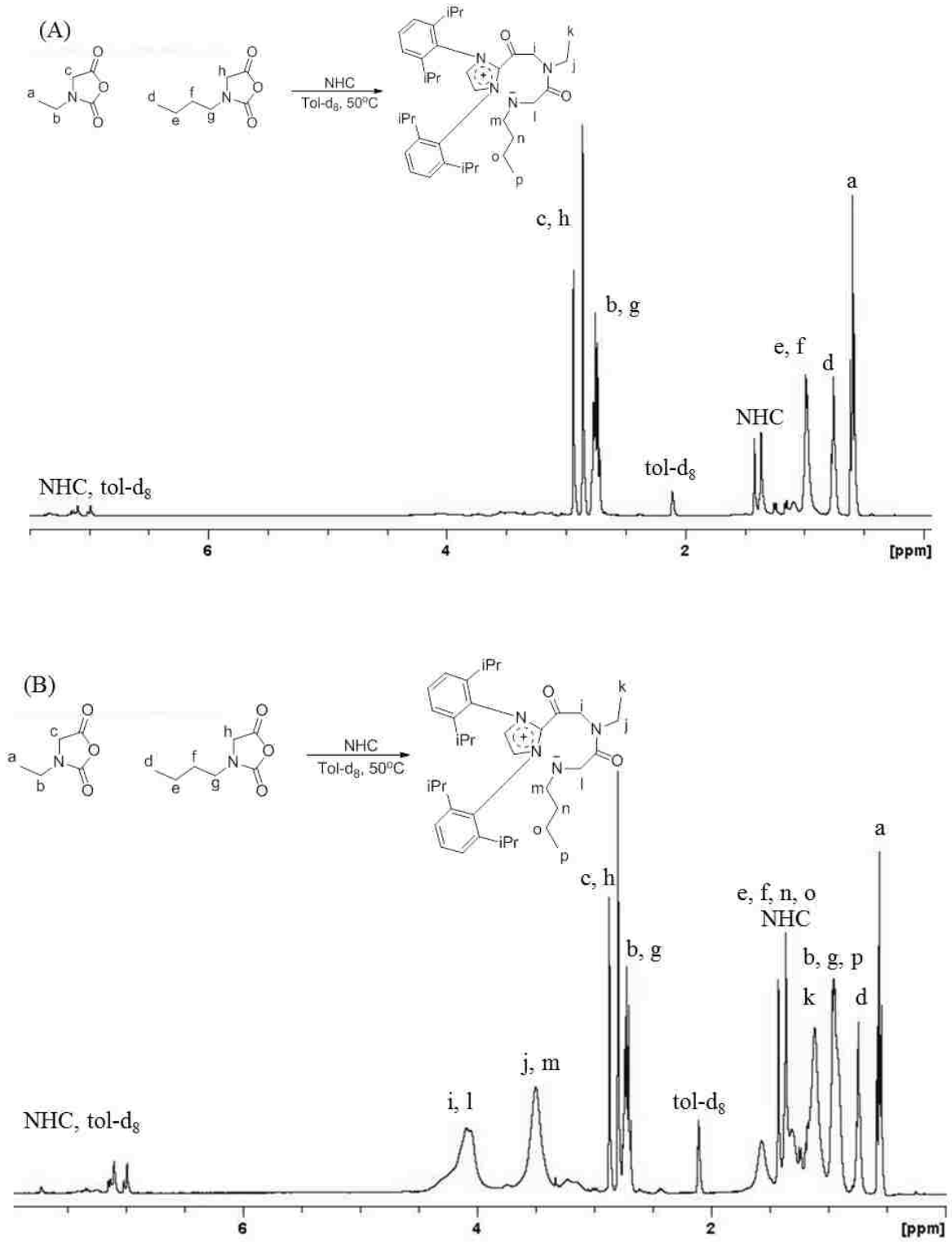

Figure 3.6. ^{1}H NMR of copolymerization of ethyl- and butyl-NCAs using NHC at monomer conversions of 0% (A), 47% (B) and 89% (C).

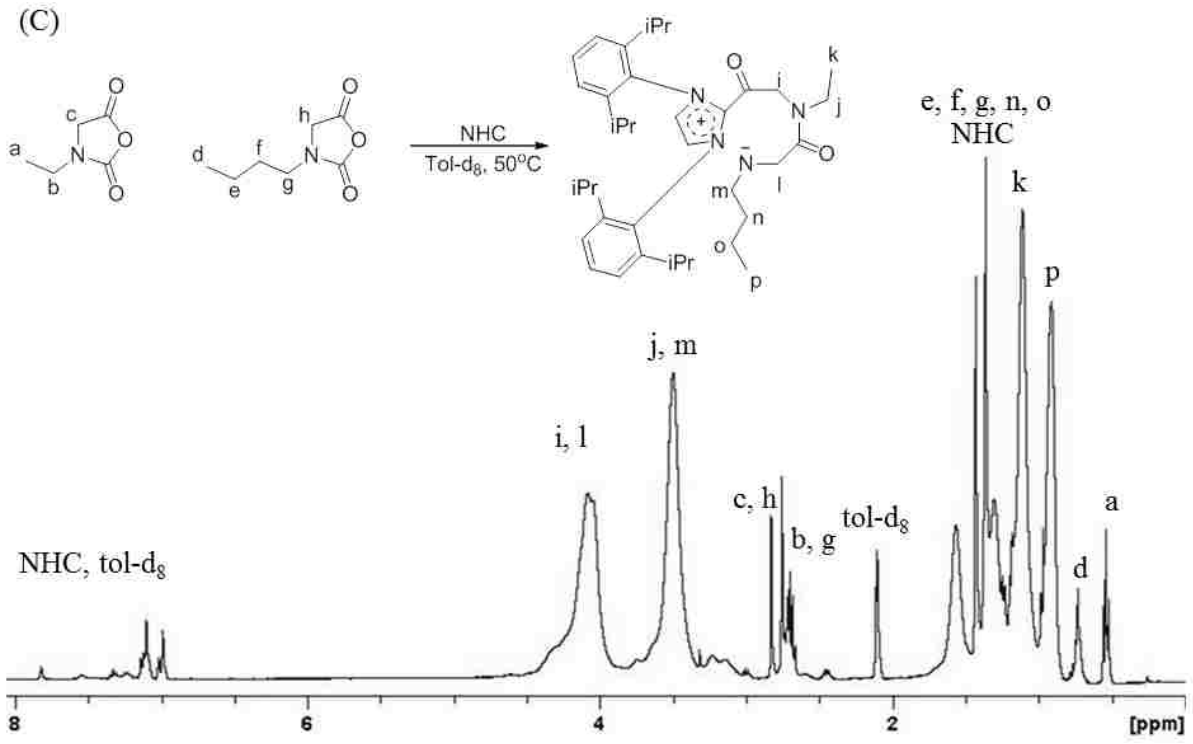

Figure 3.6 continued

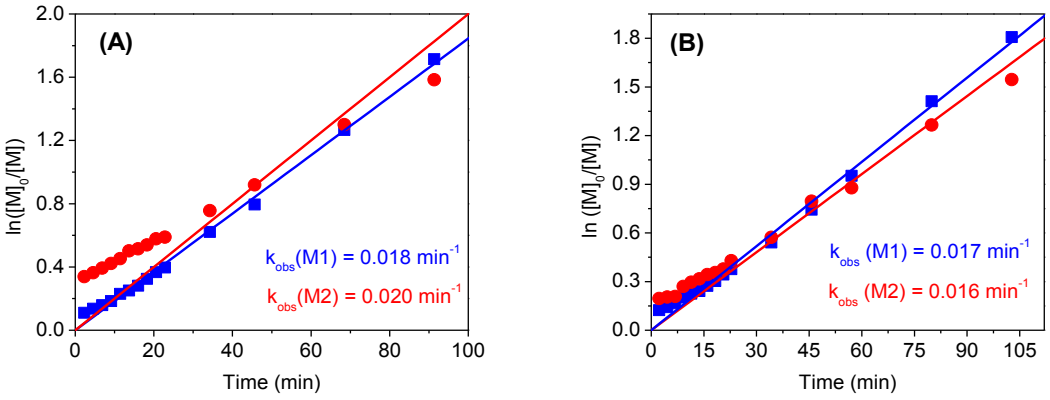

Figure 3.7. Plots of ln([M]$_0$/[M]) versus time for the NHC-mediated copolymerization of ethyl-NCA (■) and butyl-NCA (●) in toluene-d$_8$ at 50°C where the initial monomer feed ratio was varied [(**A**) [ME]$_0$:[MB]$_0$= 80:20; (**B**) [ME]$_0$:[MB]$_0$= 62:38; (**C**) [ME]$_0$:[MB]$_0$= 44:56; (**D**) [ME]$_0$:[MB]$_0$= 40:60; (**E**) [ME]$_0$:[MB]$_0$= 21:79] and their linearly fitted curves [ME(—); MB(—)] whose slopes are the k_{obs}s. [For all polymerizations: ([ME]$_0$+[MB]$_0$):[NHC]$_0$=100:1, ([ME]$_0$+[MB]$_0$)=0.4 M].

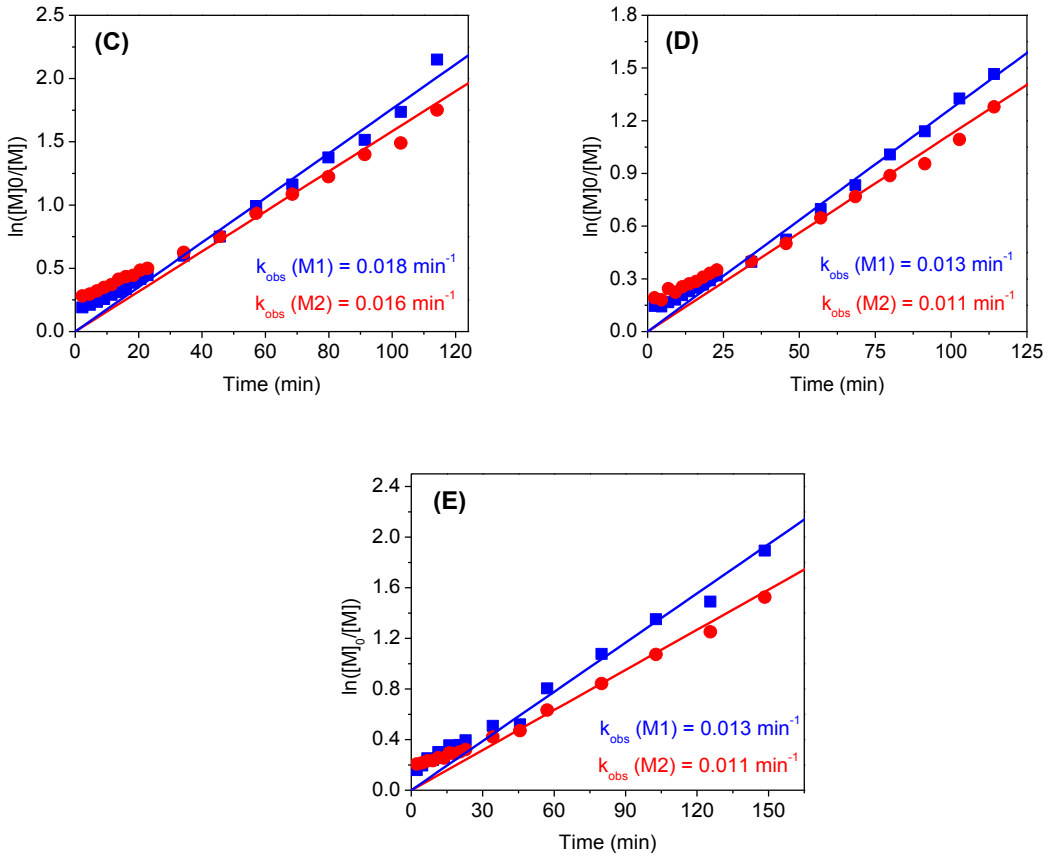

Figure 3.7 Continued

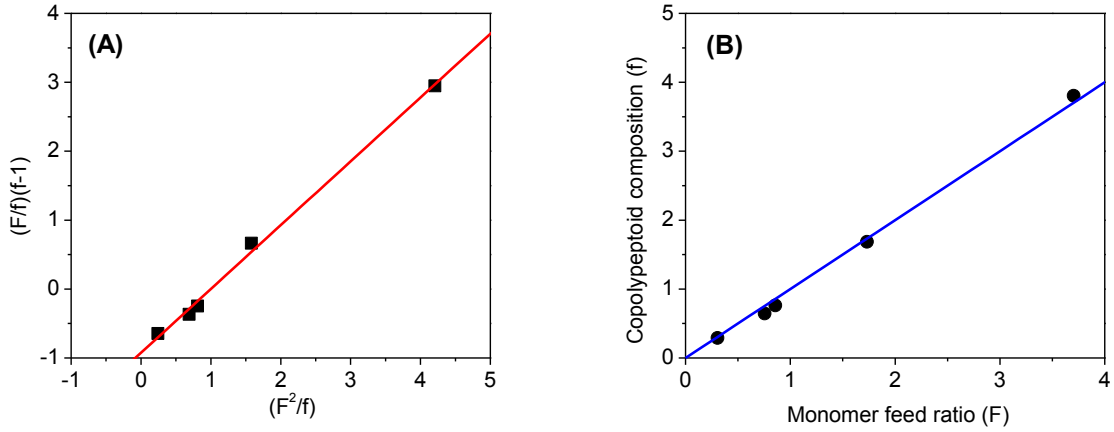

Figure 3.8. (**A**) Plot of (F/f)(f-1) versus (F^2/f) (■) for the NHC-mediated copolymerization of ME and MB and the linearly fitted line (—) whose slope is r_{ME} [0.93(3), ME] and intercept is r_{MB} [0.92(7), MB] by the Fineman-Ross method; (**B**) plot of copolypeptoid composition at low monomer conversion (25%) versus the monomer feed ratio (●) and the theoretical trend line (—) for random copolymers (r_{ME} = r_{MB} =1.0).

3.6.2.3. Determination of the reactivity ratios for butyl amine-initiated copolymerization of ME and MB.

The reactivity ratios were determined analogously those for the NHC-mediated copolymerization of ME and MB by the Fineman-Ross method.[154] The kobs for each monomer was obtained from plots of ln([M]0/[M]) vs time (**Figure 3.9**) and the reactivity ratios were calculated from the Finemann-Ross method (**Figure 3.10**).

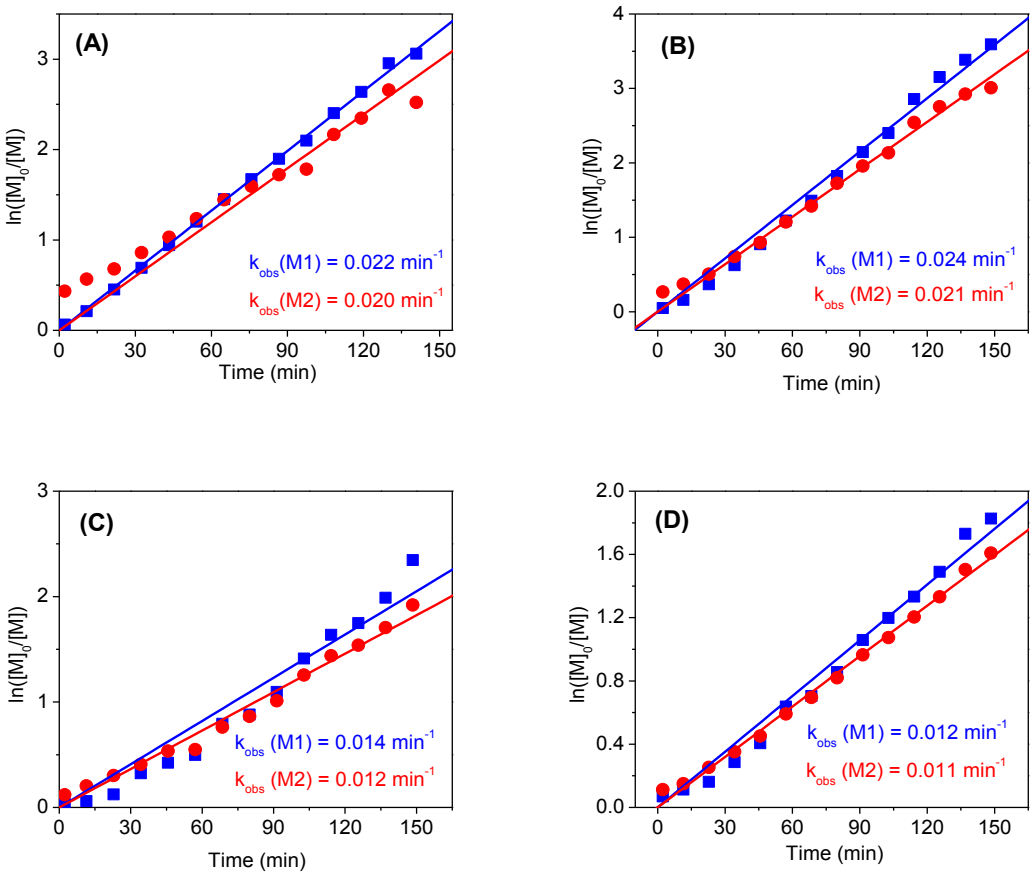

Figure 3.9. Plots of ln([M]$_0$/[M]) versus time for the butylamine-initiated batch-mode copolymerization of ME (■) and MB (●) in toluene-d$_8$ at 50°C where the initial monomer feed ratio was varied [(**A**) [ME]$_0$:[MB]$_0$= 81:19; (**B**) [ME]$_0$:[MB]$_0$= 68:32; (**C**) [ME]$_0$:[MB]$_0$= 39:61; (**D**) [ME]$_0$:[MB]$_0$= 28:72] and their linearly fitted curves [ME(—); MB(—)] whose slopes are the k_{obs}s. [For all polymerizations: ([ME]$_0$+[MB]$_0$):[NHC]$_0$=100:1, ([ME]$_0$+[MB]$_0$)=0.4 M].

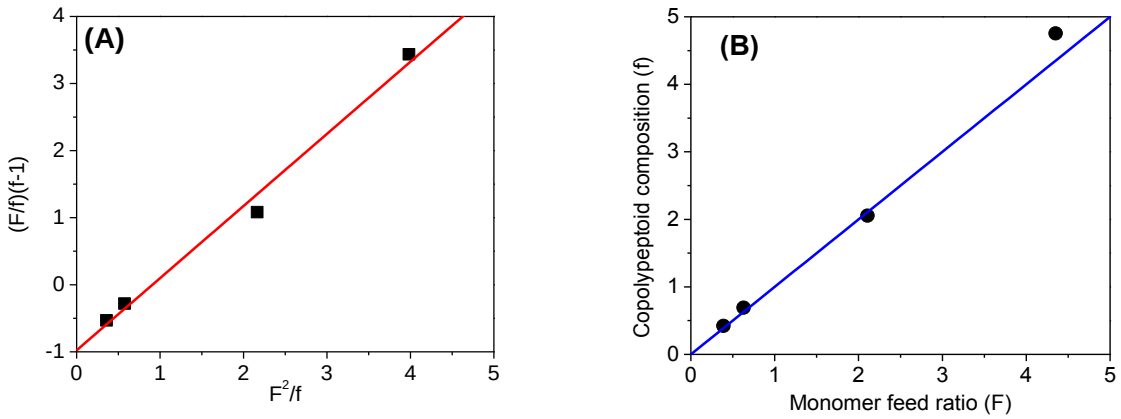

Figure 3.10. (**A**) Plot of (F/f)(f-1) versus (F^2/f) (■) for the butylamine-initiated copolymerization of ME and MB and the linearly fitted line (—) whose slope is r_{ME} [1.08(8), ME] and intercept is r_{MB} [0.98(17), MB] by the Fineman-Ross method; (**B**) plot of copolypeptoid composition at low monomer conversion (25%) versus the monomer feed ratio (●) and the theoretical trend line (—) for random copolymers (r_{ME} = r_{MB} =1.0).

The reactivity ratios for both the cyclic and linear initiated systems are near one (r_{ME} = 0.93 and r_{MB} = 0.92 for the NHC and r_{ME} = 1.08 and r_{MB} = 0.98 for the primary amine initiated systems) indicating that these copolypeptoids have a random microstructure. A consequence of the random structures is that the composition should not fluctuate throughout the length of the copolymer, resulting in an evenly dispersed hydrophilicity throughout the copolymer chain. There should be no hydrophobic patches along the backbone of either initiated system, which could affect the collapse of the thermoresponsive copolymers.

Using the kinetic data obtained from the ^{1}H NMR plots can also be used to plot the kinetic chain length, which is the average number of monomers consumed for each initiator,[29] can be used to observe if the molar fraction of the NEG segment changes throughout the reaction. If the copolymerization is a random copolymerization, then the plot of the molar fraction of one of the comonomers (in this case the NEG segment) against the normalized kinetic chain length should give a horizontal line. **Figure 3.11** is the plot of the molar fraction of NEG against the normalized kinetic chain length of the copolymer when the NHC initiator is used. At

different monomer loadings, each copolymerization yields a horizontal line for NEG molar fraction, thus further confirming that the copolymerization is random.

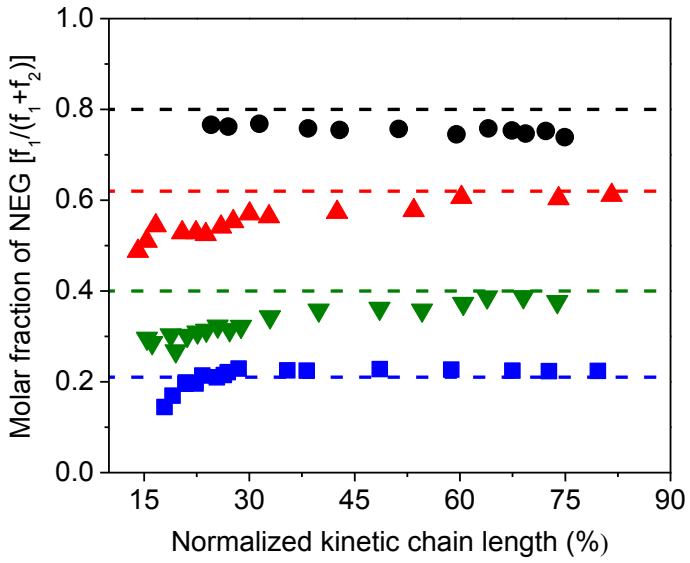

Figure 3.11. Plots of the copoly(α-peptoid) composition [i.e., the molar fraction of the NEG segment, f1/(f1+f2)] versus the normalized chain length of the *c*-P(NEG-*r*-NBG)s throughout copolymerization experiments conducted with different initial monomer feed ratios; $[ME]_0$:$[MB]_0$= 80:20 (●), 62:38 (▲), 44:56 (▼) and 21:79 (■) as well as the theoretical trend line for a truly random copolymer (r1=r2=1.0).

From the kinetic data, the copolymerization of N-ethyl- and –butyl-NCA is similar to that of the N-butyl-NCA homopolymerization with the NHC initiator. Both systems (the copolymerization and homo-polymerization) are controlled polymerizations, having a linear relationship between M_n and monomer conversion (**Figure 3.12**).[7]

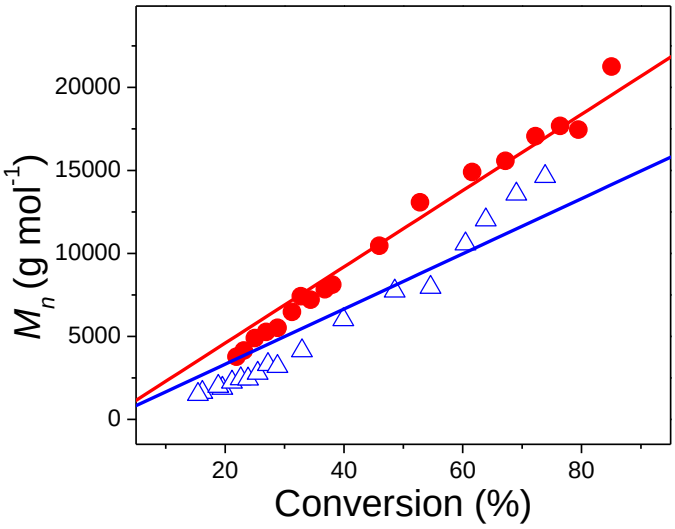

Figure 3.12. Plot of M_n and combined comonomer ([ME] + [MB]) conversion as determined by ^{1}H NMR in toluene-d8.

3.6.3. T_{cp} Determination (Turbidity Measurements).

All polymer samples were dissolved in distilled water at room temperature. The samples were placed in quartz cuvettes and heated to 75 °C (the maximum instrumentally allowed temperature), at which they were allowed to equilibrate for 15 min. The samples were then cooled at a rate of 1°C·min^{-1} and the absorption was taken every several minutes without stirring. Once past the T_{cp}, the temperature was held constant for 10 min, followed by heating at a rate of 1°C·min^{-1} back to 75°C. T_{cp}s were determined at λ=450 nm and at 50% transmittance. The transition window (ΔT_{cp}) corresponds to the temperature difference at 1% and 99% transmittance.

3.6.3.1 Turbidity measurements of methyl- and butyl-NCA copolymers.

By combining the methyl-NCA (water soluble) and butyl-NCA (water insoluble) monomers in the copolymerization, macromolecules that exhibit phase transition responses to temperature while in water can be synthesized. Below is the raw and processed (**Figure 3.13**)

experimental data for a cyclic copolymer made from the bulk copolymerization of these two monomers.

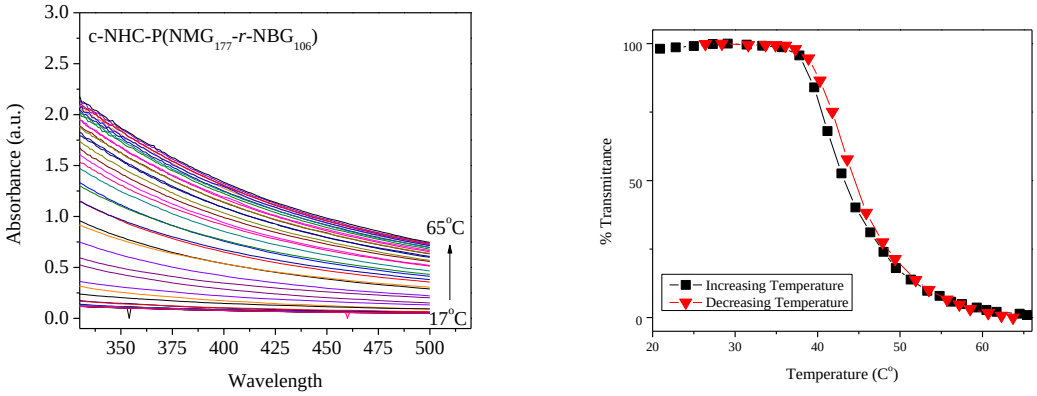

Figure 3.13. (Left) UV-vis raw data of recorded absorbance against wavelength for temperatures ranging from 17°C to 65°C for the random copolymer c-NHC-P(NMG_{177}-*r*-NBG_{106}). (Right) Processed UV-vis data for the copolymer c-NHC-P(NMG177-r-NBG106). The Tcp of this copolymer is 43.2°C.

The thermoresponsive behaviors of the methyl and butyl substituted copolymers that were synthesized from either a NHC (cyclic) or butylamine (linear) initiator are compared in the appendix (**Figure 3.14**). The results were inconclusive when regarding the topology as a primary effect on the thermalresponse of the copolymer in water. **Figure 3.14** (A-C) shows three different copolymers with NMG molar fractions of 60, 55 and 40 percent. The turbidity measurement graphs had no trend amongst the cyclic and linear copolymers. The discrepancies between the topological effects on the copolymer's phase transition properties can be ascribed to the lack of control during the copolymerization. The inability to synthesize a well-controlled copolymer in a solvent that was permissible to both hydrophobic and hydrophilic monomers was the reason accredited for in inconsistencies amongst the turbidity data for the P(NMG-r-NBG).

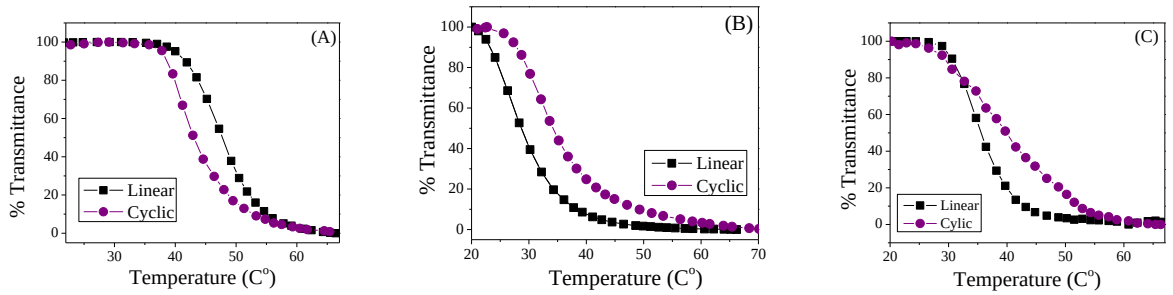

Figure 3.14. Turbidity measurements for linear and cyclic P(NMG-r-NBG)s at different NMG molar fractions of roughly 60, 55 and 40 percent for A, B and C respectively.

3.6.3.2. Turbidity Measurements for cyclic P(NEG-r-NBG)

Control of the copolymerization was greatly enhanced when the N-ethyl-NCA was substituted for the N-methyl-NCA. This control was attributed to the solubility of the polymer and is exemplified in the Tcp measurements (**Figure 3.15** and **Table 3.1**). As the water soluble NEG content is increased, the Tcp is also increased. All transitions are reversible with a miminal hysteresis (unfilled symbols in **Figure 3.15**).

Typically for polymers that exhibit LCST-like behavior, the T_{cp} can be lowered if the concentration of the polymer is increased.[176] **Figure 3.16** shows the turbidity measurement and T_{cp}'s as functions of temperatures and polymer concentrations respectively. As the concentration of the cyclic polypeptoid is increased, the T_{cp} of that polymer is lowered correspondingly. This phenomenon is attributed to the enhancement of hydrophobic interaction by simply increasing the amount of hydrophobic moieties in the solution.[177]

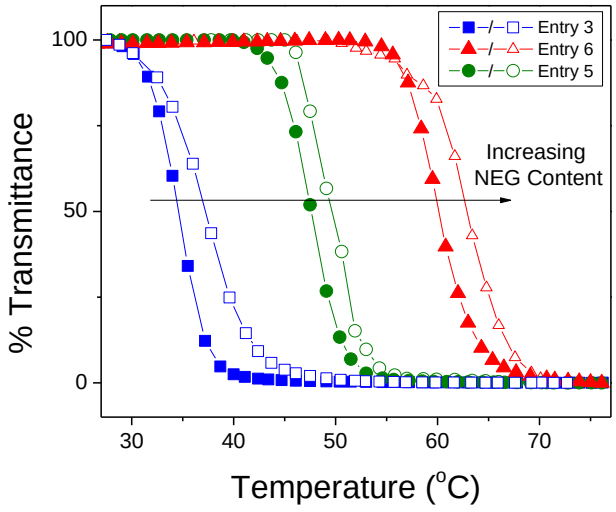

Figure 3.15. Plots of transmittance at λ=450 nm versus temperature for the selected aqueous solutions of cyclic copoly(α-peptoid)s prepared by the NHC-mediated copolymerization of ME and MB (polymer concentration= 1.0 mg·mL^{-1}; heating and cooling cycles are symbolized by the filled and unfilled symbols, respectively); *c*-NHC-P(NEG$_{70}$-*r*-NBG$_{47}$) (■,□); *c*-NHC-P(NEG$_{65}$-*r*-NBG$_{30}$) (●,○); *c*-NHC-P(NEG$_{101}$-*r*-NBG$_{34}$) (▲,Δ) (Entry 3, 5 and 6, respectively, **Table 3.1**).

Table 3.1. Characterization of cyclic and linear random copoly(α-peptoid) *c*/*l*-P(NEG$_m$-*r*-NBG$_n$)s synthesized from NHC or BuNH$_2$-initiated copolymerizations of Et-NCA (ME) and Bu-NCA (MB).

Entry #	[ME]$_0$:[MB]$_0$:[I]$_0$	Copolypeptoid Composition [b]	NEG [b] (mol%)	M_n [b] (g·mol^{-1})	M_n [c] (g·mol^{-1})	PDI [c]	T_{cp} [d] (°C)	ΔT_{cp} [h] (°C)
1	42:58:1	*c*-P(NEG$_{30}$-*r*-NBG$_{49}$)	38	8.1	24.2	1.12	-[f]	-[f]
2	60:40:1	*c*-P(NEG$_{71}$-*r*-NBG$_{62}$)	53	13.1	15.2	1.16	23.5	11.7
3	70:30:1	*c*-P(NEG$_{70}$-*r*-NBG$_{47}$)	60	11.3	15.5	1.19	34.5	13.3
5	80:20:1	*c*-P(NEG$_{65}$-*r*-NBG$_{30}$)	68	8.9	14.4	1.21	47.5	14.1
6	90:10:1	*c*-P(NEG$_{101}$-*r*-NBG$_{34}$)	75	12.4	15.2	1.15	60.1	16.4

Continued from previous page

Entry #	$[ME]_0$:$[MB]_0$:$[I]_0$	Copolypeptoid Composition [b]	NEG [b] (mol%)	M_n [b] (g·mol^{-1})	M_n [c] (g·mol^{-1})	PDI [c]	T_{cp} [d] (°C)	ΔT_{cp} [h] (°C)
7	91:9:1	*c*-P(NEG$_{74}$-*r*-NBG$_{15}$)	83	8.0	25.8	1.09	>75[e]	-[e]
8	21:9:1	*c*-P(NEG$_{17}$-*r*-NBG$_{11}$)	61	2.7	5.6	1.16	34.6	21.6
9	140:60:1	*c*-P(NEG$_{189}$-*r*-NBG$_{111}$)	63	28.7	24.8	1.18	34.4	10.7
10	44:56:1	*l*-Bu-P(NEG-*r*-NBG)[g]	39	-[g]	21.8	1.10	-[f]	-[f]
11	55:45:1	*l*-Bu-P(NEG-*r*-NBG)[g]	50	-[g]	13.9	1.12	23.1	10.3
12	60:40:1	*l*-Bu-P(NEG-*r*-NBG)[g]	53	-[g]	13.7	1.09	26.4	11.6
13	74:26:1	*l*- Bu-P(NEG-*r*-NBG)[g]	63	-[g]	18.2	1.14	44.3	12.4
14	75:25:1	*l*- Bu-P(NEG-*r*-NBG)[g]	67	-[g]	13.5	1.12	49.3	16.9
15	60:40:1	*l*- Bn-P(NEG$_{45}$-r-NBG$_{43}$)	51	8.7	12.2	1.10	26.0	12.0
16	70:30:1	*l*- Bn-P(NEG$_{76}$-r-NBG$_{50}$)	60	12.1	14.2	1.28	38.4	14.6
17	74:26:1	*l*- Bn-P(NEG$_{77}$-r-NBG$_{44}$)	64	11.5	16.0	1.14	43.8	12.1
18	80:20:1	*l*- Bn-P(NEG$_{110}$-r-NBG$_{45}$)	71	14.5	12.6	1.27	54.5	18.0
19	90:10:1	*l*- Bn-P(NEG$_{94}$-r-NBG$_{35}$)	73	12.0	13.7	1.64	61.1	16.1

[a.] all reactions were allowed to reach full conversion and isolated yields are typically 50%; [b.] Units are in kg•mol^{-1} and the copoly(α-peptoid) composition was determined by ^{1}H NMR analysis, assuming that each NHC initiates a chain growth; [c.] Units are kg•mol^{-}1 and were determined by SEC-DRI using polystyrene standards in DMF/LiBr (0.1 M); [d.] determined by turbidity measurement with a UV-Vis spectrometer where the transmittance at λ=450 nm is measured in the 20-75 °C temperature range and the temperature at 50% transmittance is the

experimental T_{cp}; [e.] T_{cp} is out of range of instrumentation; [f.] sample was not soluble in water; [g.] measured at 99% transmittance; [h.] the temperature window corresponds to the temperature difference at 99% (i.e., the onset of phase transition) and 1% transmittance (i.e., near completion of the phase transition). [g.] polymer M_n and composition cannot be accurately determined by ^{1}H NMR analysis due to the overlap of the polymer backbone and end group resonances.

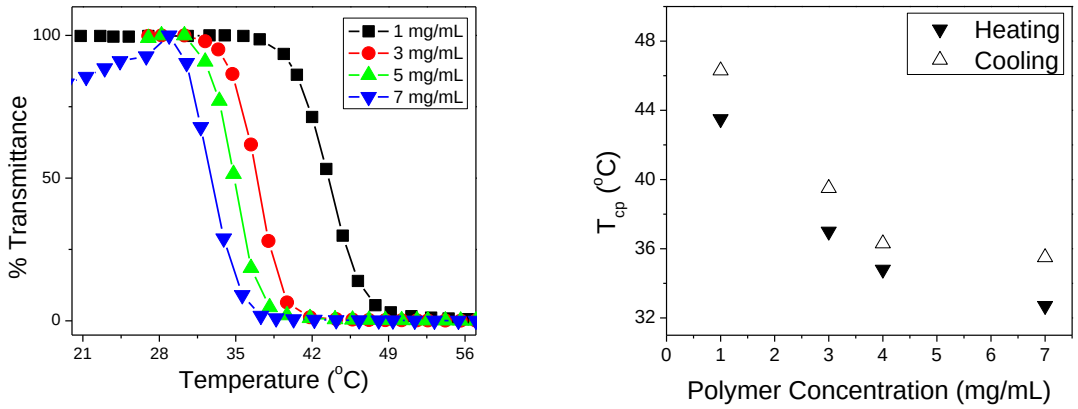

Figure 3.16. (Left) Plot of transmittance at λ=450 nm versus temperature for *c*-P(NEG_{55}-*r*-NBG_{26}) at varying copolymer concentrations in water, ranging from 1.0 mg·mL^{-1} to 7.0 mg·mL^{-1}. (Right) Plot of T_{cp}s of *c*-NHC-P(NEG_{55}-*r*-NBG_{26}) versus the polymer concentration in water for heating (▼) and cooling (Δ) cycles.

The T_{cp} of PNIPAAm and other thermoresponsive homopolymers are molecular weight dependent.[178] It has been observed by Lutz et al that this dependence on molecular weight does not apply to copolymers that exhibit LCST-like behavior.[160] The reason for the copolymer's phase transition characteristic's lack of dependence on molecular size is unknown. To test if the copolypeptoid's phase transition characteristics are dependent on molecular weight, three copolymers of different molecular weight were synthesized, and their turbidity measurements were taken. The GPC-DRI traces clearly display the differences in sizes between the copolypeptoids (**Figure 3.17**), while the turbidity measurements show little to no variation in the phase transition temperature among the three macromolecules. It appears as if the T_{cp}s of these copolypeptoids are not strongly affected by the molecular weight of the copolymer.

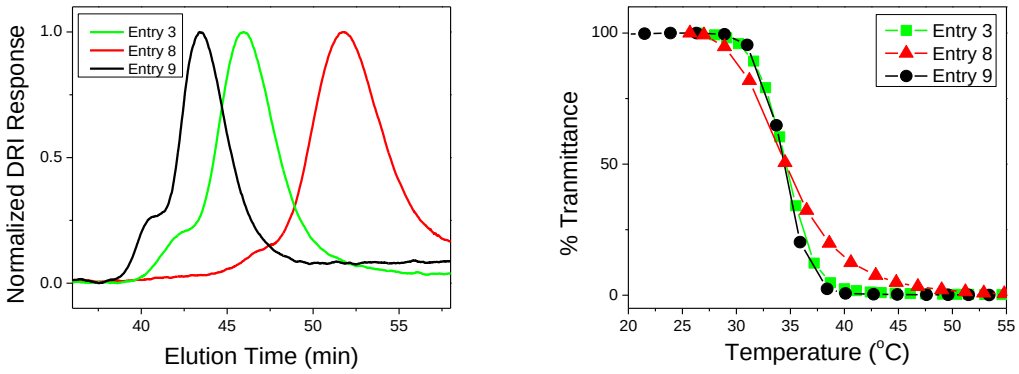

Figure 3.17. (Left) SEC-DRI chromatograms of *c*-P(NEG-*r*-NBG) having different polymer compositions (Entry 3, 8 and 9 Table S1) in DMF/LiBr (0.1M) at 50°C. (Right) Plot of transmittance versus temperature for three different c-P(NEG-r-PNBG) (Entries 3, 8 and 9) with similar NEG content (~61 mol %) but different molecular weights.

3.6.4. Hofmeister Salt series

The Hofmeister salt series, named after Franz Homeister, involves the propensity of certain ions to affect the solubility of proteins or polymers in aqueous solutions.[179, 180] These ions have the ability to either salt in (increase solubility) or salt out (decrease solubility) macromolecules. Salts are classified into two categories; kosmotropic and chaotropic. Kosmotropic salts cause the water molecules to become ordered and in doing so they decrease the T_{cp} (salt-out) the polymer. Chaotropic salts disorder water molecules, which increases the T_{cp} (salt-in) of the polymeric solution.[181] Though the exact reasoning behind this phenomenon is still being studied, it has been observed that the anions tend to have the larger effect on the stability of the protein than do their corresponding cations.[181] Several theories regarding the Hofmeister salt series have been proposed, including the hydration, water dipole, eletctrostatic, internal pressure and van der Waals forces theories, all of which provide reasoning for this phenomenon.[181] Some salts have been known to unfold or denature protiens (i.e. I- and SCN-), which indicates that these salts directly interact with the protein.[182] Other studies suggest that the rearrangement of the water molecules indirectly causes this salting-out of the protein.[183]

To test if these cyclic copolypeptoids responded and correlated with the Hofmeister series, the chaotropic salt (NaI), kosmotropic salt (Na_2SO_4) and a salt that lies in between the two (NaCl) were used. The cyclic copolypeptoids were dissolved in different concentrations of the certain salt and turbidity measurements were taken. **Figures 3.18** and **3.19** are the turbidity measurements for NaCl, NaI and Na_2SO_4, while **Figure 3.21** is the normalized response of the copolypeptoids to each salt in the Hofmeister series. At the highest salt concentration, each of the salts lowered the T_{cp} of the copolypeptoid used which indicates that the polymers were eventually 'salted-out' from their aqueous solution. As expected, these copolymers had the typical response to these Hofmeister salts, and the stronger salt (Na_2SO_4) 'salted-out' the polymer at much lower concentrations than did the weakest salt (NaI). At low concentrations, the salt with the lowest strength in the series, NaI, appeared to 'salt-in' the copolypeptoid, though at higher NaI concentrations, the T_{cp} of the copolypeptoid was lowered, and eventually 'salted-out' the polymer.

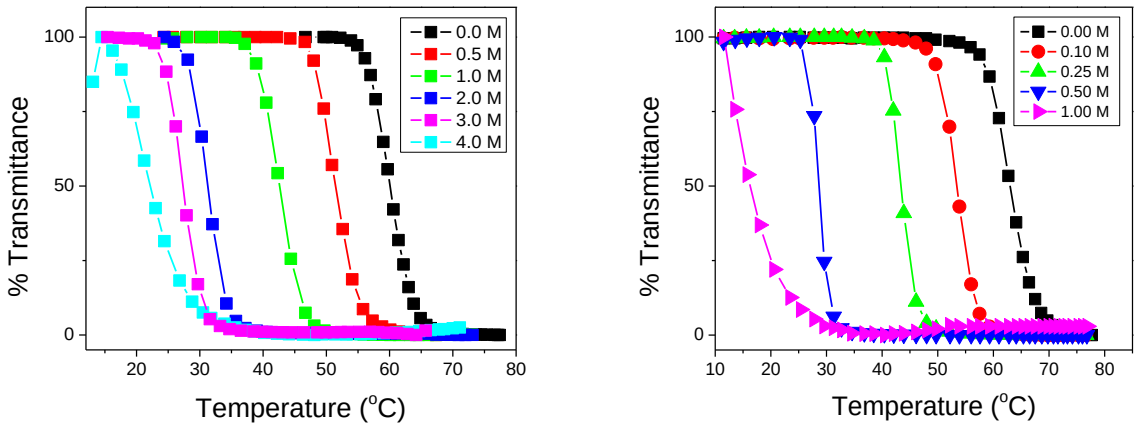

Figure 3.18. (Left)Representative plot of transmittance at λ=450 nm versus temperature for the *c*-P(NEG_{62}-*r*-NBG_{23}) in aqueous NaCl salt solutions ranging in molarity from 0.5 M to 4.0 M at a constant polymer concentration of 1.0 mg·mL^{-1}. (Right) Representative plot of transmittance at λ=450 nm versus temperature for *c*-P(NEG_{71}-*r*-NBG_{28}) in aqueous Na_2SO_4 salt solution ranging in molarity from 0.10M to 1.00 M at a constant polymer concentration of 1.0 mg·mL^{-1}.

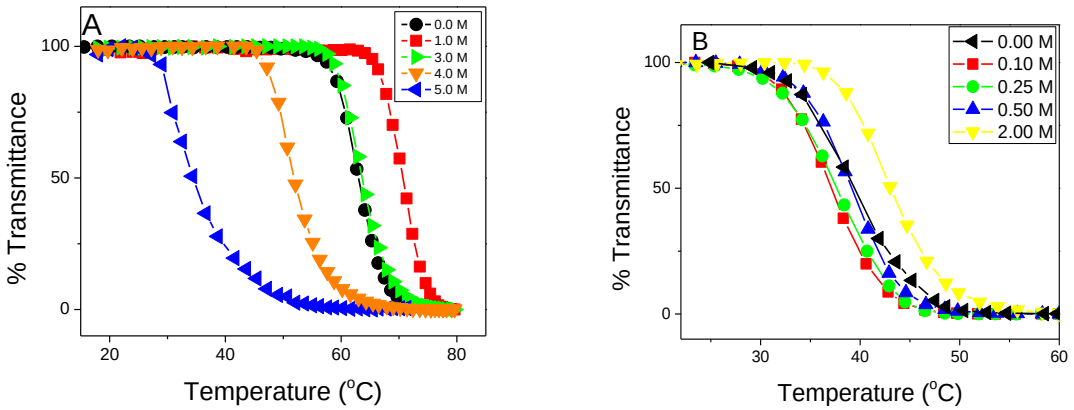

Figure 3.19. Representative plots of transmittance at λ=450 nm versus temperature for *c*-P(NEG$_{71}$-*r*-NBG$_{28}$) (A) and *c*-P(NEG$_{66}$-*r*-NBG$_{34}$) (B) in aqueous NaI salt solutions ranging in molarity from 0.10 M to 7.0 M at a constant polymer concentration of 1.0 mg·mL^{-1}.

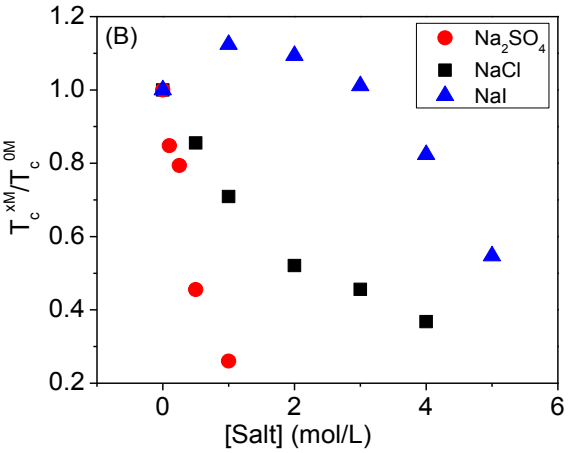

Figure 3.21. Plot of T_{cp}s of *c*-NHC-P(NEG$_{62}$-*r*-NBG$_{23}$) at various salt concentration (T_{cp}^{xM}) relative to that with no salt (T_{cp}^{0M}) versus the salt concentration in water (●: Na_2SO_4; ■: NaCl; ▲: NaI).

3.6.5. Turbidity Measurements for linear-Bu-P(NEG-r-NBG) and Bn-P(NEG-r-NBG)

The turbidity measurements for the linear copolypeptoids (copolymerizations initiated with either butyl- or benzyl-amines) were taken using the same techniques as the cyclic copolypeptoids. Similar to the cyclic copolypeptoids, as the NEG content is increased in the copolymer composition, the T_{cp} is increased (**Figure 3.22**, **3.23** and **Table 3.1**).

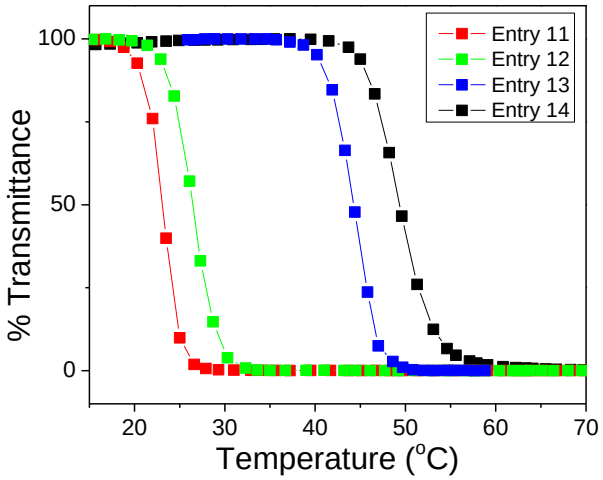

Figure 3.22. Representative plots of transmittance at λ=450 nm versus temperature for the selected aqueous solutions of butylamine-initiated linear copoly(α-peptoid)s *l*-Bu-P(NEG_{56}-*r*-NBG_{44}) (Entries 11-14, Table S1) prepared from the butylamine-initiated copolymerization of ME and MB(polymer concentration= 1.0 mg·mL^{-1}).

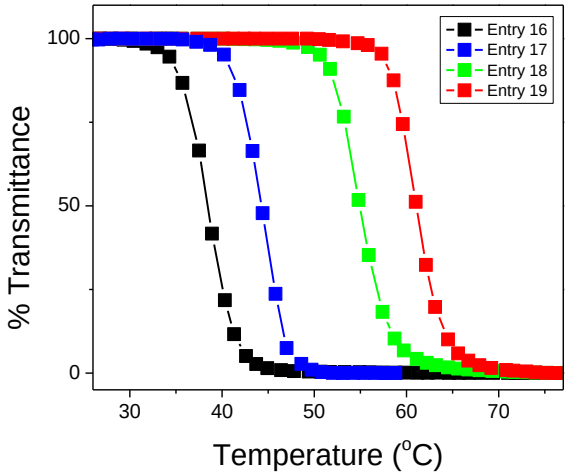

Figure 3.23. Representative plots of transmittance at λ=450 nm versus temperature for the heating cycles for the selected aqueous solutions of benzylamine-initiated linear copoly(α-peptoid)s (Entries 16-19) prepared from the benzylamine-initiated copolymerization of ME and MB (polymer concentration= 1.0 mg·mL^{-1}.)

3.6.6. Comparison of thermal phase transitions between linear and cyclic copolypeptoids

During these experiments, it was observed that the linear copolypeptoid of nearly identical NEG moiety (hydrophilic) had an increased T_{cp} as compared to its cyclic equivalent.

Similar phenomena have been observed between cyclic and linear PNIPAAm systems, however, the results from these previous studies were inconclusive. Qui et al observed that by cyclizing PNIPAAm through end-group functionalization, the T_{cp} can be increased from its linear precursor.[84] They were able to confirm this change in the thermoresponsive properties of the cyclic PNIPAAm through both turbidity (UV-vis) and specific heat capacity (mDCS) measurements. Within the same journal issue, it was observed by Xu that the T_{cp} of cyclic-PNIPAAm was dependent on polymer concentration, and that the cyclic polymer had a lower T_{cp} than its linear precursor at certain concentrations.[59] At similar concentrations (1 mg•mL^{-1}), the two journal entries disagreed with one another in regards to the relationship between the linear and cyclic T_{cp}s. Xu also reported that there was no change in T_{cp} between the linear and cyclic PNIPAAm when measuring the specific heat capacity (mDSC), a technique used to differentiate between the thermoresponsive characteristics of the two architectures in the former report. Both journal entries report a distinct broadening the phase transition window from the linear to cyclic PNIPAAm for reasons yet to be understood.

Our observations of the thermoresponsive behaviors between the linear and cyclic copolypeptoids agree with the previous assertions that the cyclic PNIPAAm has a lower T_{cp} than its linear counterpart. **Figure 3.24** illustrates the differences between linear and cyclic copolypeptoids of varying NEG content along the copolymer composition. Molecular weights were controlled and held relatively constant by controlling the initial monomer-to-initiator ratio for all polymerization systems (**Table 3.1**). Comparing copolypeptoids of different composition allowed for a direct comparison between the two architectures, and it was observed that the cyclic copolypeptoids have a depressed T_{cp} as compared to a linear polypeptoid.

Two linear copolymers were synthesized (using the butyl- and benzyl-amine intiators) to determine if the end-group affected the thermoresponsive behaviors of the copolymers. It has been previously noted that in some cases, the size and hydrophobicity of the chain end can affect the transition.[178] It appears that there is no significant difference between the butyl- and benzyl-amine initiated linear copolypeptoids (blue and green symbols in **Figure 3.24**), and in all cases, the linear copolymer's thermoresponse is elevated as compared to the cyclic's T_{cp}.

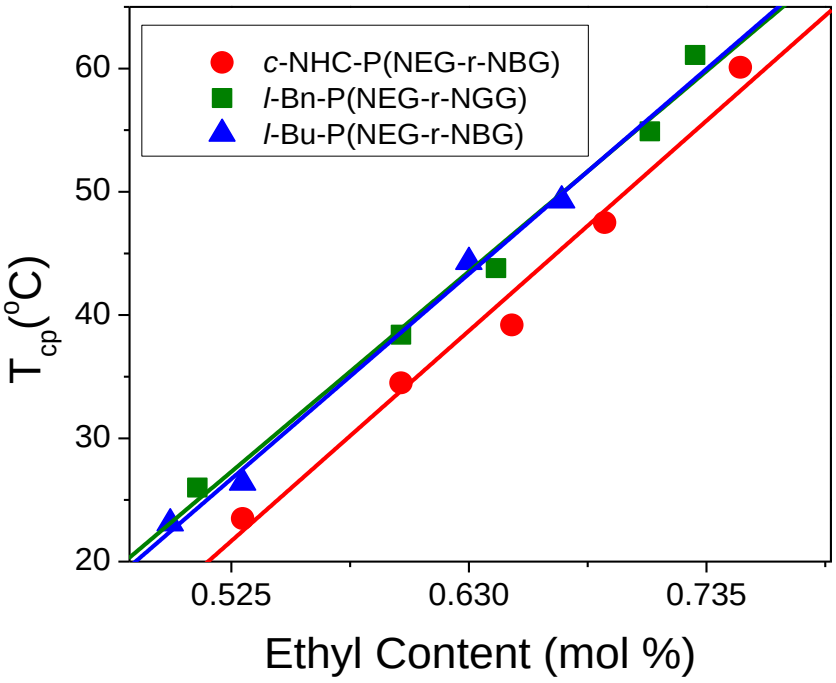

Figure 3.24. Plots of cloud point temperature (T_{cp}) versus the molar fraction of NEG segment in the cyclic and linear P(NEG-*r*-NBG) random copolymers bearing different end groups and their respective linearly fit curves [*c*-NHC-P(NEG-*r*-NBG) (●, —), *l*-Bu-P(NEG-*r*-NBG) (▲,—) and *l*-Bn-P(NEG-*r*-NBG) (■, —)].

Though these experiments lead to the conclusion that linear copolypeptoids have elevated thermoresponses as compared to their cyclic counterparts, a copolypeptoid with identical microstructure but different architecture could not be tested while using different initiators. To

compare a cyclic and linear copolypeptoid of identical microstructure, low molecular weight c-NHC-P(NEG_{17}-r-NBG_{11}) was synthesized and subsequently subjected to an acyl-chloride treatment. This reaction has been known to open the ring of cyclic-zwitterionic polypeptoids, allowing for direct comparison of identical microstructures but dissimilar topologies.[44] To confirm that the acyl-chloride treatment opened the macrocycle, ^{1}H NMR, MALDI-TOF and GPC-DRI characterizations were performed. The ^{1}H NMR confirmed that the structure of the acyl-chlorided treated copolymer had nearly identical molecular weight and NEG molar content to its cyclic precursor (**Figure 3.43**). The ^{1}H NMR also confirmed that NHC and the acyl chloride were attached to the copolymer as end-groups. GPC-DRI showed that there was a decrease in elution volume of the acyl-chloride treated copolypeptoid, which is indicative of a change in conformation (size) of the polymer in solution. This change in conformation is a result of either an increase in molecular weight or a change in polymer architecture (i.e. a transformation of cyclic-to-linear topology, **Figure 3.25,** left). MALDI-TOF data displayed no change in molecular weight (**Figure 3.25**, right), leaving the change in architecture as the reason for the decreased elution volume in the GPC-DRI. The MALDI-TOF data indicated a change in the end-group (possibly an addition of the acyl-group) to the polymer (**Figure 3.25**, right). This shift is evidence for a change in the end-group of the copolymer.

The turbidity measurements of the cyclized and opened (acyl-chloride treated) copolypeptoids further supported the observation that linear copolypeptoids have elevated T_{cp}s (**Figure 3.26**). In addition to the identical microstructure, an NHC moiety is attached to both

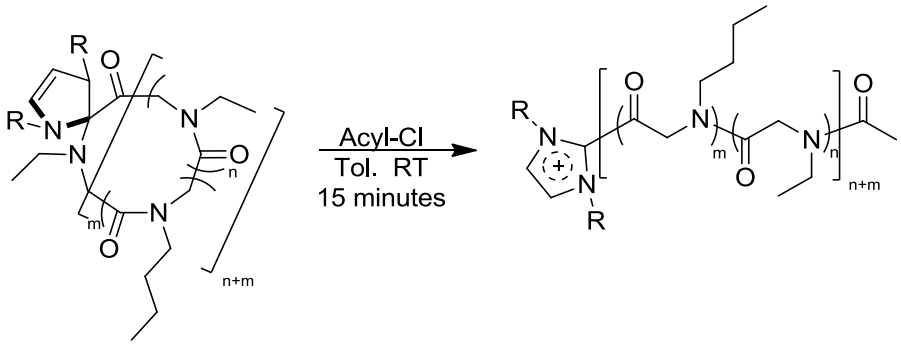

Scheme 3.4. Conversion of cyclic copolypeptoid by treatment with acyl-chloride.

copolypeptoids. This further supported the observation that the T_{cp}s of copolypeptoids in this molecular weight range was not strongly dependent on the end-group. This technique allowed for direct observation of the thermoresponsive behaviors of copolypeptoids that have identical NEG molar content and similar end-groups, but differed in their architectures. In agreement with earlier experimentation, linear copolypeptoids have increased T_{cp}s of roughly 5°C.

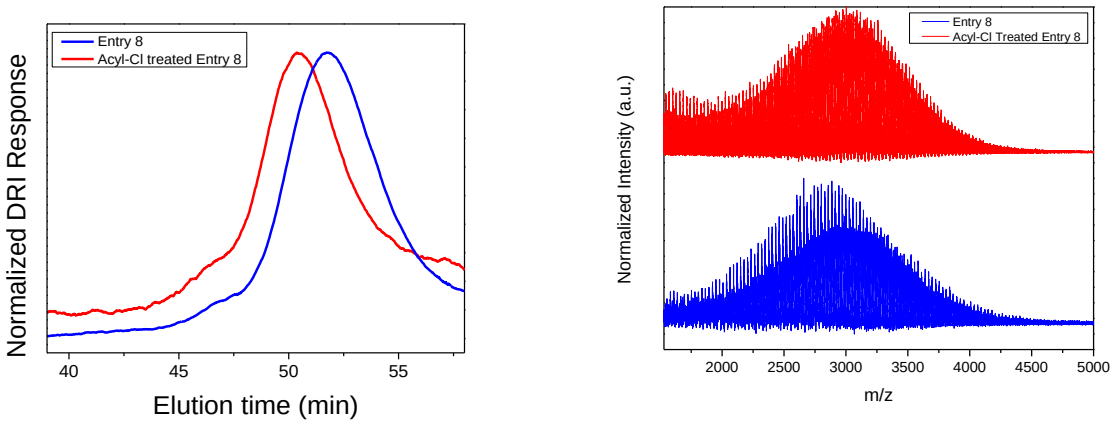

Figure 3.25. (Left) GPC-DRI traces of c-P(NEG_{17}-r-NBG_{11}) and its linear acyl-chloride counterpart (blue and red respectively) in DMF/LI (0.1M) at 50°C. (Right) MALDI-TOF spectra of c-P(NEG_{17}-r-NBG_{11}) (blue) and its corresponding acyl-chloride treated linear counterpart (red), where the molecular weights and dispersities for the cyclic and linear are M_n = 2.68 kg•mol^{-1} PDI = 1.07 and M_n = 2.74 kg•mol^{-1} and PDI 1.07 respectively.

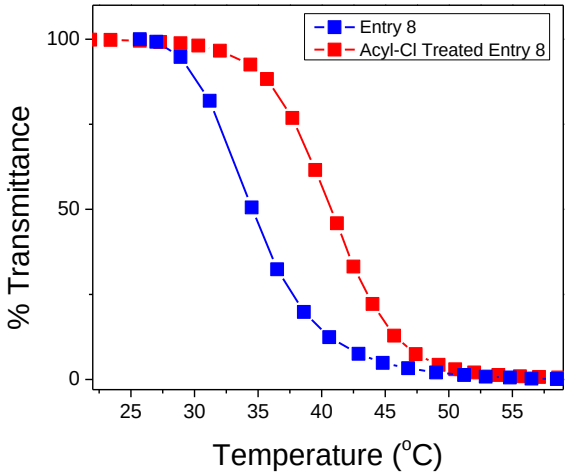

Figure 3.26. Representative plot of transmittance at λ=450 nm versus temperature for *c*-P(NEG$_{17}$-*r*-NBG$_{11}$) (blue) and *l*-P(NEG$_{17}$-*r*-NBG$_{11}$) (red) in aqueous solution at a constant polymer concentration of 1.0 mg·mL^{-1}.

3.6.7. DLS Studies of the Thermal Properties of Linear and Cyclic Copolypeptoids

Dynamic light scattering studies using a Malvern Zetasizer instrument were performed on the cyclic (*c*-P(NEG$_{77}$-*r*-NBG$_{23}$)) and linear (*l*-Bu-P(NEG$_{77}$-*r*-NBG$_{23}$)) copolypeptoids to illustrate a change in size as the temperature is increased. As the temperature is increased, thermoresponsive polymers are known to aggregate in solution (allowing for turbidity measurements). These aggregates are measured using light scattering experiments. **Figure 3.27** illustrates the increase in particle size (aggregation of the copolypeptoid) as the temperature is increased. The T_{cp} for both the cyclic (blue) and the linear (red) were measured separately using the UV-vis turbidity measurements and are indicated on the graph. Though only one angle was used to measure the size of these aggregates (limitations of the Malvern instrument), preliminary evidence for polymer aggregation (increase in particle size) exists using this instrumentation. Further investigation into the aggregation may lead to some insight into the differences in the thermoresponsive behaviors of the cyclic and linear copolypeptoids. Using a stopped-flow temperature jump and light scattering techniques, it was observed that the average aggregation

number cyclic PNIPAAm was far less than that of its linear precursor. As the temperature was increased, the average aggregation number of the linear PNIPAAm had a more pronounced increase (not a linear relationship), as opposed to its cyclic counterpart. This phenomonen was explained that the cyclic PNIPAAm formed stable mesoglobules with relatively lower chain density. The lack of interchain entanblement and penetration was the reason for this mesoglobule formation. Future DLS studies of the cyclic and linear copolypeptoids could prove fruitful in confirming this mesoglobule formation in the cyclic species.

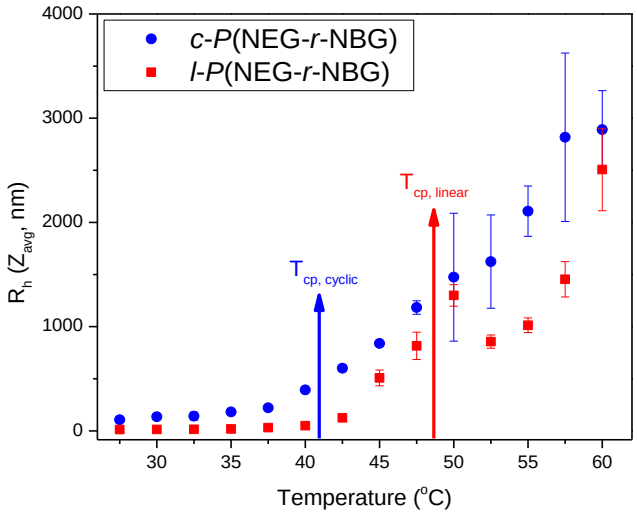

Figure 3.27. Plot of Rh as a function of temperature for butyl-amine and NHC initiated copolypeptoids. Size data of *c*-P(NEG$_{77}$-*r*-NBG$_{23}$) (blue) and *l*-Bu-P(NEG$_{77}$-*r*-NBG$_{23}$) (red) in water at various temperatures. Each copolymer's respective T_{cp}s ($T_{cp,cyclic}$ = 41.9°C, $T_{cp,linear}$ = 48.7°C) is indicated in the graph and was determined by the UV-vis turbidity measurement (polymer concentration: 5.0 mg·mL^{-1}). DLS data reveal the formation of polymer aggregates in addition to the unimers (R_h=~2 nm) below T_{cp}s. As temperature increases, the particle size increases. This is consistent with intermolecular aggregation, giving rise to the polymer/solution phase separation.

3.6.8. FTIR Study of the LCST Copolypeptoid Behavior

Minimal research has been reported on the Fourier Transform InfraRed (FTIR) studies of thermoreponsive polymers.[184, 185] In aqueous solution, PNIPAAm's thermoresponsive characteristics have been studied using the FTIR which illustrated the polymer's ability to

hydrogen bond to water molecules through the change of certain amide bands. In PNIPAAm, the amide stretchings has been classified into three distinct bands, including the intramolecular hydrogen bonded carbonyl band at 1631 cm^{-1}, the intermolecular hydrogen bonded carbonyl band at 1620 cm^{-1} and the free form of the non-hydrogen bonded carbonyl at 1643 cm^{-1}.[186] By measuring the amount of each amide bond in PNIPAAm while increasing the temperature, it was demonstrated that 70% of the polymer's hydrogen bonding was intramolecular above the polymer's T_{cp}, which indicated a collapse of the polymer.[187] Below PNIPAAm's T_{cp}, the predominant hydrogen bonding was shown to be intermolecular (50-70%) between either polymer/water or polymer/polymer interactions.

To investigate the amide carbonyl stretchings of the copolypeptoid, l-Bu-(NEG-r-NBG) (NEG 67%) was dissolved in distilled water (5 $mg \bullet mL^{-1}$) and measurements using an in-situ FTIR were taken at different temperatures. The T_{cp} of this copolypeptoid, 48.6^{o}C, was measured separately using UV-vis. It was noticed that the carbonyl stretching at 1640 cm^{-1} increased strongly after the T_{cp} of the polymeric solution (**Figure 3.28**). Due to the absence of hydrogen donors (N-substituted glycines), the amide band at 1640 cm^{-1} must be a consequence of either an intermolecular hydrogen bonded carbonyl band (polymer-to-water) or the free form of the non-hydrogen bonded carbonyl band. Changes in the intensity of this band were observed as the temperature increased. The temperature control was much more difficult while using the reactive FTIR and to compensate, the solution was allowed to equilibrate at each set temperature for 30 minutes before the measurements were taken. When plotted alongside to the transmittance there appears to be a transition in the carbonyl band intensity near the T_{cp} of the copolypeptoid. (**Figure 3.29**). It is also interesting that the fingerprint region of copolypeptoid becomes much sharper above the T_{cp} than before. The reasoning for this increase in intensity

and fingerprint region signal is currently unknown and unreported in the literature for polypeptoids.

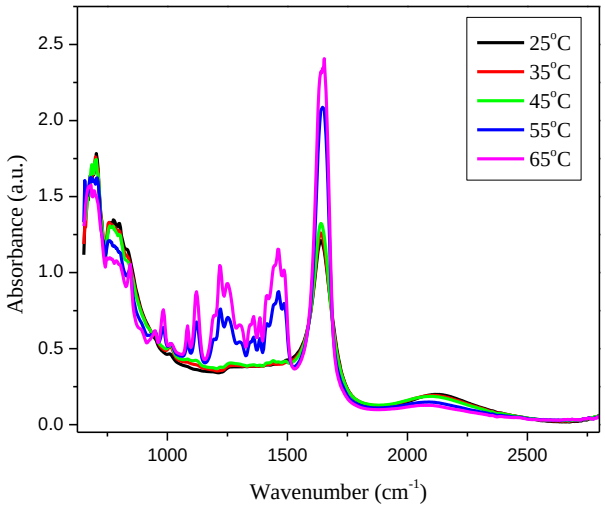

Figure 3.28. Reactive-FTIR of l-Bn-P(NEG-r-NBG) (ethyl mol, 67%) in aqueous solution at different temperatures.

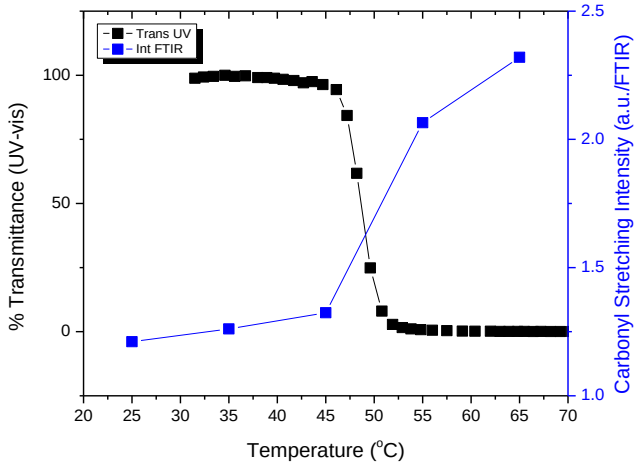

Figure 3.29. Thermoresponsive characteristics of l-Bu-P(NEG-r-NBG) (ethyl mol, 67%) as measured by the % transmittance using the UV-vis (black, left axis) and intensity of the carbonyl stretching in the FTIR (blue, right axis).

3.6.9. Potential Explanation for Depressed T_{cp} in Cyclic Copolypeptoids.

There are two arguments that help to explain the discrepancy between the T_{cp} of the cyclic and linear copolypeptoids; the entropic constraints on the cyclic polymer and the decreased hydrogen bonding capabilities of cyclic polymers. By combining chain ends to form cyclic polymer, the entropy of that polymer is decreased due to hindered rotation, which results in a decreased amount of conformations[188]. By decreasing the entropy of the polymer (i.e. the allowable amount of conformations), less energy is needed for the cyclic polymers to collapse because the polymer is already in a semi-collapsed state. Cyclic polymers lose less energy during their collapse than do their linear counterparts.[85] The amount of energy (heat) to require the polymer to collapse in solution is less than that of the linear polymer (as evident by the depression in the T_{cp} of cyclic copolypeptoids).

Another argument is related to the hydrogen bonding of the water molecules to the cyclic polymer backbone. Hydrogen bonds possess a high directionality, relying heavily on the correct alignment of the H-donor/acceptor atom and the hydrogen. The ability to align correctly will result in a stronger hydrogen bond. Due to the stiff constraints along the backbone of a cyclic polymer, this directionality may be more difficult to achieve, resulting in a less hydrated polymer. Hindered rotation along the cyclic backbone results in less structural conformations available to accommodate the directionality needed to make strong hydrogen bonds with water. If the polymer is less hydrated, then less energy is required to reach the T_{cp}.[59] These conformational constraints are not prevalent in the linear polymer, allowing for more hydrogen bonds and an elevated T_{cp}.

3.6.10. Biocompatibility of c-NHC-P(NEG-r-NBG)

The biocompatibility of *c*-NHC-P(NEG-*r*-NBG)s has been assessed by cell culture studies using the CellTiter Blue cell viability assay. Human embryonic lung fibroblasts

(HEL229) were incubated for 24 h in PBS buffers containing increasing concentrations (0.039-5.0 mg·mL^{-1} or 4.9 μM-0.63 mM) of *c*-NHC-P(NEG$_{74}$-*r*-NBG$_{15}$). The copoly(α-peptoid) exhibits minimal cytotoxicity in this concentration range (**Figure 3.30**), on par with low molecular weight poly(ethylene glycol) (PEG, M_n=8 kg·mol^{-1}), a benchmark biocompatible polymer. A more extensive biocompatibility assessment of copoly(α-peptoid)s with varying compositions is currently in progress.

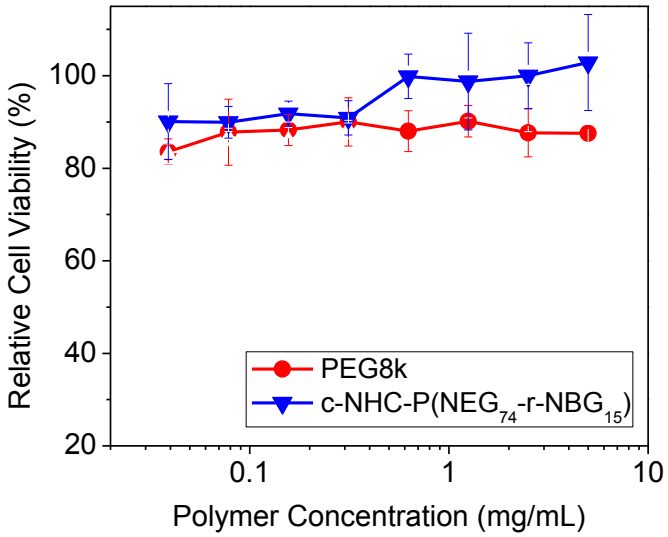

Figure 3.30. Plots of percentage cell viability (relative to the PBS buffer) versus the polymer concentration [i.e., *c*-NHC-P(NEG$_{74}$-*r*-NBG$_{15}$) (83 mol% NEG) (▼) and poly(ethylene glycol) (PEG, M_n=8 kg·mol^{-1}) (●)] for HEL229 cells after 24 h incubation. (The x-axis is plotted in logarithmic scale to enable an unobstructed view of data at low concentration range).

3.7 Conclusions

Thermoresponsive copolypeptoids have been synthesized via the copolymerization technique that combines water soluble and water insoluble repeat units. The ability to tune the thermoresponse of these polypeptoids was achieved by controlling the composition of the copolymers (NEG mol %). The use of different initiators (primary amine and NHC) allowed for comparisons of the thermoresponsive behaviors of different architectures and it was observed that the cyclic copolypeptoids have a lower T_{cp} than their linear counterparts.

These thermoresponsive copolypeptoids are the first stimuli-responsive polymers synthesized from a polypeptoid backbone. Stimuli-responsive polymers are currently being studied in many scientific fields, and the addition of these thermoresponsive, biocompatible polypeptoids could prove fruitful. Future studies with these thermoresponsive copolypeptoids include physical studies into the aggregation of cyclic polymers and cellular imaging of these copolypeptoids (where these copolypeptoids are delivered into the cells).

3.8 Synthetic Procedures

Materials. Glyoxylic acid monohydrate (98%), butylamine (98%), ethylamine (99%) di-*tert*-butyl dicarbonate (97%), triethylamine, phosphorous trichloride and poly(ethylene glycol) (M_n=8 kg·mol^{-1}) were all purchased from Sigma Aldrich and used as received. All the solvents used in this study was purchased from Sigma-Aldrich, and purified by passing through alumina columns under argon. *N*-methyl *N*-carboxyanhydride (MM), *N*-ethyl *N*-carboxyanhydride (ME) and *N*-butyl *N*-carboxyanhydride (MB) was synthesized by adapting a reported procedure (**Scheme 3.3**).[7]

Instrumentation. ^{1}H and ^{13}C ^{1}{H} ^{189} NMR spectra were recorded on a Bruker AV-400 spectrometer, and the chemical shifts in parts per million (ppm) were referenced relative to protio impurities or ^{13}C isotope of deuterated solvents (e.g., $CDCl_3$ or toluene-d_8), respectively. SEC analyses were conducted using an Agilent 1200 system (Agilent 1200 series degasser, isocratic pump, auto sampler and column heater) equipped with three Phenomenex 5 μm, 300×7.8 mm columns [100 Å, 1000 Å and Linear(2)], Wyatt DAWN EOS multi-angle light scattering (MALS) detector (GaAs 30 mW laser at λ=690 nm), Wyatt ViscoStar viscometry(VISC) detector and Wyatt Optilab rEX differential refractive index (DRI) detector with a 690 nm light source. DMF containing 0.1 M LiBr was used as the eluent at a flow rate of

0.5 mL·min^{-1}. The column temperature was 50°C and the detectors temperature was 25°C. All data analyses were performed using Wyatt Astra V 5.3 software. Polymer molecular weight (M_n) and molecular weight distribution (PDI) were obtained by conventional SEC analysis with a calibration curve. The calibration curve was constructed from twenty three pauci-disperse polystyrene standards (M_n =590 g·mol^{-1}-1472 kg·mol^{-1}, Polymer Laboratories, Inc.) using Astra's column calibration template. Relative M_ns and PDIs were then calculated using Astra's conventional calibration template. UV-Vis spectra were recorded on a Varian Cary 50 Bio-UV-Vis spectrophotometer equipped with a Thermo/Neslab RTE-7 refrigerated bath circulator for temperature control. All UV-Vis absorptions were referenced against distilled water. Dynamic light scattering (DLS) analysis was conducted on a Malvern Zetasizer Nano-ZS instrument while using the Zetasizer software version 6.12. The aqueous solutions of *c*/*l*-P(NEG-*r*-NBG) copolymers (5 mg·mL^{-1}) were prepared by dissolving the polymers in nanopure water obtained from a Barnstead NANOpure ultrapure water system and filtering through a 0.2 micron PTFE filter prior to DLS data collection. The data were collected in triplicates between 25 to 60 °C at a 2.5 °C increment interval. Matrix-assisted laser desorption ionization-time of flight (MALDI-TOF) mass spectra were collected on a Bruker ProFLEX III MALDI-TOF mass spectrometer in the reflector mode and α-cyano-4-hydroxycinnamic acid (CHCA) was used as matrices and the major cation source.

Cell Culture. All tissue culture media and reagents were obtained from Invitrogen. Human embryonic lung HEL299 cells were grown in DMEM with high glucose supplemented with 10% fetal calf serum, 15mM hepes, glutamax, NaPyruvate, and NEAA in a humidified CO_2 incubator (37, 5% CO_2). The cells were subcultured twice weekly to maintain subconfluent stocks. The 4th to 15th passage cells were used for all the experiments.

Assessment of Cytotoxicity. The HEL299 cells (100 uL) were plated at 10000 cells per well in a Costar 96-well plate and allowed to grow for 48 h. All polymers were purified by dialysis (cutoff M_n= 3.5 kg·mol^{-1}) against distilled water for three and half days followed by drying and dissolution in PBS to give a 10 mg·ml^{-1} concentration. Serial dilutions were then conducted to prepare polymer solutions with lower concentrations (down to 0.039 mg·ml^{-1}). The polymer/PBS solution (100 uL) was added to each well, and the cells were incubated in the polymer/PBS solution for 24 h. The polymer concentration in the well is in the range of 0.039 to 5 mg·ml^{-1}. Cell toxicity was measured using Promega's CellTiter-Blue Viability Assay Kit as per manufacturer's instructions, with untreated cells in the PBS buffer considered 100% viable. A total of 5 replicates were conducted for each treatment. Microsoft Excel and Origin software were used for the data processing and plotting.

3.8.1. Methyl-NCA Synthesis (MM)

Synthesis of 2-(*N*, *N*-*tert*-butoxycarbonylmethylamino)acetic acid (3M, Scheme 2.1). *N*-(*tert*-Butoxycarbonyl)glycine (5.26 g, 30 mmol) was dissolved in anhydrous THF (120 mL) and iodomethane (7.5 mL, 120 mmol) was added. Sodium hydride (3.6 g, 150 mmol) was added into the solution slowly at 0°C. The reaction mixture was stirred at room temperature overnight. Additional iodomethane (3.7 mL, 60 mmol) and sodium hydride (1.2 g, 50 mmol) was added into the reaction mixture and stirred at room temperature overnight. Ethyl acetate (60 mL) was added and distilled water (12 mL) was added dropwise. The solvent was evaporated and the residue was re-dissolved in ether (40 mL) and distilled water (60 mL). The ether phase was separated and washed with saturated $NaHCO_3$ aqueous solution (40 mL). The aqueous extracts were combined and acidified to pH=2 with 1 M HCl aqueous solution at 0 °C. The solution was extracted with ethyl acetate (2×80 mL). The extract was washed with distilled water (100 mL), Na2S2O3 aqueous solution (5 wt%, 2×80 mL), brine (100 mL) and dried with $MgSO_4$. After

filtration, the filtrate was evaporated to afford the product as a white solid (5.01 g, 88% yield). ^{1}H NMR (δ in $CDCl_3$, ppm): 1.45 (s, -(C*H*$_3$)$_3$), 2.94 (s, C*H*$_3$N-), 3.95 and 4.02 (s, -COC*H*$_2$-).

Synthesis of *N*Me-NCA (MM). **3M** (5.68 g, 30 mmol) was dissolved in dry CH_2Cl_2 (150 mL) under a nitrogen atmosphere and PCl_3 (2.1 mL, 24.4 mmol) was added dropwise to the solution at 0°C. The reaction mixture was stirred for 2 hrs and then the solvent was removed under vacuum. The solid residue was re-dissolved in anhydrous CH_2Cl_2 and filtered. The filtrate was evaporated to afford a white solid. Further purification by recrystallization in anhydrous CH_2Cl_2/hexane and sublimation afforded white crystals (2.27 g, 66% yield) that were to be used for polymerizations. ^{1}H NMR (δ in CDCl3, ppm): 3.06 (s, C*H*$_3$N-), 4.12 (s, -COC*H*$_2$-). ^{13}C{^{1}H} NMR (δ in $CDCl_3$, ppm): 30.5 (*C*H$_3$N-), 51.1 (-CO*C*H$_2$-), 152.5 (-N*C*OOCO-), 165.4 (-NCOO*C*O-).

3.8.2. Ethyl-NCA Synthesis (ME)

Synthesis of 2-(ethylamino)acetic acid hydrochloride (1E, Scheme 2.1). Ethyl amine (2.8 g, 0.062 mol), cold CH_2Cl_2 (125 mL) and glyoxylic acid (12.0 g, 0.162 mol) was added sequentially a chilled round-bottom flask at 0°C. The reaction was allowed to react at 0°C for 3 h and then at room temperature for an additional 16 h. The volatiles were removed under vacuum to yield a yellow oil, to which 1 N HCl(aq) (175 mL) was added. The mixture was refluxed for 24 h. The water was removed by rotary evaporation. The solid residue was recrystallized from methanol/THF at 0 °C to yield a white solid (6.1 g, 70% yield). ^{1}H NMR (δ in D_2O, ppm): 1.13 (t, C*H*$_3$CH$_2$-, 3H), 3.04 (q, -C*H*$_2$CH$_3$, 2H), 3.84 (s, -C*H*$_2$-, 2H). ^{13}C {^{1}H} NMR (δ in D_2O, ppm): 10.2 (*C*H$_3$-), 42.7 (-*C*H$_2$CH$_3$), 46.7 (-*C*H$_2$-), 166.9 (*C*O).

Synthesis of 2-[(tert-butoxycarbonyl)(ethyl)amino]acetic acid (2E). Compound **1E** (6.1 g, 0.04 mol), di-*tert*-butyl-dicarbonate (24.0 g, 0.11 mol) and triethylamine (30.6 mL, 0.22 mol) were dissolved in distilled water (150 mL) at room temperature. The solution was stirred for 24 h

at room temperature followed by extraction with hexane (2×200 mL). The aqueous phase was isolated, acidified with 4 N HCl_{aq} (50 mL) and extracted with ethyl acetate (200 mL). The organic phase was separated, washed with brine and dried over anhydrous $MgSO_4$. Filtration and evaporation under vacuum yielded the product as colorless oil (8.4 g, 94% yield). ^{1}H NMR (δ in $CDCl_3$, ppm): 0.88 (t, C*H*$_3$CH$_2$-, 3H), 1.45 (s, (C*H*$_3$)$_3$-, 9H), 3.22 (q, -C*H*$_2$CH$_3$, 2H), 3.93 (s, -C*H*$_2$-, 2H). ^{13}C {^{1}H} NMR (δ in $CDCl_3$, ppm): 10.6 (-*C*H$_3$), 41.5 (-*C*H$_2$-), 52.4 (-*C*H$_2$-), 168.2 (*C*=O)

Synthesis of *N*-ethyl *N*-carboxyanhydride (ME). Compound **2E** (8.4 g, 0.041 mol) was dissolved in anhydrous CH_2Cl_2 (100 mL) under nitrogen. The solution was cooled to 0°C followed by dropwise addition of PCl_3 (4.0 mL, 0.046 mol). The reaction mixture was stirred at 0°C for 1 h and was allowed to warm to room temperature for additional 2 h. The volatiles were removed under vacuum to yield an oily residue. Inside the glovebox, the residue was extracted with anhydrous CH_2Cl_2 (20 mL) and filtered. The filtrate was stirred with NaH (100 mg) for 30 min and filtered. The volatiles were removed under vacuum to afford a faint yellow liquid, which was distilled under vacuum to yield a clear liquid (2.1 g, 40% yield). ^{1}H NMR (δ in toluene-d8, ppm): 0.63 (t, C*H*$_3$CH$_2$-, 3H), 2.80 (m, CH$_3$C*H*$_2$-, 2H), 2.94 (s, -COC*H*$_2$-, 2H). ^{13}C {^{1}H} NMR (δ in toluene-d8, ppm): 12.1 (*C*H$_3$CH$_2$-), 38.1 (CH$_3$*C*H$_2$-), 47.7 (-CO*C*H$_2$-), 151.8 (-N*C*OOCO-), 166.2 (-NCOO*C*O-).

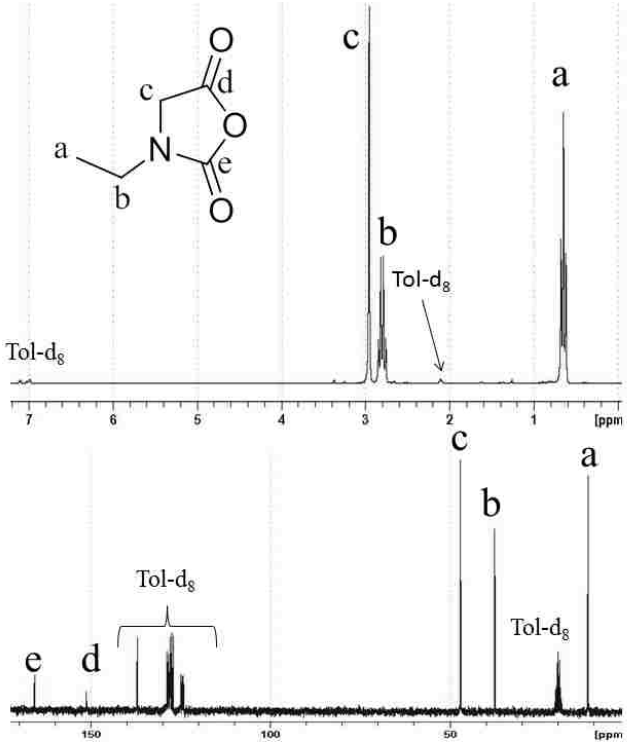

Figure 3.31. ^{1}H NMR (top) and ^{13}C {^{1}H} NMR (bottom) of ethyl-NCA (ME) in toluene-d_8.

3.8.3. Butyl-NCA Synthesis (MB)

Synthesis of 2-(*N*-butylamino)acetic acid hydrochloride (1B, Scheme 2.1).4 Glyoxylic acid (14.83 g, 158 mmol) and *n*-butylamine (7.8 mL, 79 mmol) were added to CH_2Cl_2 (400 mL) and stirred at room temperature for 24 hrs. The solvent was evaporated and 1 M HCl aqueous solution (400 mL) was added. The reaction mixture was heated under reflux overnight. The solvent was evaporated to yield a pale yellow solid. Recrystallization in methanol/ether afforded the final product as white crystals (10.9 g, 82% yield). ^{1}H NMR (δ in DMSO-D6, ppm): 0.88 (t, C*H*$_3$CH$_2$CH$_2$CH$_2$-), 1.30 (m, CH$_3$C*H*$_2$CH$_2$CH$_2$-), 1.60 (m, CH$_3$CH$_2$C*H*$_2$CH$_2$-), 2.88(s, CH$_3$CH$_2$CH$_2$C*H*$_2$-), 3.83 (s, -COC*H*$_2$-), 9.19 (s, *H*N*H*Cl).

Synthesis of 2-(*N*, *N*-*tert*-butoxycarbonyl-*n*-butylamino)acetic acid (2B). A round bottom flask was charged with **1B** (8.62 g, 51.4 mmol), di-*tert*-butyl dicarbonate (28.06 g, 128.6 mmol), triethyl amine (35.8 mL, 257.1 mmol) and distilled water (200 mL). The mixture was stirred at

room temperature overnight and extracted with hexane (2×200 mL). The aqueous phase was poured into 4 M HCl aqueous solution (50 mL) and extracted with ethyl acetate (3×50 mL). The organic phase was washed with brine (1×200mL), separated and dried over anhydrous $MgSO_4$. After filtration, the solvent was evaporated to afford the product as colorless oil (10.70 g, 90% yield). ^{1}H NMR (δ in $CDCl_3$, ppm): 0.91 (t, C*H*$_3$CH$_2$CH$_2$CH$_2$-), 1.29 (m, CH$_3$C*H*$_2$CH$_2$CH$_2$-), 1.47 (s, - (C*H*$_3$)$_3$), 1.48 (m, CH$_3$CH$_2$C*H*$_2$CH$_2$-), 3.26 (m, CH$_3$CH$_2$CH$_2$C*H*$_2$-), 3.90 and 3.97 (s, -COC*H*$_2$-).

Synthesis of *N*Bu-NCA (MB). **2B** (10.7 g, 46.3 mmol) was dissolved in dry CH_2Cl_2 (230 mL) under a nitrogen atmosphere and PCl_3 (3.2 mL, 37 mmol) was added dropwise to the solution at 0°C. The reaction mixture was stirred for 2 hrs and the solvent was removed under vacuum. The solid residue was extracted with anhydrous CH_2Cl_2 (3×20mL) and filtered. The filtrate was evaporated to afford a white solid. Further purification by recrystallization in anhydrous CH_2Cl_2/hexane and sublimation afforded white crystals (4.72 g, 65% yield) that were to be used for polymerizations. ^{1}H NMR (δ in $CDCl_3$, ppm): 0.95 (t, C*H*$_3$CH$_2$CH$_2$CH$_2$-), 1.37 (m, CH$_3$C*H*$_2$CH$_2$CH$_2$-), 1.57 (m, CH$_3$CH$_2$C*H*$_2$CH$_2$-), 3.39 (t, CH$_3$CH$_2$CH$_2$C*H*$_2$-), 4.09 (s, COC*H*$_2$-). ^{13}C {^{1}H} NMR (δ in $CDCl_3$, ppm): 13.4 (*C*H$_3$CH$_2$CH$_2$CH$_2$-), 19.6 (CH$_3$*C*H$_2$CH$_2$CH$_2$-), 29.0 (CH$_3$CH$_2$*C*H$_2$CH$_2$-), 43.2 (CH$_3$CH$_2$CH$_2$*C*H$_2$-), 48.9 (-CO*C*H$_2$-), 152.1 (-N*C*OOCO-), 166.2 (-NCOO*C*O-).

3.8.4. Synthesis of P(NMG-ran-NBG)

Representative Synthesis of P(NMG-ran-NBG). Methyl-NCA (31.2 mg, 0.273 mmol) and butyl-NCA (26.6 mg, 0.169 mmol) were both dissolved in acetonitrile (1 mL). The initiator was taken from a 58 mM stock solution in THF, where the THF was removed under vacuum to give solid NHC (76 uL, 0.0044 mmol). The total ratio of all three components, methyl-to-butyl-to-

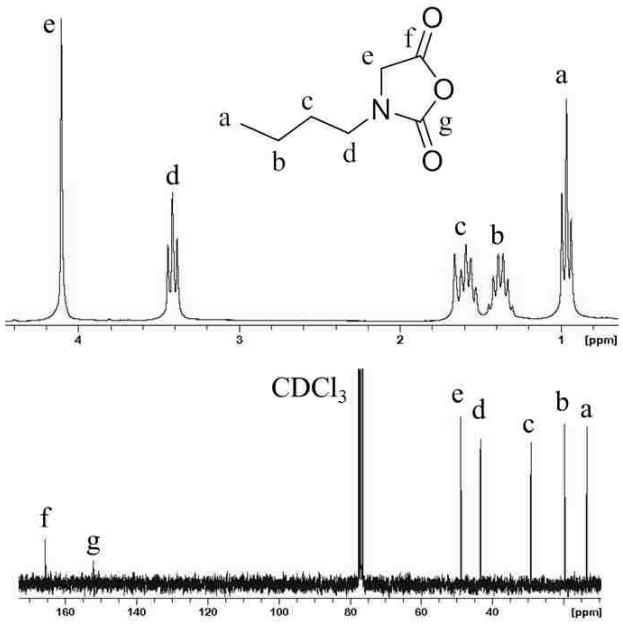

Figure 3.32. ^{1}H NMR (top) and ^{13}C {^{1}H} NMR (bottom) of butyl-NCA (MB) in toluene-d_8.

NHC was 60:40:1 respectively; however the first experiment from the ^{1}H NMR showed a slightly higher ratio 91:68:1. Some of the NHC may have been removed during the evaporation of the THF, but the same ratio of each monomer subunit was still intact. The solution was allowed to react overnight at 50^{o}C, after which, diethyl ether was used to precipitate the polymer. The white solid was filtered and washed with diethyl ether (yield 10 mg, 52%).

3.8.5. Synthesis of P(NEG-ran-NBG)

Representative Synthesis of *c*-NHC-P(NEG-*r*-NBG). Inside the glovebox, two toluene stock solutions of ME (1.1 mL, 1.0 M, 1.1 mmol) and MB (1.1 mL, 0.4 M, 0.44 mmol) were mixed with additional toluene (1.7 mL) in a vial. A measured volume of NHC/toluene stock solution (29 μL, 12.5 μmol, 69.5 mM) was then added to the above monomer solution. The vial was sealed under nitrogen and stirred at 50°C for 16 h. An aliquot of the reaction mixture was taken for conversion analysis. Excess cold hexane (~10 mL) was added to the remaining solution to precipitate the polymer. Filtration and drying under vacuum yielded the final product as a pale

yellow powder (86 mg, 60% yield). 1H NMR (δ in $CDCl_3$, ppm): 0.78-0.97 (bt, C*H*$_3$CH$_2$-, NEG), 1.03-1.20 (bt, C*H*$_3$CH$_2$-, NBG), 1.24-2.07 (bm, -C*H*$_2$C*H*$_2$CH$_3$), 3.20-3.57 (bm, -NC*H*$_2$CH$_3$, -NC*H*$_2$CH$_2$), 3.85-4.40 (bm, -COC*H*$_2$-), 7.33 (d, -CC*H*CHC*H*C-, NHC end group), 7.60 (t, -CCHC*H*CHC-, NHC end group), 8.10 (s, -NC*H*C*H*N-, NHC end group).

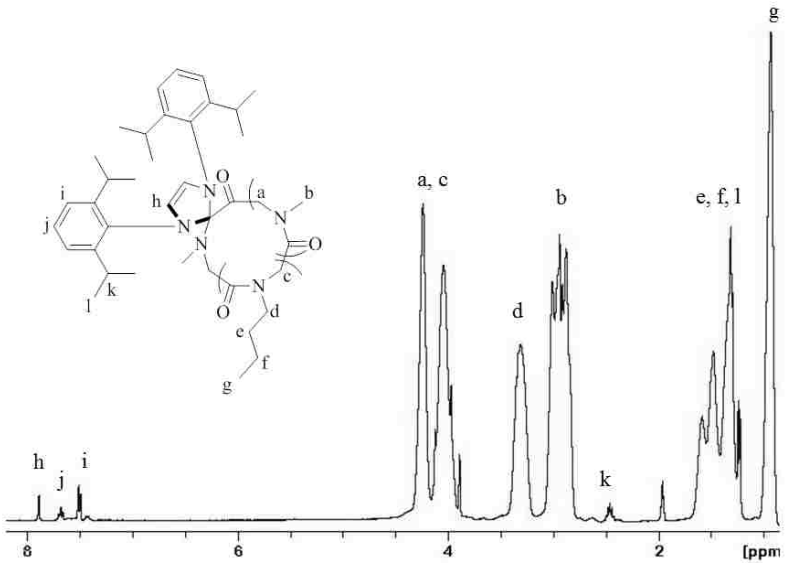

Figure 3.33. ^{1}H NMR of P(NMG-r-NBG) in CD_3CN.

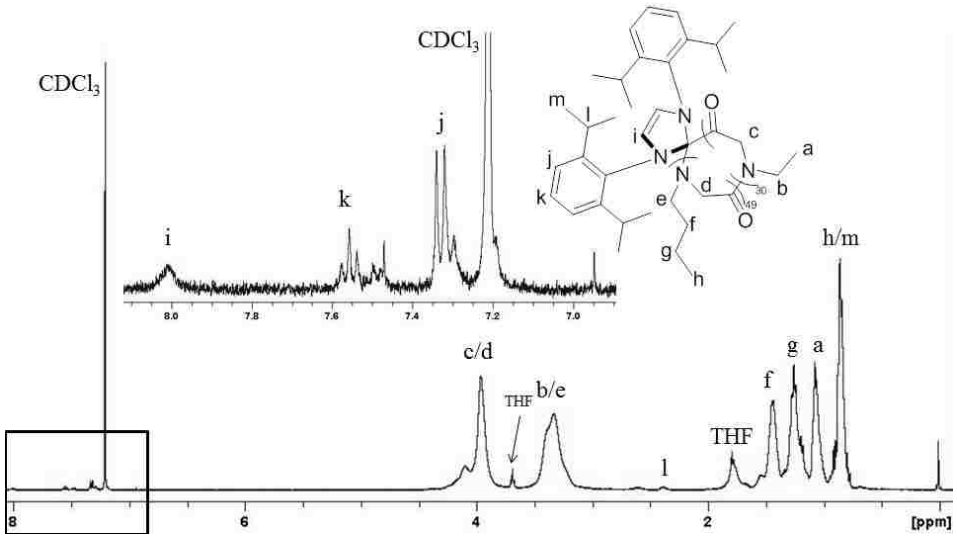

Figure 3.34. ^{1}H NMR spectrum of *c*-P(NEG$_{30}$-*r*-NBG$_{49}$) in $CDCl_3$. Integration of the methyl protons (h, a) at 1.11 and 0.88 ppm, corresponding to the NEG and NBG segments respectively, relative to that of the aromatic protons of the NHC (j, 7.37 ppm) was used to determine the polymer composition and thereby the polymer molecular weight.

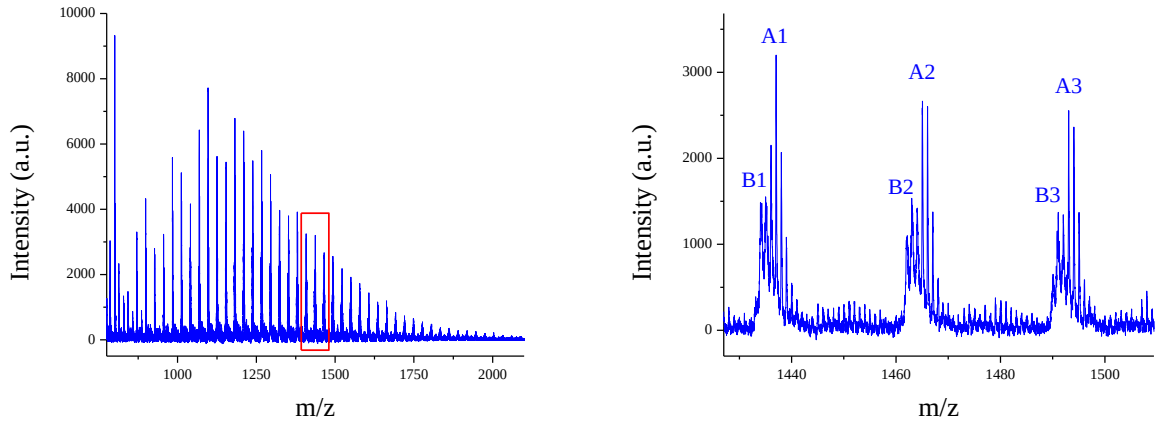

Figure 3.35. MALDI-TOF using CHCA matrix of c-P(NEG-r-NBG); M_n = 1.3 kg • mol^{-1}, PDI = 1.05.

A1 (1437.03) - [c-NHC-P(NEG$_7$-r-NBG$_4$)] H$^+$

A2 (1465.06) - [c-NHC-P(NEG$_6$-r-NBG$_5$)] H$^+$

A3 (1493.07) - [c-NHC-P(NEG$_5$-r-NBG$_6$)] H$^+$

B1 (1434.04) - [c-NHC-P(NEG$_8$-r-NBG$_3$)] Na$^+$

B2 (1462.15) - [c-NHC-P(NEG$_7$-r-NBG$_4$)] Na$^+$

B3 (1490.07) - [c-NHC-P(NEG$_6$-r-NBG$_5$)] Na$^+$

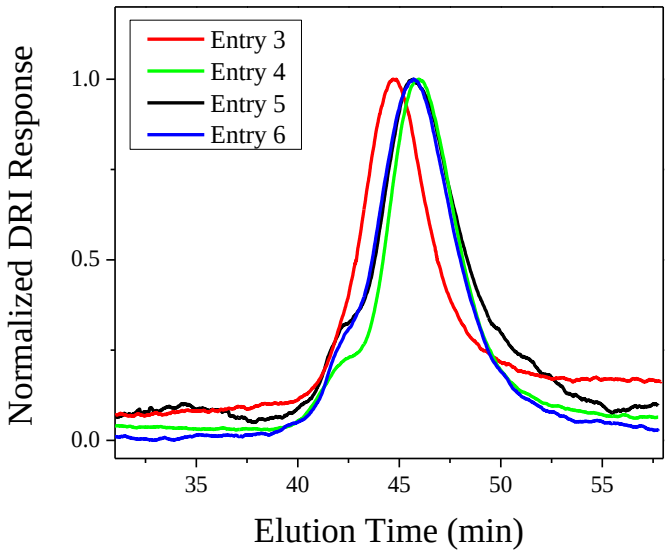

Figure 3.36. Representative SEC-DRI chromatograms of *c*-P(NEG-*r*-NBG) having different NEG compositions (Entry 3-6 **Table 3.1**) in DMF/LiBr (0.1M) at 50°C, but similar hydrodynamic radii.

Representative Synthesis of *l*-Bu-P(NEG-*r*-NBG). Inside the glovebox, two toluene stock solutions of ME (0.7 mL, 1.0 M, 0.7 mmol) and MB (585 µL, 0.4 M, 0.233 mmol) were mixed

with additional toluene (1.0 mL) in a vial. A measured volume of butylamine/toluene stock solution (116 μL, 9.3 μmol, 80.1 mM) was added to the above monomer solution. The vial was sealed under nitrogen and stirred at 50 °C for 16 h. An aliquot of the reaction mixture was taken for conversion analysis. Excess cold hexane (~10 mL) was added to the remaining solution to precipitate the polymer. Filtration and drying under vacuum yielded the final product as a white powder (36 mg, 42% yield). ^{1}H NMR (δ in $CDCl_3$, ppm): 0.82-1.00 (bt, C*H*$_3$CH$_2$-, NEG), 1.05-1.21 (bt, C*H*$_3$CH$_2$-, NBG), 1.23-1.70 (bm, -C*H*$_2$C*H*$_2$CH$_3$), 3.13-3.64 (bm, -NC*H*$_2$CH$_3$, -NC*H*$_2$CH$_2$-), 3.88-4.43 (bm, -COC*H*$_2$-).

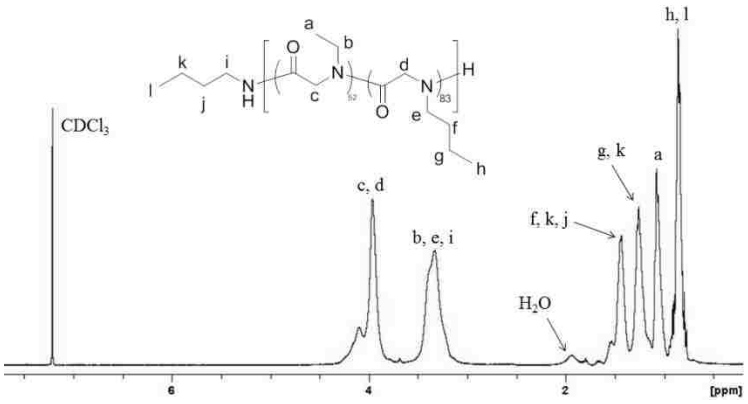

Figure 3.37. ^{1}H NMR spectrum of *l*-But-P(NEG$_{52}$-*r*-NBG$_{83}$) in $CDCl_3$.

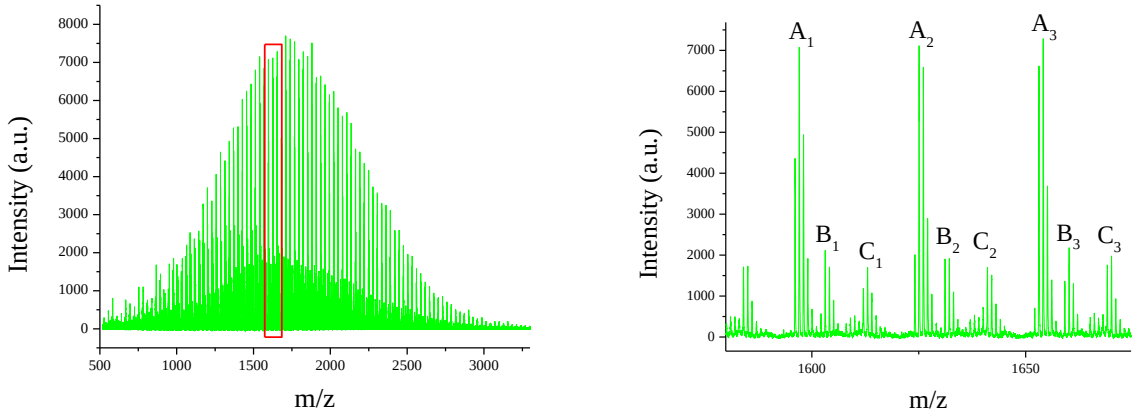

Figure 3.38. MALDI-TOF using CHCA matrix of butylamine initiated l-But-P(NEG-r-NBG); M_n = 1.5 kg • mol^{-1}, PDI = 1.08.

A_1 (1597.06) [l-Bu-P(NEG_7-r-NBG_8)] Na^+

A_2 (1625.08) [l-Bu-P(NEG_6-r-NBG_9)] Na^+

A_3 (1625.08) [l-Bu-P(NEG_5-r-NBG_{10})] Na^+

B_1 (1603.13) [l-Bu-P(NEG_{10}-r-NBG_6)] H^+

B_2 (1631.15) [l-Bu-P(NEG_9-r-NBG_7)] H^+

B_2 (1659.18) [l-Bu-P(NEG_8-r-NBG_8)] H^+

C_1 (1612.05) [l-Bu-P(NEG_9-r-NBG_7)] H^+

C_2 (1641.00) [l-Bu-P(NEG_9-r-NBG_7)] H^+

C_3 (1669.08) [l-Bu-P(NEG_9-r-NBG_7)] H^+

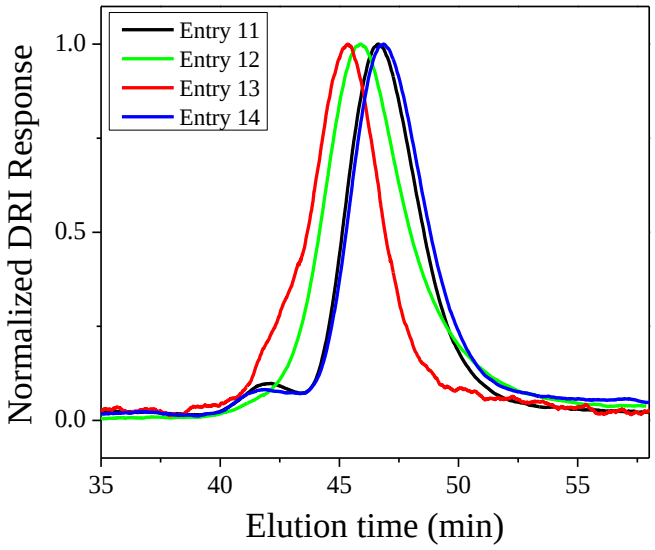

Figure 3.39. SEC-DRI chromatograms of butylamine initiated *l*-P(NEG-*r*-NBG)s having different polymer composition (Entries 11-14, **Table 3.1**) in DMF/LiBr (0.1M) at 50°C.

Representative Synthesis of *l*-Bn-P(NEG-*r*-NBG). Inside the glovebox, two toluene stock solutions of ME (0.4 mL, 1.0 M, 0.4 mmol) and MB (332 µL, 0.4 M, 0.133 mmol) were mixed with additional toluene (1.0 mL) in a vial. A known volume of benzylamine/toluene stock solution (51 µL, 3.6 µmol, 70.9 mM) was added to the above monomer solution. The vial was sealed under nitrogen and stirred at 50 °C for 16 h. An aliquot of the reaction mixture was taken for conversion analysis. Excess cold hexane (~10 mL) was added to the remaining solution to precipitate the polymer. Filtration and drying under vacuum yielded the final product as a white

powder (23 mg, 47% yield). ^{1}H NMR (δ in CD_2Cl_2, ppm): 0.82-1.00 (bt, C*H*$_3$CH$_2$-, NEG), 1.05-1.21 (bt, C*H*$_3$CH$_2$-, NBG), 1.23-1.70 (bm, -C*H*$_2$C*H*$_2$CH$_3$), 3.13-3.64 (bm, -NC*H*$_2$CH$_3$, -NC*H*$_2$CH$_2$-), 3.88-4.43 (bm, -COC*H*$_2$-), 7.26 (m, aromatic benzyl Hs).

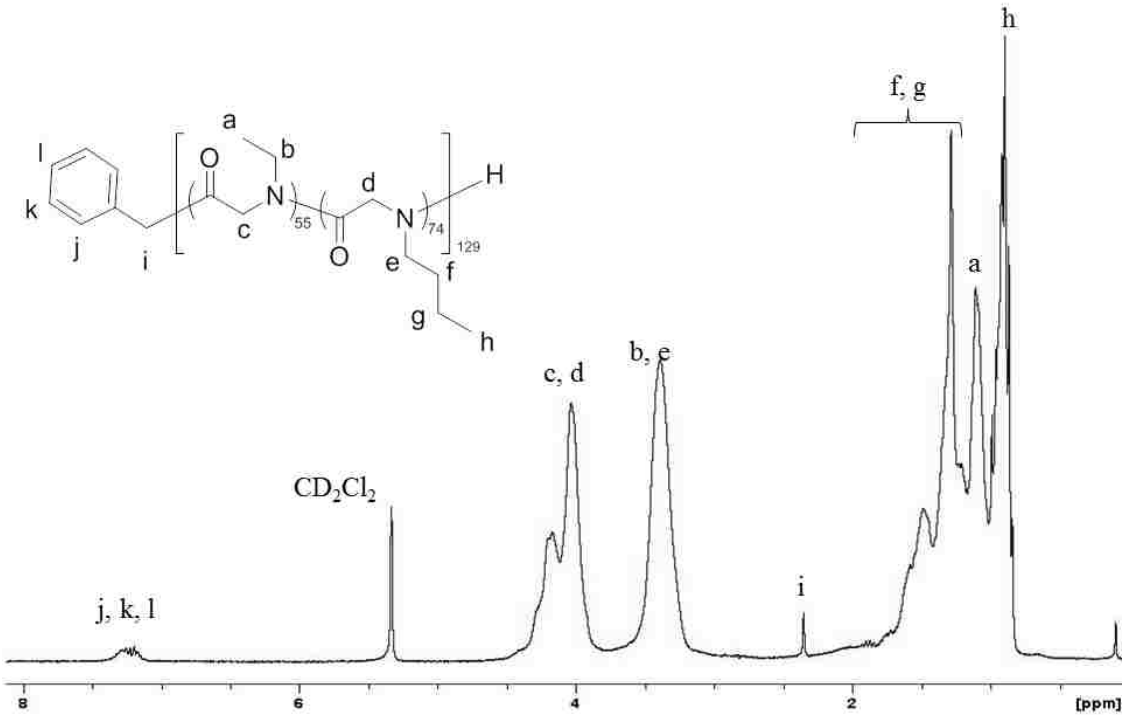

Figure 3.40. ^{1}H NMR spectrum of *l*-Bn-P(NEG$_{55}$-*r*-NBG$_{74}$) in CD_2Cl_2.

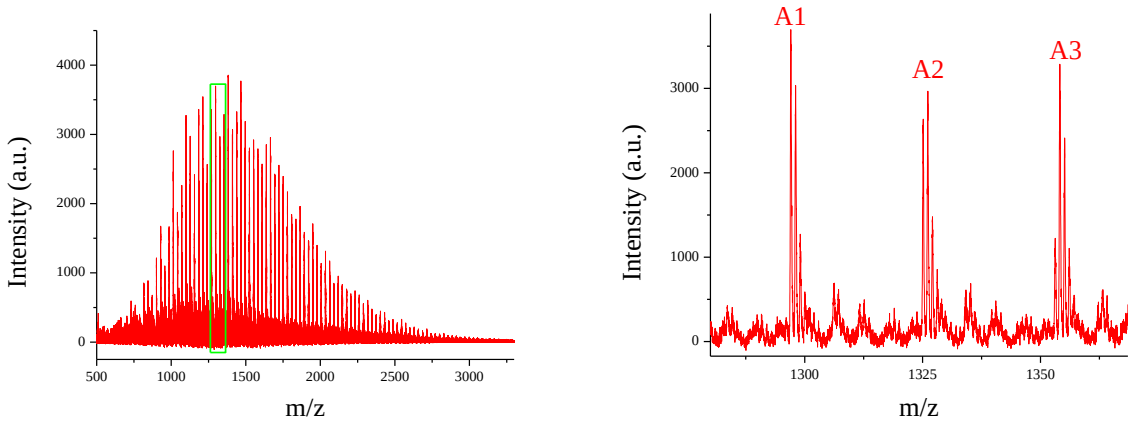

Figure 3.41. MALDI-TOF using CHCA matrix of benzylamine initiated l-Bnz-P(NEG-r-NBG); M_n = 1.4 kg • mol^{-1}, PDI = 1.16.

A_1 (1297.1) [l-Bn-P(NEG_6-r-NBG_6)] H^+

A_2 (1325.1) [l-Bn-P(NEG_5-r-NBG_7)] H^+

A_3 (1354.1) [l-Bn-P(NEG_4-r-NBG_8)] H^+

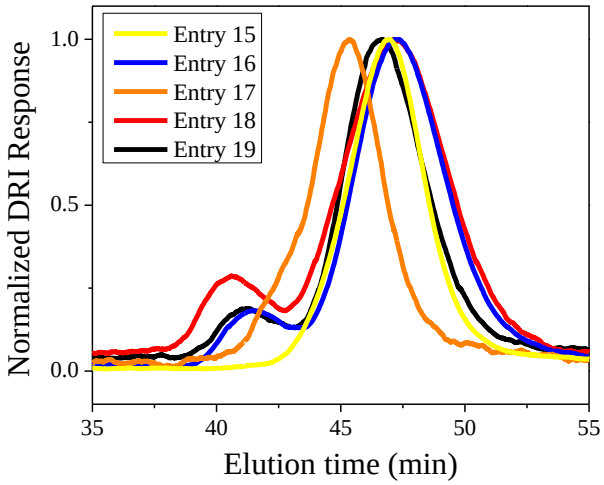

Figure 3.42. Representative SEC-DRI chromatograms of benzylamine initiated *l*-Bn-P(NEG-*r*-NBG)s having different polymer composition (Entries 15-19 in **Table 3.1**) in DMF/LiBr (0.1M) at 50°C.

3.8.6. Representative Synthesis of conversion of c-P(NEG-*r*-NBG) into l-P(NEG-r-NBG) using Acyl-Chloride Treatment

c-NHC-P(NEG_{17}-r-NBG_{11}) (27 mg, 0.009 mmol) was dissolved in toluene (1 mL). From a stock solution in toluene (0.76 M), an excess of acyl-chloride (10 equive, 0.09 mmol, 115 uL) was added to the polymer solution. The reaction was allowed to stir at room temperature for 15 minutes, during which the solution turned from yellow to clear. The polymer was purified by precipitation from hexanes (3x). Filtration and drying under vacuum yielded the final product as a white powder (22.4 mg, 83% yield). ^{1}H NMR (δ in $CDCl_3$, ppm): 0.82-1.00 (bt, C*H*$_3$CH$_2$-, NEG), 1.05-1.21 (bt, C*H*$_3$CH$_2$-, NBG), 1.23-1.70 (bm, -C*H*$_2$C*H*$_2$CH$_3$), 2.36 (s, -CCH$_3$, Acyl), 2.43 (m, -C*H*(CH$_3$)$_2$, NHC), 3.13-3.64 (bm, -NC*H*$_2$CH$_3$, -NC*H*$_2$CH$_2$-), 3.88-4.43 (bm, -COC*H*$_2$-), 7.39 (d, - C*H*CHC*H* -, NHC), 7.61 (t, -CHC*H*CH-, NHC) and 8.11 (s, -NC*H*C*H*N-, NHC).

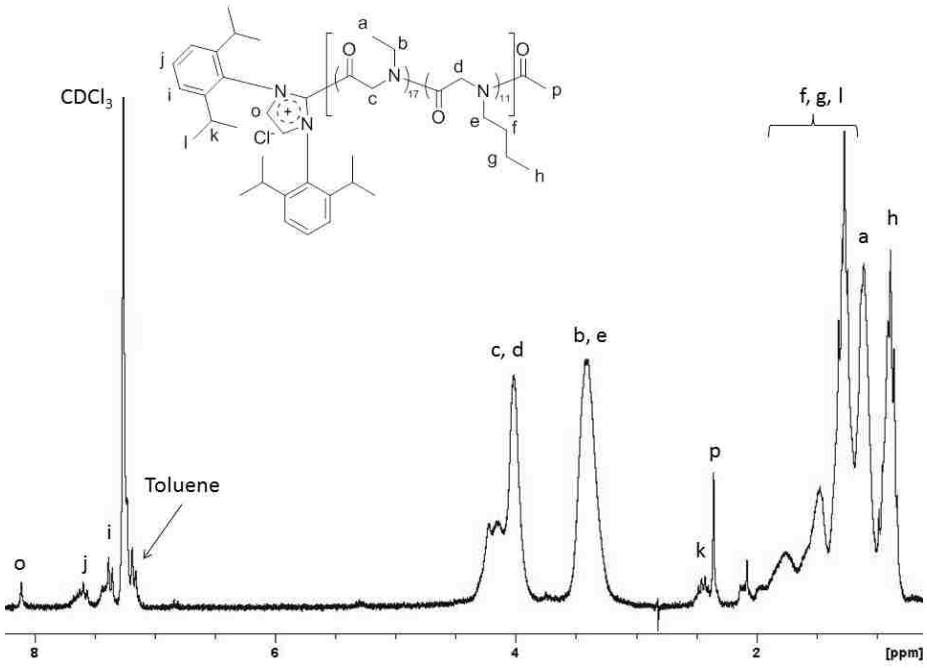

Figure 3.43. ^{1}H NMR of acyl-chloride treated copolymer in $CDCl_3$. According to the ^{1}H NMR, the ratio of the integration of the methyl protons of the ethyl and butyl moieties (a and h respectively) quantifies the ethyl composition as being 60.8%, which suggests that the composition of the original cyclic copolypeptoid (Entry 8, *c*-P(NEG_{17}-r-NBG_{11}) was not disturbed during the acylation (61% ethyl composition for Entry 8).

Chapter 4. Synthesis and Characterization of Brush-Star Copolypeptoids.

4.1 Objectives and First Observations

Using the copolymerization technique towards the synthesis of thermoresponsive copolypeptoids allowed for the access of many temperatures that are not typically witnessed in a hompolymeric system. These copolypeptoids proved helpful in learning more about architecture's effect on the physical aspects of thermoresponsive polymer. The desire to learn more about these architectural effects on the thermoresponsive behavior of copolypeptoids inspired the work presented in this chapter. The ROP of R-NCA monomers allows for a variety of end groups. Many primary amines (butyl-, benzyl-, propargyl, allyl-, and pyrene-) have been used to polymerize R-NCAs. By installing functionality into the end-groups of these thermoresponsive polymers, post-polymerization modifications can be made to synthesize interesting architectures. In Chapter 2, post-polymerization modifications (CuAAC of PEG-N_3 and PNPgG) have already been used in the synthesis of macrocyclic brushes. These macrocyclic brushes were prepared using the grafting-to approach to make brush copolymers. A different method, grafting-through, was used to synthesize linear brush copolypeptoids.

In this chapter, norbornene-end-group functionalized thermoresponsive copolypeptoid will be used to synthesize a brush copolymer. These brush copolypeptoids are named 'brush-stars' due to a combination of the shape and synthetic approach used to make this structures. The thermoresponsive characteristics of these copolypeptoids were observed to have profound differences from their linear components. The synthesis of brush copolymers has already been discussed (**Chapter 2.2.1**) and only the synthesis and characterization of thermoresponsive brush copolymers will be discussed here. As seen in Chapter 3, the architecture appears to affect the thermoresponsive behavior of these copolypeptoids.

4.2 Stimuli Responsive Materials

Stimuli-responsive materials have been widely explored due to their potential applications in "smart" materials.[190, 191] These thermoresponsive polymerss demand interest due to their applicability to the nano- and biotechnological fields.[127, 191-193] Polymer's whose solubility decreases in a solvent as the temperature increases are considered to exhibit lower critical solution temperature (LCST) behavior. The LCST behavior of thermoresponsive polymers in aqueous media has been widely studied due to their applicability in biological applications.[101] The most often investigated thermoresponsive polymer is poly(*N*-isopropylacrylamide) (PNIPAAm).[194] This homopolymer has a phase transition at nearly 32^{o}C, which makes PNIPAAm appealing towards biomedical applications.[194] While PNIPAAm's importance to the understanding of this physical transition cannot be overstated, investigations to find novel thermoresponsive systems have led to interesting discoveries regarding LCST behavior.

The ability to tune the LCST behavior of PNIPAAm (i.e. control the temperature at which the physical response occurs) is accomplished by using a salt (kosmotropic or chaotropic), controlling the concentration of the homopolymer in solution, changing the end-groups of PNIPAAm or controlling the molecular weight.[179, 195] Alternatively, polymerizing two monomers that have varying water solubilities allows for control of the LCST behavior.[177] This method is commonly referred to as the co-monomer approach. The thermal response of co-poly(methyl ethylene oxide methacrylate-oligo ethylene glycol methacrylate) has been investigated and it was demonstrated that the temperature at which the copolymer underwent a physical response could be increased or decreased by adjusting the copolymer composition.[137] This co-monomer synthetic route has also been used in the investigation of polyoxazolines. The

LCST behavior of ethyl and *n*-propyl copolyoxazolines is tuned by varying the monomer ratio and the molecular weight of the copolymer.[196] In a similar fashion, copolypeptoids were shown to undergo physical responses to changes in temperatures that were dependent on the co-monomer ratio and chain topology. The ability to tune the thermal response of these copolypeptoids spanned many different temperatures (23-63^{o}C).[197]

4.3 Thermoresponsive Brush Copolymers

Using thermoresponsive polymers in the design of interesting polymer architectures such as brush and star polymers has been an investigated topic.[101] New synthetic strategies have allowed for more direct routes to previously difficult-to-obtain molecular architectures. Synthetic strategies including the grafting-to, grafting-from and grafting-through approaches allow for direct routes towards brush polymers.[198] With a poly-2-bromisobutyryloxyethyl methacrylate macroinitiator, the grafting-from approach was utilized to grow PNIPAAm side chains using atom transfer radical polymerization (ATRP).[199] These brush copolymers collapsed in aqueous solution at the cloud point temperature of PNIPAAm. The grafting-from method has also been exploited to tune the response of core-shell thermoresponsive brush copolymers of poly(propylene oxide)-*block*-poly(ethylene oxide).[200] Core-shell brushes exhibited both intramolecular chain contraction/association along with intermolecular aggregation at varying temperatures. The grafting-to approach towards thermoresponsive brush polymers has also been implemented in several accounts. The grafting-to approach was utilized with the reactive butenyl repeat unit of the statistical co-poly[2-(isopropyl/3-butenyl)-2-oxazoline] copolymer.[201] Using the thiol/ene reaction, small molecules were grafted onto the oxazoline backbone which allowed for precise control of the cloud point temperature. The thermal properties of polypeptoid-based brush copolymers have been utilized in the grafting-to approach as well.[83] 1-

thiolglycerol was grafted onto the poly-(*N*-allyl glycine) backbone and was shown to increase the temperature at which the thermal response took place.

Here, we present an investigation into the synthetic challenges and physical differences of polypeptoid brush-star copolymers containing a polynorbornene backbone. We have named these molecules 'brush-stars' because their shape resembles a star but their architecture is that of a brush. Via the grafting-through approach, the brush-stars were synthesized using a norbornene macromonomer (**Scheme 4.1**). The LCST behavior of the system can be controlled during the macromonomer synthesis, which is the ring-opening copolymerization of a water soluble (ethyl) and water insoluble (butyl) N-substituted *N*-carboxyanhydride (NCA) monomer. The monomer determines the temperature at which the copolymer undergoes the physical response. The macromonomer is then polymerized using Grubb's 2nd generation catalyst in the ring-opening metathesis polymerization (ROMP) of norbornene. Due to the amine functionality on the end-groups of the macromonomer, the ROMP of norbornene was limited to low conversions and low degrees of polymerization (~25). The low DP of the brush backbone is the reason for the star-like shape. These brush-stars exhibited different LCST behaviors from their corresponding macromonomers.

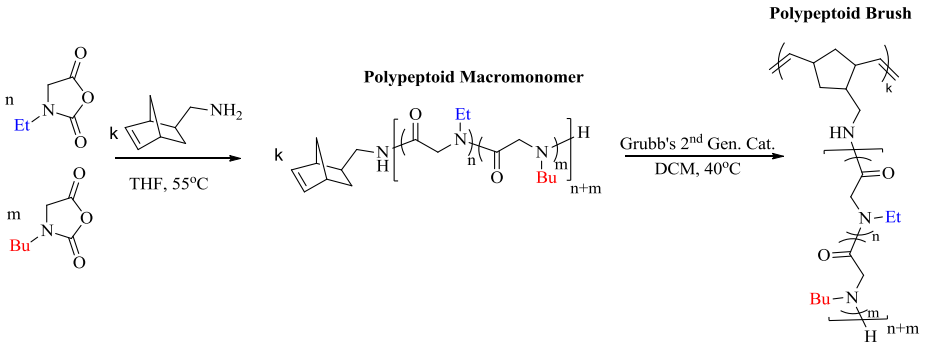

Scheme 4.1. Synthesis copolypeptoid macromonomer and copolypeptoid brush-star

The thermoresponsive behaviors of the macromonomers and the brush-stars were measured using an optical microscope with a Mettler FP 80 central processor temperature control system heating stage and a photomonitor. Each sample was sealed in a Vitrocom cell and heated at a constant rate of 1^{o}C/min. The cloud point temperatures (T_{CP}) and the transmittance windows (TW) are considered to be the temperature at 50% transmittance and the difference of the temperatures at 1% and 99% transmittance respectively.

4.4. Results and Discussion

4.4.1 Macromonomer Synthesis

The macromonomer synthesis was achieved through the ring-opening copolymerization of the water soluble ethyl- (ME) and water insoluble butyl-NCA (MB) monomers initiated by a primary amine functionalized 5-norbornene-2-methylamine. When using a butylamine initiator, ME and MB have a reactivity ratio near one (r_{ME} = 1.08(8) and r_{MB} = 0.98(2)), indicating that the primary-amine initiated copolymerization of these two monomers yields a random copolymer.[197] Molecular weights and hydrophilicity of the macromonomers are controlled through the monomer-to-initiator and ME:MB ratios respectively (**Table 4.1**). M_n values were determined using end group analysis of the norbornene allyl protons in toluene-d8 (**Figure 4.10**). As the ethyl moiety is increased within the copolymer, the T_{CP} increases (**Figure 4.2** and **4.3**), which is in good agreement with previous findings.[197]

4.4.2. Brush-Star Synthesis

Grubb's 2^{nd} generation catalyst was used for the ring-opening metathesis polymerization of the macromonomer. Kinetic studies using Grubb's catalysts (2^{nd} and 3^{rd}) indicated that neither catalyst allowed for the complete conversion of the macromonomer. The inability to reach high macromonomer conversions (i.e. obtain a longer backbone) could potentially be attributed to the secondary amine end-group of the polypeptoid side chain. Primary and

secondary amine functionalized norbornenes have been found to be inactive towards some metal-mediated catalytic ROMP systems.[202-204] Attempts to extend the polynorbornene backbone resulted in lower macromonomer conversions, so the polynorbonene backbone was kept to low degrees of polymerization (DP = 25) to maximize macromonomer conversion (**Table 4.6**). After termination and precipitation, the unreacted macromonomer was removed from the solution prior to LCST measurements by a centrifugal filter tube (10 kDa MWCO, **Figure 4.11**). ^{1}H NMR was used to confirm the structure of the brush star (**Figure 4.12**).

4.4.3. Thermoresponsive Behaviors of Macromonomers and Brush-Stars

The LCST behavior of the brush-stars with thermoresponsive polypeptoid side chains exhibited different characteristics than their macromonomer components. The linear polypeptoid (macromonomer: Nor-P(NEG_{38}-*ran*-NBG_{30})) experienced a phase transition in distilled water that corresponded to the ethyl mole percent (T_{CP} 46.6 ^{o}C at an ethyl mol% of 56%). However, the brush-star made from this macromonomer ($PNor_{25}$-g-P(NEG_{38}-*ran*-NBG_{30})) had no noticeable turbidity changes in the temperature range studied (**Figure 4.1A**). To induce LCST behavior in the brush-star, the bio-relevant and kosmotropic salt NaCl (1 M) was added to the system. Not only did the kosmotropic salt induce LCST-like behavior in the brush-star, the T_{CP} of the brush-star was decreased beyond that of the macromonomer in the same salted conditions (**Figure 4.1B**).

4.4.4. Use of Kosmotropic Salts to Lower T_{cp} of Brush-Star

While in the salted solution, the brush-star also exhibited a decreased TW as compared to the macromonomer. A decrease in the TW for the brush-star was observed as compared to its corresponding macromonomer for samples that contained varying amounts of ethyl mole percentages (i.e. hydrophilic content, **Figure 4.2 and 4.3**). The brush-star appears to be more resistant towards the suppression of the T_{CP} as the polymer concentration is increased (**Figure**

4.3 Right). The LCST behaviors of the macromonomer and the brush-star correlate to the amount of salt in solution; as the salt concentration is decreased, the T_{CP} of both increased (**Figure 4.4**). The macromonomer appears to have a linear relationship for T_{CP} and salt

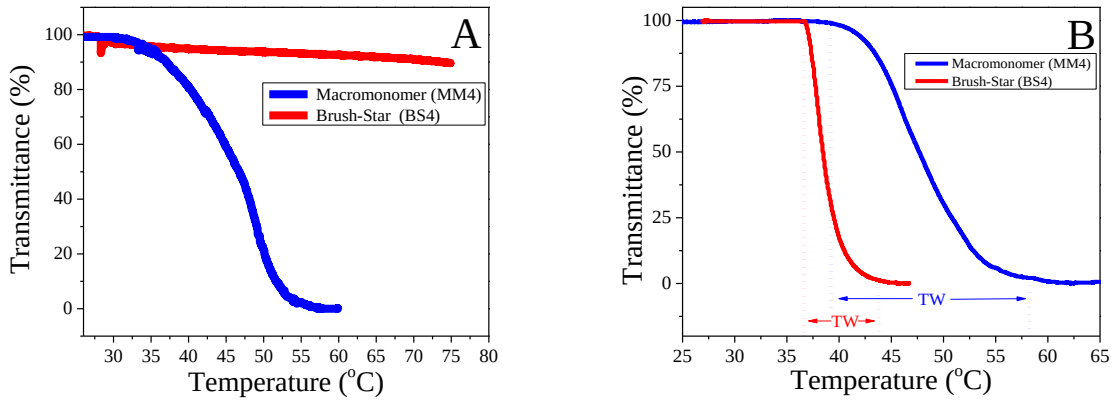

Figure 4.1. Plot of transmittance vs. temperature for the polypeptoid macromonomer (blue) and the brush-star (red) in distilled water (A) and in 1 M NaCl (B). The heating rate was 1 °C per minute for all heating cycles and the polymer concentration was 1 mg•mL^{-1}.

concentration, a phenomenon that has been documented for linear thermoresponsive polymers.[179] This differs for the brush-star system, where at low salt concentrations; the system exhibits a high sensitivity towards salt.

Kosmotropic salts have been known to decrease the solubility of proteins, polypeptoids and other thermoresponsive polymers.[181, 205] These salts can decrease the T_{CP} of thermoresponsive polymers (though the exact mechanism for this reduction in the thermoresponse is not known). Due to their high charge density, kosmotropic salts will bind to water more strongly than water can hydrogen bond to other water molecules. These salts cause the water molecules to order themselves around the ions, possibly disrupting the polymer-to-water complex, which could facilitate the precipitation of the polymer.[180] Typically, there is a linear relationship between the thermoreponsive polymer's T_{CP} and the salt concentration.[179, 183]

The T_{CP}s of these polypeptoid brush-stars appear to be very sensitive to the amount of salt in solution and do not exhibit a linear

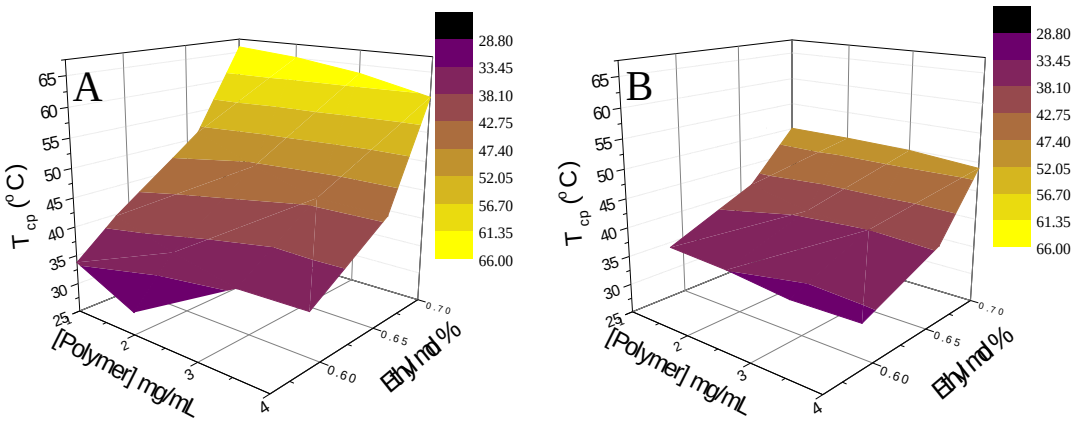

Figure 4.2. Colored surface maps of the polypeptoid macromonomers (A) and the brush-stars (B) in an aqueous solution of 1 M NaCl. Cloud point temperatures (T_{cp}) were measured as a function of polymer concentration and NEG mol content.

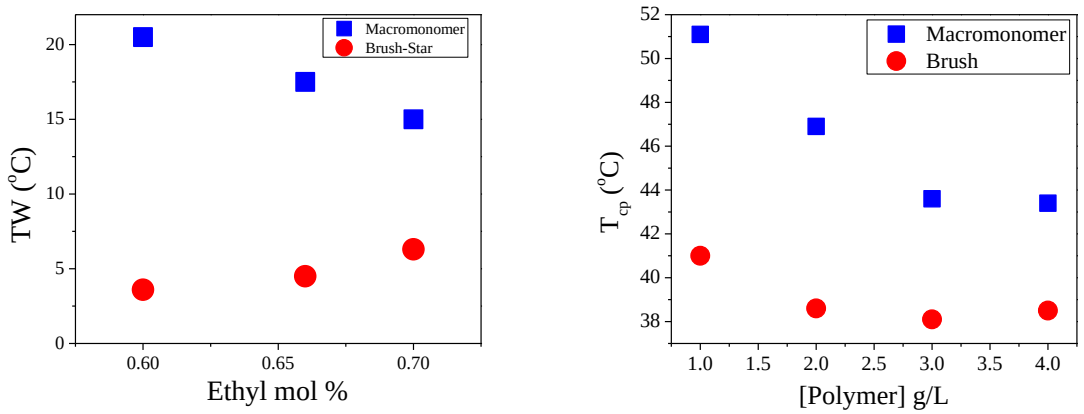

Figure 4.3. (Left) Plot of the transition window (TW) versus the ethyl mol percent for the polypeptoid macromonomer (blue) and the brush-star (red) at a 4 mg/mL concentration. (Right) Plot of T_{CP} as a function of polymer concentration for the macromonomer (Nor-P(NEG_{40}-*ran*-NBG_{21})) and its corresponding brush-star ($PNor_{25}$-g-P(NEG_{40}-*ran*-NBG_{21})).

relationship. A recent study of the effects on thermoresponsive hyperbranched dendritic polymers illustrated a similar sensitivity of 'crowded' polymers towards diluted salt conditions.[206] Hyperbranched dendritic thermoresponsive polymers exhibited a nonlinear

relationship with komsotropic salts. The thermoresponse of dendritic polymers was divided into two distinct linear regions whose characteristics are governed by the concentration of the kosmotropic salt. The densely crowded brush-star (BS3) also exhibits these two distinct linear

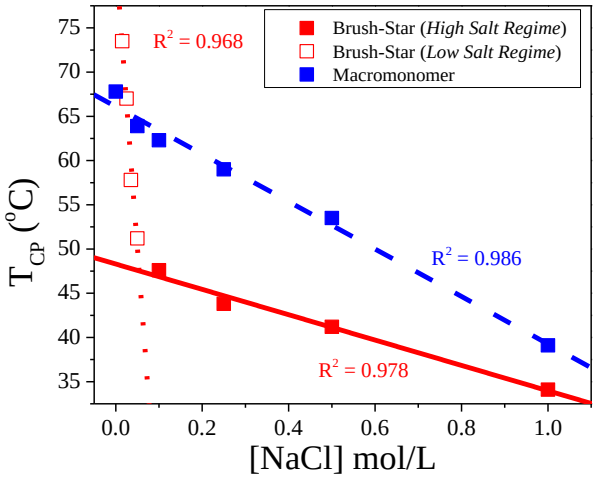

Figure 4.4. Plot of cloud point temperatures for the macromonomer (blue, Nor-P(NEG_{36}-r-NBG_{25})) and the brush-star ($PNor_{25}$-g-P(NEG_{36}-r-NBG_{25})) as a function of salt concentration. At a 0.0 M concentration of NaCl, the brush-star exhibited no cloud point temperature.

regions (filled and unfilled red squares in **Figure 4.4**) which are attributed to a *high salt regime* (filled red squares) and *low salt regime* (unfilled red squares). The linear fit from the *high salt regime* data has less drastic slope than that from the *low salt regime*, indicating that the brush-star has a hypersensitivity to the concentration of salts within the *low salt regime*. This behavior is similar to what was observed with the highly crowded dendritic polymers. However, it was observed that the dendritic polymers do have a T_{CP} in a pure aqueous solution (no salt), whereas these brush-stars do not have an observable T_{CP} (**Figure 4.5** and **Table 4.6**).

4.4.5. DLS Study of Brush-Star Size in Salted and Unsalted Solution

To help understand why these brush-stars do not have a T_{CP} in an unsalted solution, dynamic light scattering (DLS) experiments were performed to observe changes in particle size

as the temperature is varied. In a pure aqueous media, the brush-star, $PNor_{25}$-P(NEG_{38}-r-NBG_{30}) (BS4), which has no T_{CP} (**Figure 4.1A**), appears to undergo a decrease in particle size as the temperature is increased (**Figure 4.6**) (R_H sizes are roughly 40 nm at 20°C to 18 nm at 65°C).

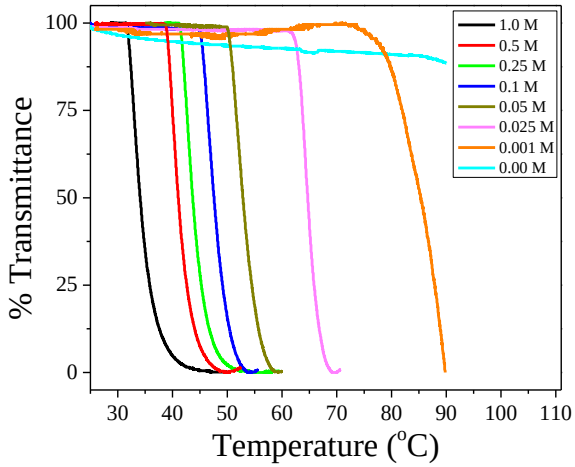

Figure 4.5. Transmittance versus temperature plot of the brush-star ($PNor_{25}$-g-P(NEG_{36}-*r*-NBG_{25})) in various concentrations of salt. At 0.01 M, a TCP could not be determined because no baseline at 0% transmittance was formed. There was no significant change in transmittance for the 0.00 salt concentrations (cyan lines respectively).

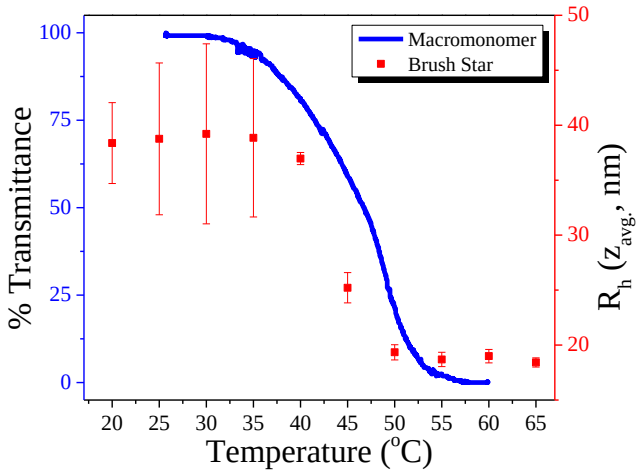

Figure 4.6. Double Y-plot of the transmittance of the macromonomer, Nor-P(NEG_{38}-r-NBG_{30}) (blue, left) and the particle size of the brush-star, $PNor_{25}$-P(NEG_{38}-r-NBG_{30}) (red, right), as

determined by multiple dynamic light scattering (DLS) experiments. Each polymer sample was in an aqueous solution (1 mg/mL). The heating rate for the transmittance experiments was 1°C/min. The brush-star was allowed to equilibrate at each temperature for 5 minutes before the DLS experiment was performed.

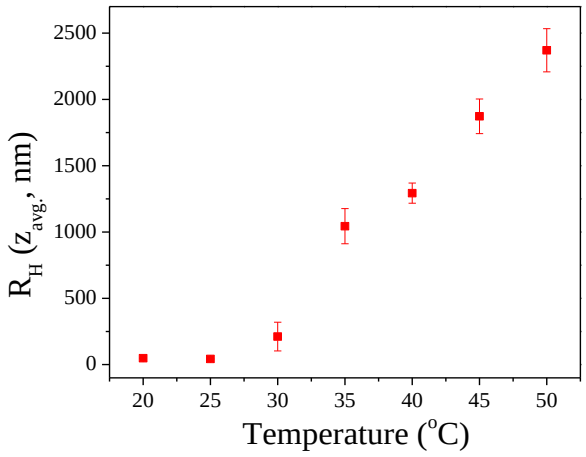

Figure 4.7. Dynamic light scattering experiment (DLS) of the brush-star $PNor_{25}$-g-P(NEG_{38}-r-NBG_{30}) dissolved in a 0.25 M NaCl aqueous solution (1 mg/mL). The sample was allowed to equilibrate at each temperature for 5 minutes before the experiment was performed.

This decrease in particle size corresponds well to the thermoresponsive behavior of the brush-star's macromonomer component (MM4) (blue transmittance overlaid in **Figure 4.6**). The decrease in size could be attributed to an intra-molecular collapse of the brush-star in an unsalted solution. Star polymers have been shown to decrease in size at low polymer concetrations (0.3 wt.%).[207] However, in a salted solution (0.25 M), the same brush-star appears to increase in particle size as the temperature is increased, which could correspond to inter-molecular aggregation (**Figure 4.7**). Intra-molecular collapses and inter-molecular aggregation has been observed in other thermoresponsive brush systems, though the addition of a kosmotropic salt did not appear to be the reasons for the observed collapse and aggregation.[200]

4.4.6 AFM Characterization of Brush-Star Copolymers

Tapping mode atomic force microscopic (AFM) characterization of the brush-stars was performed on sample $PNor_{25}$-g-P(NEG_{36}-*ran*-NBG_{25}) to illustrate the architecture of the polymer nano-particles (**Figure 4.8**). The AFM sample was prepared by drop cast of a 0.02 mg/mL aqueous solution of the polymer. Since the brush-stars' copolypeptoid side chains have are longer (theoretical length 23.7 nm) than the average polynorbornene backbone length (theoretical length 16.2 nm), the morphologies of these particles appear to be star-like. The large distribution of sizes witnessed in the AFM can be attributed to the lack of control of the macromonomer (norbornene) polymerization.

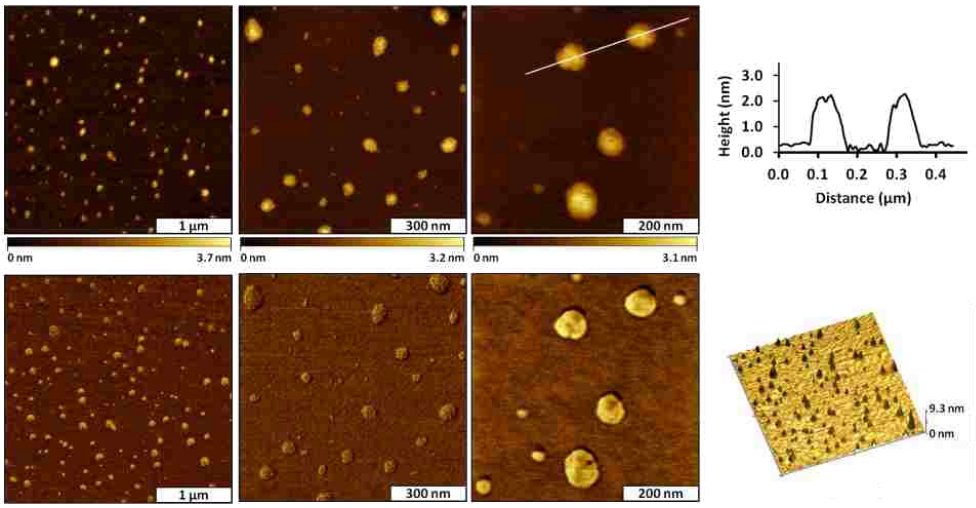

Figure 4.8. AFM topography and phase images of $PNor_{25}$-g-P(NEG_{36}-*ran*-NBG_{25}). Sample was drop-casted onto a micah surface from a 0.02 mg/mL aqueous solution.

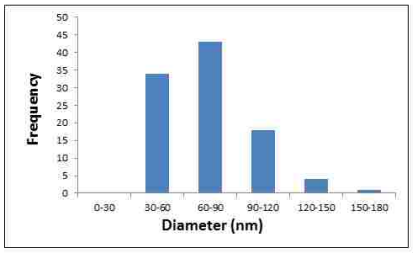

Average diameter: 74.4 nm

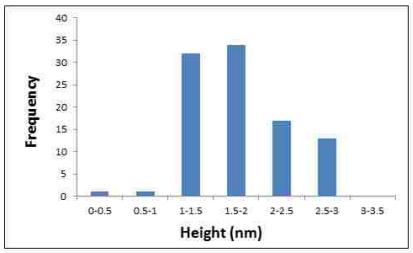

Average height: 1.8 nm

Figure 4.9. Histograms of diameter and height (nm) of $PNor_{25}$-g-P(NEG_{36}-*ran*-NBG_{25}) from samples that were drop-casted onto a micah surface from a 0.02 mg/mL aqueous solution.

4.5 Potential Explanation of Differences between the Thermoresponsive Behavior of Linear and Brush-Stars Copolypeptoids

Limited research has been performed on the potential reasons for the observed occurrence that sterically crowded polymers exhibit a high sensitivity towards the concentration of salts. This is the first report of a brush-star that does not have a T_{CP} in an aqueous solution. A potential reason for this interesting thermoresponse in the brush star could be linked to concentration of the polymer structure in solution. Just as there is a critical concentration for micelles to form in amphiphilic block copolymers,[208] there may be a critical concentration for these brush copolymers to exhibit a thermoresponse. Though the amount (moles) of each copolypeptoid segment is identical when comparing the linear to the brush-star copolymers, the concentration of each polymer is not. The linear copolypeptoids have a much higher polymer concentration than do the brush-stars because the copolypeptoids are covalently linked in the brush-star structure. There may be a polymer concentration dependence on the thermoresponsive behaviors for the entire copolypeptoid system. It was shown that the T_{cp} of the

linear copolypeptoids is dependent on their concentration (**Chapter 3.6.3.2**) and this may be dependence could be related to the number of moles of polymers in solution and not its weight percent. Further concentration studies into the brush-star and linear copolypeptoid systems need to be performed to confirm this assertion.

4.6 Conclusion

Thermoresponsive brush-star copolymers have been synthesized using the grafting-through method. These copolymers were synthesized by the ROMP of a norbonene modified thermoresponsive copolypeptoid (ethyl- and butyl- substituted). These brush-stars exhibited notable differences in their thermoresponsive behaviors from their linear macromonomer components, including a decreased TW, higher sensitivity towards the kosmotropic salt NaCl and no observable T_{CP} in distilled water. These densely grafted copolymers may undergo an intra-molecular chain collapse in distilled water as opposed to the linear macromonomer which has been previously shown to undergo inter-molecular aggregation.[197] Distinctions in the thermoresponsive behaviors between the two architectures could help further the understanding of how architecture effects the thermoresponsive behavior of a polymer. Also, due to the compact morphology of these peptidomimetic brush-stars, this research may aid in the understanding of how proteins, which also have compact morphologies, fold in salted solutions.

4.7 Synthetic Procedure

Materials. Glyoxylic acid monohydrate (98%), butylamine (98%), ethylamine (99%) di-*tert*-butyl dicarbonate (97%), triethylamine, phosphorous trichloride and 5-norbornene-2-carbonitrile were all purchased from Sigma Aldrich and used as received. All the solvents used in this study was purchased from Sigma-Aldrich, and purified by passing through alumina columns under

argon. *N*-ethyl *N*-carboxyanhydride (M_1) and *N*-butyl *N*-carboxyanhydride (M_2) were synthesized by adapting a reported procedure[7, 197].

Instrumentation. ^1H and ^{13}C $\{^1H\}$ NMR spectra were recorded on a Bruker AV-400 spectrometer, and the chemical shifts in parts per million (ppm) were referenced relative to proton impurities or ^{13}C isotope of deuterated solvents (e.g., $CDCl_3$ or toluene-d_8), respectively. SEC analyses were conducted using an Agilent 1200 system (Agilent 1200 series degasser, isocratic pump, auto sampler and column heater) equipped with three Phenomenex 5 μm, 300×7.8 mm columns [100 Å, 1000 Å and Linear(2)], Wyatt DAWN EOS multi-angle light scattering (MALS) detector (GaAs 30 mW laser at λ=690 nm), Wyatt ViscoStar viscometry(VISC) detector and Wyatt Optilab rEX differential refractive index (DRI) detector with a 690 nm light source. DMF containing 0.01 M LiBr was used as the eluent at a flow rate of 0.5 mL·min^{-1}. The column temperature was 50°C and the detectors temperature were 25°C. All data analyses were performed using Wyatt Astra V 5.3 software. Polymer molecular weight (M_n) and molecular weight distribution (PDI) were obtained by conventional SEC analysis with a calibration curve. The calibration curve was constructed from twenty three pauci-disperse polystyrene standards (M_n =590 g·mol^{-1}-1472 kg·mol^{-1}, Polymer Laboratories, Inc.) using Astra's column calibration template. Relative M_n and PDI was then calculated using Astra's conventional calibration template. Dynamic light scattering (DLS) analysis was conducted on a Malvern Zetasizer Nano-ZS instrument using the Zetasizer software version 6.12.

T_{CP} Determination (Turbidity Measurements)

Cloud point temperatures were measured by dissolving the polymer sample in either salted or unsalted water at a predetermined polymer concentration. This aqueous solution was then

transferred to a vitro-dynamic cell which was sealed at both ends. The Vitrocom cell walls were 1.0 mm in thickness. The polymer solution was then placed in a Mettler Heating Stage, from which the control of the temperature ramp could be accessed using controller Mettler Fp 80 central processing unit. The heating rate was 1 ^{o}C/min unless otherwise stated. An Olympus optical microscope was used to collect the transmittance through the sample on the Mettler heating stage and the intensity was collected by a Mettler photomonitor. This process has been outlined in the Mettler handbook.[209] After transmittance normalization, the cloud point temperature (T_{CP}) was determined to be the temperature at 50% transmittance.

Synthesis of ethyl-N-carboxyanhydride (ME)

Ethyl-NCA were synthesized according the reported procedure.[197]

Synthesis of butyl-N-carboxyanhydride (MB)

Ethyl-NCA were synthesized according the reported procedure.[197]

Synthesis of 5-Norbornene-2-methylamine (I_N)

The synthetic procedure was taken from the reported procedure[210]. Yield: 1.92 g (62%). ESI-MS calculated for $C_8H_{18}N$, m/z is 123.19; found, m/z 124.0, which is (I_N) + H^+.

Synthesis of Nor-P(NEG_{27}-r-NBG_{17})

From a 3 M stock solution of ME in THF (1 mL, 3 mmol) and from a 1 M stock solution of MB in THF (0.75 mL, 0.75 mmol) were added to a vial and diluted with THF (0.4 M, 9.4 mL total THF). From a stock solution in THF (338 mM), the norbornene-amine (228 uL, 0.075 mmol) was added to the monomer solution. The reaction vial was sealed under nitrogen and heated to 50^{o}C for 18 hours. The polymer solution was concentrated and hexanes were added to

precipitate the polymer from solution. The dry polymer was filtered and dried under vacuum to give a white solid (223.3 mg, 66 % yield).

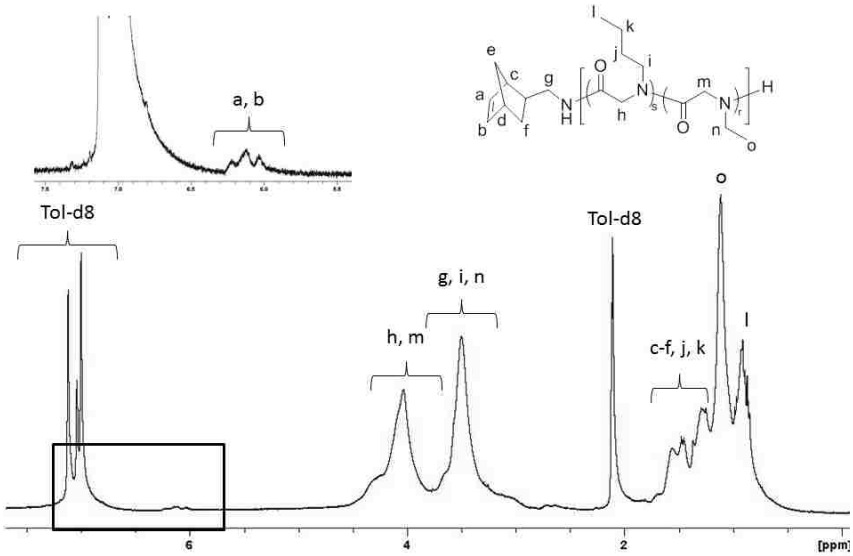

Figure 4.10. ^{1}H NMR of Nor-P(NEG$_{27}$-r-NBG$_{17}$) in toluene-d8.

Table 4.1. Macromonomer synthesis.

Trial	[ME$_0$]:[MB$_0$]:[Nor$_0$]	NEG:NBG:Nor	M_n[a]	Mol% Ethyl[b]	M_n[c]	PDI[c]
MM1(828A)	44:6:1	43:18:1	5.7	70	8.8	1.04
MM2(905A)	40:10:1	40:21:1	5.8	66	8.4	1.06
MM3(905B)	38:12:1	36:25:1	5.9	59	8.6	1.05
MM4(905D)	33:17:1	38:30:1	6.7	56	8.9	1.06

a- Determined from the ^{1}H NMR end-group integration analysis of the norbornene alkene protons. b- Determined from the ^{1}H NMR integration of the methyl side chain of the ethyl and butyl repeat units. c- Determined by SEC-DRI using polystyrene standards in DMF/LiBr (0.01 M).

Table 4.2. Macromonomer TCP by varying the polymer concentration.

Trial	Macromonomer[a]	[Polymer] mg/mL	T_{CP} (^oC)[b]	TW (^oC)[c]
MM1	Nor-P(NEG_{43}-r-NBG_{18})	1	66.0	20.2
		2	65.1	14.8
		3	63.5	13.6
		4	60.9	15.0
MM2	Nor-P(NEG_{40}-r-NBG_{21})	1	51.1	21.6
		2	46.9	17.7
		3	43.6	20.7
		4	43.4	17.5
MM3	Nor-P(NEG_{36}-r-NBG_{25})	1	39.7	19.6
		2	36.4	19.6
		3	33.9	18.8
		4	34.2	20.5
MM4	Nor-P(NEG_{38}-r-NBG_{30})	1	33.8	16.4
		2	28.9	18.3
		3	DND	-
		4	DND	-

a- Copolymer composition was determined by ^1H NMR integration of the methyl protons from the ethyl and butyl repeat units. b-Determined by turbidity measurements using an optical microscope. Cloud point temperatures are considered to be the temperature at 50% transmittance. All samples were dissolved in 1 M NaCl. c-Transition window (TW) is the temperature at 1 % transmittance minus the temperature at 99% transmittance. DND – Did not dissolve at room temperature.

Table 4.3. Macromonomer (MM3) T_{CP} by varying the salt concentration

[NaCl] (mol •L^{-1})	T_{CP}[a]	TW[b]
1.00	39.1	24.3
0.50	53.5	26.5
0.25	59.0	32.3
0.10	62.3	23.4
0.05	63.9	25.0
0.00	67.8	28.4

a-Determined by turbidity measurements using an optical microscope. Cloud point temperatures are considered to be the temperature at 50% transmittance. All samples were at a polymer concentration of 1 mg•mL^{-1}. b-Transition window (TW) is the temperature at 1 % transmittance minus the temperature at 99% transmittance.

Synthesis of the Ruthenium Catalyst

The catalyst was prepared according to the reported procedure.[120] The yield was 86%.

Synthesis of $PNor_{25}$-g-$P(NEG_{40}$-r-$NBG_{21})$

From a stock solution in toluene (13 mM), Grubbs 2nd generation catalyst (64 uL, 608 umol) was added to a solution of Nor-$P(NEG_{40}$-r-$NBG_{21})$ (120.4 mg, 0.0208 mmol) in DCM (0.01 M). The solution was sealed under nitrogen and reacted for 2 days at 40°C. The reaction solution was cooled to room temperature, concentrated and then the brush-star was precipitated using hexanes. To remove the unreacted macromonomer, the product was dissolved in a mixture of methanol and water (60:40 by volume) and transferred to a centrifugal filter tube (10 kDa MWCO). The tub was spun at 3300 rpm until nearly all the solvent had passed through the filter (roughly 0.5 mL). More of the methanol/water 60/40 solution was added and the process was repeated at least 4 times (each spin cycle was roughly 45 minutes). After the last centrifugation cycle, the solvent was removed by vacuum to yield a pink polymer product (57.0 mg, yield 47 %).

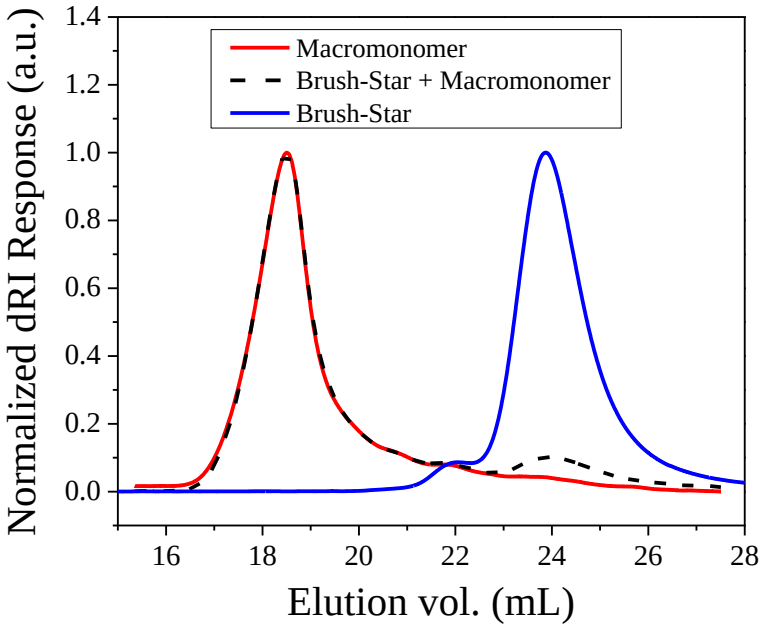

Figure 4.11. GPC-dRI traces of the macromonomer (MM2, blue) and the brush-star (BS2) before (black dashed line) and after (red) centrifugation in a 10 kDa MW cutoff Millipore centrifuge filter.

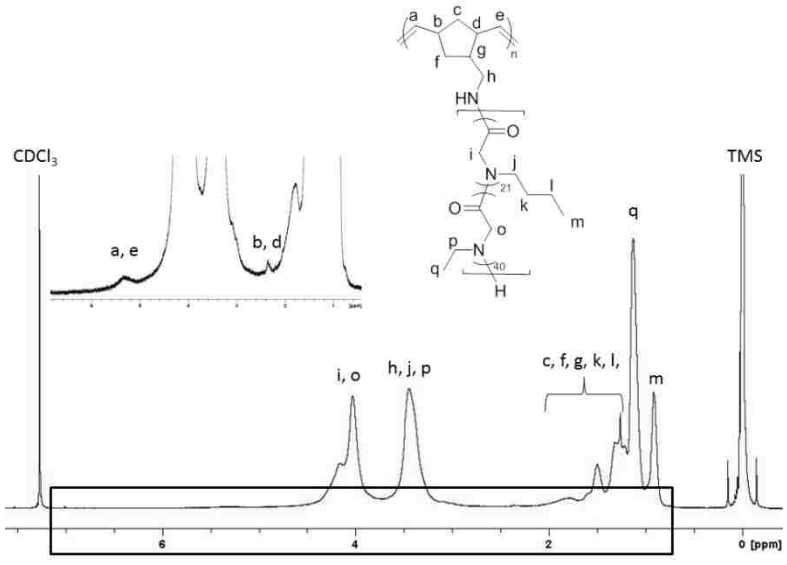

Figure 4.12. ^{1}H NMR of the brush-star BS2 (PNor-g-P(NEG$_{40}$-r-NBG$_{21}$) in $CDCl_3$.

Table 4.4. Brush-Star Synthesis.

Trial	Macromonomer (MM)	$[MM_0]:[I_{N0}]$	M_n (kg •mol^{-1})[a]	PDI[a]
BS-1	Nor-P(NEG_{43}-r-NBG_{18})	25:1	195.9	2.00
BS-2	Nor-P(NEG_{40}-r-NBG_{21})	25:1	160.0	1.82
BS-3	Nor-P(NEG_{36}-r-NBG_{25})	25:1	291.0	2.91
BS-4	Nor-P(NEG_{38}-r-NBG_{30})	25:1	290.4	2.43

a- Determined by SEC-DRI using polystyrene standards in DMF/LiBr (0.01 M).

Table 4.5. Brush-Star TCP by varying the polymer concentration.

Trial	Brush-Star[a]	[Polymer] mg/mL	T_{CP} (^oC)[b]	TW[c]
1	$PNor_{25}$-P(NEG_{43}-r-NBG_{18})	1	50.1	11
		2	50.1	7.7
		3	49.9	7.3
		4	49.0	6.3
2	$PNor_{25}$-P(NEG_{40}-r-NBG_{21})	1	41.0	12.2
		2	38.6	7.1
		3	38.1	3.9
		4	38.5	4.5
3	$PNor_{25}$-P(NEG_{36}-r-NBG_{25})	1	34.1	11.2
		2	33.5	6.7
		3	32.2	3.5
		4	32.5	3.6
4	$PNor_{25}$-P(NEG_{38}-r-NBG_{30})	1	DND	DND
		2	DND	DND
		3	DND	DND

Continued from previous page

Trial	Brush-Star[a]	[Polymer] mg/mL	T_{CP} (^{o}C)[b]	TW[c]
		4	DND	DND

a- Copolymer composition was determined by ^{1}H NMR integration of the methyl protons from the ethyl and butyl repeat units. b-Determined by turbidity measurements using an optical microscope. Cloud point temperatures are considered to be the temperature at 50% transmittance. All samples were dissolved in 1 M NaCl. c-Transition window (TW) is the temperature at 1 % transmittance minus the temperature at 99% transmittance. DND – Did not dissolve at room temperature.

Table 4.6. Brush-Star (BS3) T_{CP} by varying the salt concentration

[NaCl] (mol •L^{-1})	T_{CP}[a]	TW[b]
1.000	34.1	10.7
0.500	41.1	9.3
0.250	43.8	9.9
0.100	47.5	8.3
0.050	51.2	7.8
0.035	57.8	7.5
0.025	67.0	6.6
0.015	73.5	25.8
0.010	-	
0.000	-	

a-Determined by turbidity measurements using an optical microscope. Cloud point temperatures are considered to be the temperature at 50% transmittance. All samples were at a polymer concentration of 1 mg•mL^{-1}. b-Transition window (TW) is the temperature at 1 % transmittance minus the temperature at 99% transmittance.

Chapter 5. Concluding Remarks

5.1 Advancing the Field of Peptidomimetics through Polypeptoids

Peptidomimetic polymers, including polyacrylamides, polyoxazolines and poly-α-peptoids, are an emerging class of polymers that are more frequently being used in polymer physics, materials science and biology. Due to their similarities to proteins, peptidomimetic polymers further the fundamental understanding of protein folding and aggregation. These phenomena are applicable in cellular biology, enzymology and pathology. For example, Alzhemier's disease is thought to be strongly related to protein aggregation (beta-amyloid).[211, 212] Research into the formation of protein-like aggregates (peptidomimetic aggregates) will help our understanding of protein aggregation, ultimately allowing for the ability to prevent it in the case of beta-amyloid.

Until recently, poly-α-peptoids have been overshadowed by the extent of other research performed on peptidomimetic polymers. Polyacrylamides have been widely studied due to their ease of synthesis and use as thermoresponsive polymers (PNIPAAm). Since its first synthesis in the 1950s, PNIPAAm has been at the forefront of our understanding of LCST behavior.[213] Since their conception in the 1980s, polyoxazolines, which were first developed as a food additive, have become more frequently used in pharmaceutical and medical applications.[214] These peptidomimetic polymers, which also have LCST behavior, are currently being employed in clinical trials. Poly-α-peptoids do not have the extensive research histories that the other peptidomimetic polymers do. Being developed in the 1990s, polypeptoids have recently (past five years) been researched as a potential tool in protein and materials science. By contributing to the fundamental understanding of polypeptoid synthesis, characterization and physical

properties, the research presented in this dissertation has furthered the advancement of polypeptoid research.

The research into the LCST behavior of these polypeptoids could further understand protein folding and aggregation. These polypeptoids have been proven to be biocompatible and could someday replace some of the more frequently used polymer in pharmaceutical studies. The wide arrays of T_{cp}s that are available through the synthesis of copolypeptoids make them useful in biology and materials science. The ring-opening polymerizations of R-NCA monomers facilitated the synthesis of polypeptoids with interesting architectures, including linear, cyclic and brush (macrocyclic and linear) copolymers. Understanding the mechanism of the ROP of these monomers allows for the ability to control the molecular weight and topology of polypeptoids. Controlling the topology through initiator selection is unique to this class of peptidomimetic polymers, and has allowed for the synthesis of a macrocyclic brush copolymer. Facile architectural control of these polymers has allowed for complex research into how the architecture affects the macroscopic properties. The ability to synthesize these different architectures allowed for direct comparison of their LCST behaviors, linking the structural design of the polymer to its physical properties.

Polypeptoids are garnering more interest in many fields due to their facile synthesis, unique physical properties and biocompatibility. Future research in this area should be focused on the design of interesting architectures and the aggregation properties of these thermoresponsive copolymers. Questions like, 'how does architecture affect the aggregation of these peptidomimetic polymers?' can be answered using polypeptoids. Answering this question allows for a deeper comprehension of polymer aggregation and protein folding, which ultimately affects many areas of biology and pathology. Research in polypeptoids will forever be

intertwined with biology due to their structural similarities to proteins. Interdisciplinary work will always be part of polypeptoid research, making this field very attractive towards future studies and potential funding! This research has been at the forefront of peptidomimetic exploration and has aided in some understanding of their physical capabilities, opening doors to potential applications in pharmaceutics and materials science.

References

1. Zuckermann, R. N., *Peptide Science* **2011,** *96* (5), 545-555.

2. Zhang, D.; Lahasky, S. H.; Guo, L.; Lee, C.-U.; Lavan, M., *Macromolecules* **2012,** *45* (15), 5833-5841.

3. Simon, R. J.; Kania, R. S.; Zuckermann, R. N.; Huebner, V. D.; Jewell, D. A.; Banville, S.; Ng, S.; Wang, L.; Rosenberg, S.; Marlowe, C. K., *Proceedings of the National Academy of Sciences* **1992,** *89* (20), 9367-9371.

4. Barron, A. E.; Zuckerman, R. N., *Current Opinion in Chemical Biology* **1999,** *3* (6), 681-687.

5. Kirshenbaum, K.; Zuckermann, R. N.; Dill, K. A., *Current Opinion in Structural Biology* **1999,** *9* (4), 530-535.

6. Burkoth, T. S.; Beausoleil, E.; Kaur, S.; Tang, D.; Cohen, F. E.; Zuckermann, R. N., *Chemistry & biology* **2002,** *9* (5), 647-654.

7. Guo, L.; Zhang, D., *Journal of the American Chemical Society* **2009,** *131* (50), 18072-18074.

8. Kirshenbaum, K.; Barron, A. E.; Goldsmith, R. A.; Armand, P.; Bradley, E. K.; Truong, K. T. V.; Dill, K. A.; Cohen, F. E.; Zuckermann, R. N., *Proceedings of the National Academy of Sciences* **1998,** *95* (8), 4303-4308.

9. Armand, P.; Kirshenbaum, K.; Goldsmith, R. A.; Farr-Jones, S.; Barron, A. E.; Truong, K. T. V.; Dill, K. A.; Mierke, D. F.; Cohen, F. E.; Zuckermann, R. N.; Bradley, E. K., *Proceedings of the National Academy of Sciences* **1998,** *95* (8), 4309-4314.

10. Wu, C. W.; Sanborn, T. J.; Zuckermann, R. N.; Barron, A. E., *Journal of the American Chemical Society* **2001,** *123* (13), 2958-2963.

11. Palau, J.; Argos, P.; Puigdomenech, P., *International Journal of Peptide and Protein Research* **1982,** *19* (4), 394-401.

12. Lee, B.-C.; Zuckermann, R. N.; Dill, K. A., *Journal of the American Chemical Society* **2005,** *127* (31), 10999-11009.

13. Guo, L.; Li, J.; Brown, Z.; Ghale, K.; Zhang, D., *Peptide Science* **2011,** *96* (5), 596-603.

14. Huang, K.; Wu, C. W.; Sanborn, T. J.; Patch, J. A.; Kirshenbaum, K.; Zuckermann, R. N.; Barron, A. E.; Radhakrishnan, I., *Journal of the American Chemical Society* **2006,** *128* (5), 1733-1738.

15. Gorske, B. C.; Bastian, B. L.; Geske, G. D.; Blackwell, H. E., *Journal of the American Chemical Society* **2007,** *129* (29), 8928-8929.

16. Gorske, B. C.; Blackwell, H. E., *Journal of the American Chemical Society* **2006,** *128* (44), 14378-14387.

17. Jordan, P. A.; Paul, B.; Butterfoss, G. L.; Renfrew, P. D.; Bonneau, R.; Kirshenbaum, K., *Peptide Science* **2011,** *96* (5), 617-626.

18. Sun, H.; Zhang, J.; Liu, Q.; Yu, L.; Zhao, J., *Angewandte Chemie International Edition* **2007,** *46* (32), 6068-6072.

19. Miller, S. M.; Simon, R. J.; Ng, S.; Zuckermann, R. N.; Kerr, J. M.; Moos, W. H., *Bioorganic & Medicinal Chemistry Letters* **1994,** *4* (22), 2657-2662.

20. Miller, S. M.; Simon, R. J.; Ng, S.; Zuckermann, R. N.; Kerr, J. M.; Moos, W. H., *Drug Development Research* **1995,** *35* (1), 20-32.

21. Fields, G. B.; Noble, R. L., *International Journal of Peptide and Protein Research* **1990,** *35* (3), 161-214.

22. Barz, M.; Luxenhofer, R.; Zentel, R.; Vicent, M. J., *Polymer Chemistry* **2011,** *2* (9), 1900-1918.

23. Patch, J. A.; Barron, A. E., *Current Opinion in Chemical Biology* **2002,** *6* (6), 872-877.

24. Murphy, J. E.; Uno, T.; Hamer, J. D.; Cohen, F. E.; Dwarki, V.; Zuckermann, R. N., *Proceedings of the National Academy of Sciences* **1998,** *95* (4), 1517-1522.

25. Cornils, B.; Hermann, W. A., *Applied Homogenous Catalysis with Organometallic Compounds*. 2nd ed.; Wiley-VCH: Weinheim, 2002.

26. Galamb, V.; Palyi, G.; Ungvary, F.; Marko, L.; Boese, R.; Schmid, G., *Journal of the American Chemical Society* **1986,** *108* (12), 3344-3351.

27. Hall, I. H.; Bastow, K. F.; Warren, A. E.; Barnes, C. R.; Bouet, G. M., *Applied Organometallic Chemistry* **1999,** *13* (11), 819-828.

28. Hadjichristidis, N.; Iatrou, H.; Pitsikalis, M.; Sakellariou, G., *Chemical Reviews* **2009,** *109* (11), 5528-5578.

29. Hiemenz, P. C.; Lodge, T. P., *Polymer Chemistry Second Editino*. Taylor & Francis Group: Boca Raton, 2007.

30. Hadjichristidis, N.; Iatrou, H.; Pitsikalis, M.; Sakellariou, G., *Chemical Reviews* **2009,** *109* (11), 5528-5578.

31. Waley, S. G.; Watson, J., *Journal of the American Chemical Society* **1948,** *70* (6), 2299-2300.

32. Sisido, M.; Imanishi, Y.; Higashimura, T., *Die Makromolekulare Chemie* **1977,** *178* (11), 3107-3114.

33. Kricheldorf, H. R.; von Lossow, C.; Schwarz, G., *Macromolecular Chemistry and Physics* **2004,** *205* (7), 918-924.

34. Kricheldorf, H. R.; v. Lossow, C.; Schwarz, G.; Fritsch, D., *Macromolecular Chemistry and Physics* **2005,** *206* (12), 1165-1170.

35. Goodman, M.; Fried, M., *Journal of the American Chemical Society* **1967,** *89* (5), 1264-1267.

36. Goodman, M.; Chen, F.; Prince, F. R., *Biopolymers* **1973,** *12* (11), 2549-2561.

37. Cope, A. C.; Acton, E. M., *Journal of the American Chemical Society* **1958,** *80* (2), 355-359.

38. Fetsch, C.; Grossmann, A.; Holz, L.; Nawroth, J. F.; Luxenhofer, R., *Macromolecules* **2011,** *44* (17), 6746-6758.

39. Li, X.; Guo, L.; Casiano-Maldonado, M.; Zhang, D.; Wesdemiotis, C., *Macromolecules* **2011,** *44* (12), 4555-4564.

40. Waymouth, R. M.; Culkin, D. A.; Jeong, W.; Csihony, S.; Gomez, E. D.; Balsara, N. P.; Hedrick, J. L., *Angewadte Chemie* **2007,** *119* (15), 2681-2684.

41. Culkin, D. A.; Jeong, W.; Csihony, S.; Gomez, E. D.; Balsara, N. P.; Hedrick, J. L.; Waymouth, R. M., *Angewandte Chemie International Edition* **2007,** *46* (15), 2627-2630.

42. Jeong, W.; Shin, E. J.; Culkin, D. A.; Hedrick, J. L.; Waymouth, R. M., *Journal of the American Chemical Society* **2009,** *131* (13), 4884-4891.

43. Szwarg, M., *Die Makromolekulare Chemie* **1960,** *35* (1), 132-158.

44. Guo, L.; Lahasky, S. H.; Ghale, K.; Zhang, D., *Journal of the American Chemical Society* **2012**.

45. Clavier, H.; Nolan, S. P., *Chemical Communications* **2010,** *46* (6), 841-861.

46. Bhattacharyya, D. N.; Smid, J.; Szwarc, M., *The Journal of Physical Chemistry* **1965,** *69* (2), 624-627.

47. Dainton, F. S.; East, G. C.; Harpell, G. A.; Hurworth, N. R.; Ivin, K. J.; Laflair, R. T.; Pallen, R. H.; Hui, K. M., *Die Makromolekulare Chemie* **1965,** *89* (1), 257-262.

48. Boyd, G. V.; Wright, P. H., *Journal of the Chemical Society, Perkin Transactions 1* **1972**, 914-918.

49. Dghaym, R. D.; Dhawan, R.; Arndtsen, B. A., *Angewandte Chemie International Edition* **2001,** *40* (17), 3228-3230.

50. Wang, J. C.; Davidson, N., *Journal of Molecular Biology* **1966,** *15* (1), 111-123.

51. Laurent, B. A.; Grayson, S. M., *Chemical Society Reviews* **2009,** *38* (8), 2202-2213.

52. Szymanski, R.; Kubisa, P.; Penczek, S., *Macromolecules* **1983,** *16* (6), 1000-1008.

53. Jacobson, H.; Beckmann, C. O.; Stockmayer, W. H., *The Journal of Chemical Physics* **1950,** *18* (12), 1607-1612.

54. Kricheldorf, H. R.; Schwarz, G., *Macromolecular Rapid Communications* **2003,** *24* (5-6), 359-381.

55. Geiser, D.; Höcker, H., *Macromolecules* **1980,** *13* (3), 653-656.

56. Hild, G.; Kohler, A.; Rempp, P., *European Polymer Journal* **1980,** *16* (6), 525-527.

57. Vollmert, B.; Huang, J.-x., *Die Makromolekulare Chemie, Rapid Communications* **1980,** *1* (5), 333-339.

58. Laurent, B. A.; Grayson, S. M., *Journal of the American Chemical Society* **2006,** *128* (13), 4238-4239.

59. Xu, J.; Ye, J.; Liu, S., *Macromolecules* **2007,** *40* (25), 9103-9110.

60. Eugene, D. M.; Grayson, S. M., *Macromolecules* **2008,** *41* (14), 5082-5084.

61. Kudo, H.; Makino, S.; Kameyama, A.; Nishikubo, T., *Macromolecules* **2005,** *38* (14), 5964-5969.

62. Bielawski, C. W.; Benitez, D.; Morita, T.; Grubbs, R. H., *Macromolecules* **2001,** *34* (25), 8610-8618.

63. Bielawski, C. W.; Benitez, D.; Grubbs, R. H., An 'Endless' Route to Cyclic Polymers. In *Science*, American Association for the Advancement of Science: 2002; Vol. 297, p 2041.

64. Penczek, S.; Duda, A.; Szymanski, R., *Macromolecular Symposia* **1998,** *132* (1), 441-449.

65. Penczek, S.; Szymanski, R.; Duda, A.; Baran, J., *Macromolecular Symposia* **2003,** *201* (1), 261-270.

66. Matyjaszewski, K.; Greszta, D.; Hrkach, J. S.; Kim, H. K., *Macromolecules* **1995,** *28* (1), 59-72.

67. Higgins, J. S.; Dodgson, K.; Semlyen, J. A., *Polymer* **1979,** *20* (5), 553-558

68. Clarson, S. J.; Semlyen, J. A., *Polymer* **1986,** *27* (10), 1633-1636.

69. Freifelder, D.; Kleinschmidt, A. K.; Sinsheimer, R. L., *Science* **1964,** *146*, 254.

70. Hadziioannou, G.; Cotts, P. M.; ten Brinke, G.; Han, C. C.; Lutz, P.; Strazielle, C.; Rempp, P.; Kovacs, A. J., *Macromolecules* **1987,** *20* (3), 493-497.

71. Honda, S.; Yamamoto, T.; Tezuka, Y., *Journal of the American Chemical Society 132* (30), 10251-10253.

72. Anastasiadis, S. H.; Gancarz, I.; Koberstein, J. T., *Macromolecules* **1989,** *22* (3), 1449-1453.

73. Kricheldorf, H. R.; Schwarz, G., *Macromolecular Rapid Communications* **2003,** *24* (5-6), 359-381.

74. Kricheldorf, H. R., *Journal of Polymer Science Part A: Polymer Chemistry* **2010,** *48* (2), 251-284.

75. Hoskins, J. N.; Grayson, S. M., *Macromolecules* **2009,** *42* (17), 6406-6413.

76. Lee, C.-U.; Smart, T. P.; Guo, L.; Epps, T. H.; Zhang, D., *Macromolecules* **2011,** *44* (24), 9574-9585.

77. Bloomfield, V.; Zimm, B. H., *The Journal of Chemical Physics* **1966,** *44* (1), 315-323.

78. Kobayashi, S.; Endo, K., Synthesis and Properties of Cyclic Polymers. In *New Frontiers in Polymer Synthesis*, Springer Berlin / Heidelberg: 2008; Vol. 217, pp 121-183.

79. Rosales, A. M.; Murnen, H. K.; Zuckermann, R. N.; Segalman, R. A., *Macromolecules* **2010,** *43* (13), 5627-5636.

80. Kidchob, T.; Kimura, S.; Imanishi, Y., *Journal of Applied Polymer Science* **1997,** *63* (4), 453-458.

81. Tanisaka, H.; Kizaka-Kondoh, S.; Makino, A.; Tanaka, S.; Hiraoka, M.; Kimura, S., *Bioconjugate Chemistry* **2007,** *19* (1), 109-117.

82. Sun, J.; Stone, G. M.; Balsara, N. P.; Zuckermann, R. N., *Macromolecules* **2012,** *45* (12), 5151-5156.

83. Robinson, J. W.; Schlaad, H., *Chemical Communications* **2012,** *48* (63), 7835-7837.

84. Qiu, X.-P.; Tanaka, F.; Winnik, F. M., *Macromolecules* **2007,** *40* (20), 7069-7071.

85. Ye, J.; Xu, J.; Hu, J.; Wang, X.; Zhang, G.; Liu, S.; Wu, C., *Macromolecules* **2008,** *41* (12), 4416-4422.

86. Muir, H., *Biochemical Society Transactions* **1983,** *11*, 613-622.

87. Lecommandoux, S.; Chécot, F.; Borsali, R.; Schappacher, M.; Deffieux, A.; Brûlet, A.; Cotton, J. P., *Macromolecules* **2002,** *35* (23), 8878-8881.

88. Feuz, L.; Leermakers, F. A. M.; Textor, M.; Borisov, O., *Macromolecules* **2005,** *38* (21), 8891-8901.

89. Subbotin, A.; Saariaho, M.; Ikkala, O.; ten Brinke, G., *Macromolecules* **2000,** *33* (9), 3447-3452.

90. Vlassopoulos, D.; Fytas, G.; Loppinet, B.; Isel, F.; Lutz, P.; Benoit, H., *Macromolecules* **2000,** *33* (16), 5960-5969.

91. Wintermantel, M.; Gerle, M.; Fischer, K.; Schmidt, M.; Wataoka, I.; Urakawa, H.; Kajiwara, K.; Tsukahara, Y., *Macromolecules* **1996,** *29* (3), 978-983.

92. Zhang, M.; Müller, A. H. E., *J. Polym. Sci., Part A: Polym. Chem.* **2005,** (43), 3461-3481.

93. Sheiko, S. S.; Sun, F. C.; Randall, A.; Shirvanyants, D.; Rubinstein, M.; Lee, H.-i.; Matyjaszewski, K., *Nature* **2006,** *440* (7081), 191-194.

94. Huang, K.; Rzayev, J., *Journal of the American Chemical Society* **2009,** *131* (19), 6880-6885.

95. Müller, M. T.; Yan, X.; Lee, S.; Perry, S. S.; Spencer, N. D., *Macromolecules* **2005,** *38* (13), 5706-5713.

96. Kumaraswamy, G.; Dibaj, A. M.; Caruso, F., *Langmuir* **2002,** *18* (10), 4150-4154.

97. Sheiko, S. S.; Sumerlin, B. S.; Matyjaszewski, K., *Progress in Polymer Science* **2008,** *33* (7), 759-785.

98. Yamada, K.; Miyazaki, M.; Ohno, K.; Fukuda, T.; Minoda, M., *Macromolecules* **1998,** *32* (2), 290-293.

99. Beers, K. L.; Gaynor, S. G.; Matyjaszewski, K.; Sheiko, S. S.; Moller, M., *Macromolecules* **1998,** *31* (26), 9413-9415.

100. Gao, H.; Matyjaszewski, K., *Journal of the American Chemical Society* **2007,** *129* (20), 6633-6639.

101. Lee, H.-i.; Pietrasik, J.; Sheiko, S. S.; Matyjaszewski, K., *Progress in Polymer Science* **2010,** *35* (1–2), 24-44.

102. Cheng, C.; Khoshdel, E.; Wooley, K. L., *Macromolecules* **2007,** *40* (7), 2289-2292.

103. Binder, W. H.; Sachsenhofer, R., *Macromol. Rapid Commun.* **2008,** *29*, 952-981.

104. Kolb, H. C.; Sharpless, K. B.; Finn, M. G., *Angewadt Chemie International Edition* **2001,** *40* (11), 2004-2021.

105. Sumerlin, B. S.; Tsarevsky, N. V.; Louche, G.; Lee, R. Y.; Matyjaszewski, K., *Macromolecules* **2005,** *38*, 7540-7545.

106. Helms, B. M., J. L.; Hawker, C. J.; Fréchet, J. M., *J. Am. Chem. Soc.* **2004,** *126*, 15020-15021.

107. Parrish, B.; Breitenkamp, R. B.; Emrick, T., *Journal of the American Chemical Society* **2005,** *127* (20), 7404-7410.

108. Gondi, S. R.; Vogt, A. P.; Sumerlin, B. S., *Macromolecules* **2007,** *40* (3), 474-481.

109. Golas, P. L. M., K., *Chem. Soc. Rev.* **2010,** *39*, 1338-1354.

110. Meldal, M., *Macromol. Rapid Commun.* **2008,** *29*, 1016-1051.

111. Tsarevsky, N. V., *J. Polym. Sci., Part A: Polym. Chem.* **2010,** *48*, 966-974.

112. Wu, J.; Gao, C., *Macromolecules* **2010,** *43* (17), 7139-7146.

113. Kreutzer, G. T., C.; Nguyen, T. Q.; Plummer, C. J. G.; Månson, J.-A. E.; Castelletto, V.; Hamley, I. W.; Sun, F.; Sheiko, S. S.; Herrmann, A.; Ouali, L.; Sommer, H.; Fieber, W.; Velazco, M. I.; Klok, H.-A., *Macromolecules* **2006,** *39*, 4507-4516.

114. Schappacher, M.; Deffieux, A., *Science* **2008,** *319* (5869), 1512-1515.

115. Schappacher, M.; Deffieux, A., *Macromolecules* **2005,** *38* (11), 4942-4946.

116. Schappacher, M. D., A., *Angew. Chem. Int. Ed.* **2009,** *48*, 5930-5933.

117. Jia, Z.; Fu, Q.; Huang, J., *Macromolecules* **2006,** *39* (16), 5190-5193.

118. Coulembier, O.; Moins, S. b.; De Winter, J.; Gerbaux, P.; Lecleὶ€re, P.; Lazzaroni, R.; Dubois, P., *Macromolecules* **2009,** *43* (1), 575-579.

119. Xia, Y. B., A. J.; Grubbs, R. H. , *Angew. Chem. Int. Ed.* **2011,** *0*, 5882-5885.

120. Zhang, K.; Lackey, M. A.; Wu, Y.; Tew, G. N., *Journal of the American Chemical Society* **2011,** *133* (18), 6906-6909.

121. Semlyen, J. A., *Cyclic Polymers*. Kluwer Academic Publishers: Norwell, MA, 2000.

122. Ostaci, R.-V.; Damiron, D.; Grohens, Y.; Léger, L.; Drockenmuller, E., *Langmuir* **2009,** *26* (2), 1304-1310.

123. Villarrubia, J. S., *J. Res. Natl. Inst. Stand. Technol.* **1997,** *102*, 425-454.

124. Arduengo, A. J.; Krafczyk, R.; Schmutzler, R.; Craig, H. A.; Goerlich, J. R.; Marshall, W. J.; Unverzagt, M., *Tetrahedron* **1999,** *55* (51), 14523-14534.

125. Stanford, M. J. P., R. L.; Dove, A. P., *Macromolecules* **2010,** *43*, 6538-6541.

126. Liu, F.; Urban, M. W., *Progress in Polymer Science* **2010,** *35* (1–2), 3-23.

127. Schmaljohann, D., *Advanced Drug Delivery Reviews* **2006,** *58* (15), 1655-1670.

128. Gao, C.; Leporatti, S.; Moya, S.; Donath, E.; Möhwald, H., *Chemistry – A European Journal* **2003,** *9* (4), 915-920.

129. Suzuki, A.; Tanaka, T., *Nature* **1990,** *346* (6282), 345-347.

130. Shimizu, K.; Fujita, H.; Nagamori, E., *Biotechnology and Bioengineering* **2010,** *106* (2), 303-310.

131. Vasilevskaya, V. V.; Khokhlov, A. R.; Matsuzawa, Y.; Yoshikawa, K., *The Journal of Chemical Physics* **1995,** *102* (16), 6595-6602.

132. Sherman, E.; Haran, G., *Proceedings of the National Academy of Sciences* **2006,** *103* (31), 11539-11543.

133. Moore, M. A., *Journal of Physics A: Mathematical and General* **1977,** *10* (2), 305.

134. Vasile, C.; Kulshreshtha, A. K., *Handbook of Polymerblends and Composites*. Rapra Technology Ltd

Shawbury, UK, 2003.

135. Southall, N. T.; Dill, K. A.; Haymet, A. D. J., *The Journal of Physical Chemistry B* **2001,** *106* (3), 521-533.

136. Ward, M. A.; Georgiou, T. K., *Polymers* **2011,** *3* (3), 1215-1242.

137. Lutz, J.-F., *Journal of Polymer Science Part A: Polymer Chemistry* **2008,** *46* (11), 3459-3470.

138. Cowie, J. M. G., *Polymers: Chemistry and Physics of Modern Materials*. 2nd ed.; Blackie: 1991.

139. Bae, Y. C.; Lambert, S. M.; Soane, D. S.; Prausnitz, J. M., *Macromolecules* **1991,** *24* (15), 4403-4407.

140. Boutris, C.; Chatzi, E. G.; Kiparissides, C., *Polymer* **1997,** *38* (10), 2567-2570.

141. Yong-Hee, K.; You Han, B.; Sung Wan, K., *Journal of Controlled Release* **1994,** *28* (1–3), 143-152.

142. Xiao, X.; Fu, Y.-q.; Zhou, J.-j.; Bo, Z.-s.; Li, L.; Chan, C.-M., *Macromolecular Rapid Communications* **2007,** *28* (9), 1003-1009.

143. Fuwa, K.; Valle, B. L., *Analytical Chemistry* **1963,** *35* (8), 942-946.

144. Mitchell, K.; Ford, J. L.; Armstrong, D. J.; Elliott, P. N. C.; Rostron, C.; Hogan, J. E., *International Journal of Pharmaceutics* **1990,** *66* (1–3), 233-242.

145. Xia, Y.; Burke, N. A. D.; Stöver, H. D. H., *Macromolecules* **2006,** *39* (6), 2275-2283.

146. Liu, Z.; Guo, Y.; Inomata, K., *Polym J* **2011,** *43* (8), 676-682.

147. Idziak, I.; Avoce, D.; Lessard, D.; Gravel, D.; Zhu, X. X., *Macromolecules* **1999,** *32* (4), 1260-1263.

148. Ranganathan, K.; Deng, R.; Kainthan, R. K.; Wu, C.; Brooks, D. E.; Kizhakkedathu, J. N., *Macromolecules* **2008,** *41* (12), 4226-4234.

149. Yamamoto, S.-i.; Pietrasik, J.; Matyjaszewski, K., *Macromolecules* **2008,** *41* (19), 7013-7020.

150. Bütün, V.; Liu, S.; Weaver, J. V. M.; Bories-Azeau, X.; Cai, Y.; Armes, S. P., *Reactive and Functional Polymers* **2006,** *66* (1), 157-165.

151. Liu, R.; Fraylich, M.; Saunders, B., *Colloid & Polymer Science* **2009,** *287* (6), 627-643.

152. Skrabania, K.; Kristen, J.; Laschewsky, A.; Akdemir, Ö.; Hoth, A.; Lutz, J.-F., *Langmuir* **2006,** *23* (1), 84-93.

153. Mayo, F. R.; Lewis, F. M., *Journal of the American Chemical Society* **1944,** *66* (9), 1594-1601.

154. Fineman, M.; Ross, S. D., *Journal of Polymer Science* **1950,** *5* (2), 259-262.

155. Chung, J. E.; Yokoyama, M.; Aoyagi, T.; Sakurai, Y.; Okano, T., *Journal of Controlled Release* **1998,** *53* (1–3), 119-130.

156. Sugihara, S.; Kanaoka, S.; Aoshima, S., *Macromolecules* **2004,** *37* (5), 1711-1719.

157. Sosnik, A.; Cohn, D., *Biomaterials* **2005,** *26* (4), 349-357.

158. Ito, Y.; Chen, G.; Guan, Y.; Imanishi, Y., *Langmuir* **1997,** *13* (10), 2756-2759.

159. Huber, S.; Jordan, R., *Colloid & Polymer Science* **2008,** *286* (4), 395-402.

160. Lutz, J.-F.; Akdemir, Ö.; Hoth, A., *Journal of the American Chemical Society* **2006,** *128* (40), 13046-13047.

161. Savoji, M. T.; Strandman, S.; Zhu, X. X., *Macromolecules* **2012,** *45* (4), 2001-2006.

162. da Silva, R. M. P.; Mano, J. F.; Reis, R. L., *Trends in Biotechnology* **2007,** *25* (12), 577-583.

163. Ganta, S.; Devalapally, H.; Shahiwala, A.; Amiji, M., *Journal of Controlled Release* **2008,** *126* (3), 187-204.

164. Lavigne, M. D.; Pennadam, S. S.; Ellis, J.; Yates, L. L.; Alexander, C.; Górecki, D. C., *The Journal of Gene Medicine* **2007,** *9* (1), 44-54.

165. Mao, Z.; Ma, L.; Yan, J.; Yan, M.; Gao, C.; Shen, J., *Biomaterials* **2007,** *28* (30), 4488-4500.

166. Yang, J.; Zhang, P.; Tang, L.; Sun, P.; Liu, W.; Sun, P.; Zuo, A.; Liang, D., *Biomaterials* **2010,** *31* (1), 144-155.

167. Zhou, Y.-M.; Ishikawa, A.; Okahashi, R.; Uchida, K.; Nemoto, Y.; Nakayama, M.; Nakayama, Y., *Journal of Controlled Release* **2007,** *123* (3), 239-246.

168. Tanaka, T., *Scientific American* **1981,** *244*, 124-138.

169. Gulrez, S. K. H.; Al-Assaf, S., *Hydrogels: Methods of Preparation, Characterisation and Applications*. 2011.

170. Okuyama, Y.; Yoshida, R.; Sakai, K.; Okano, T.; Sakurai, Y., *Journal of Biomaterials Science, Polymer Edition* **1993,** *4* (5), 545-556.

171. Kozhunova, E. Y.; Makhaeva, E. E.; Khokhlov, A. R., *Polymer* **2012,** *53* (12), 2379-2384.

172. Lyman, D. J.; Loo, B. H.; Crawford, R. W., *Biochemistry* **1964,** *3* (7), 985-990.

173. Fasman, G. D.; Blout, E. R., *Biopolymers* **1963,** *1* (2), 99-109.

174. Fujita, K.; Kimura, S.; Imanishi, Y., *Langmuir* **1999,** *15* (13), 4377-4379.

175. Park, J.-S.; Kataoka, K., *Macromolecules* **2007,** *40* (10), 3599-3609.

176. Tam, K. C.; Wu, X. Y.; Pelton, R. H., *Journal of Polymer Science Part A: Polymer Chemistry* **1993,** *31* (4), 963-969.

177. Feil, H.; Bae, Y. H.; Feijen, J.; Kim, S. W., *Macromolecules* **1993,** *26* (10), 2496-2500.

178. Plunkett, K. N.; Zhu, X.; Moore, J. S.; Leckband, D. E., *Langmuir* **2006,** *22* (9), 4259-4266.

179. Zhang, Y.; Furyk, S.; Sagle, L. B.; Cho, Y.; Bergbreiter, D. E.; Cremer, P. S., *The Journal of Physical Chemistry C* **2007,** *111* (25), 8916-8924.

180. Zhang, Y.; Cremer, P. S., *Current Opinion in Chemical Biology* **2006,** *10* (6), 658-663.

181. Lo Nostro, P.; Ninham, B. W., *Chemical Reviews* **2012,** *112* (4), 2286-2322.

182. Baldwin, R. L., *Biophysical Journal* **1996,** *71* (4), 2056-2063.

183. Zhang, Y.; Furyk, S.; Bergbreiter, D. E.; Cremer, P. S., *Journal of the American Chemical Society* **2005,** *127* (41), 14505-14510.

184. Maeda, Y.; Higuchi, T.; Ikeda, I., *Langmuir* **2001,** *17* (24), 7535-7539.

185. Cheng, H.; Shen, L.; Wu, C., *Macromolecules* **2006,** *39* (6), 2325-2329.

186. Musto, P.; Karasz, F. E.; MacKnight, W. J., *Macromolecules* **1991,** *24* (17), 4762-4769.

187. Lin, S.-Y.; Chen, K.-S.; Liang, R.-C., *Polymer* **1999,** *40* (10), 2619-2624.

188. Ruzicka, L., *Chem. Ind. (London)* **135,** (43), 2.

189. Deshmukh, M. V.; Vaidya, A. A.; Kulkarni, M. G.; Rajamohanan, P. R.; Ganapathy, S., *Polymer* **2000,** *41* (22), 7951-7960.

190. Stuart, M. A. C.; Huck, W. T. S.; Genzer, J.; Muller, M.; Ober, C.; Stamm, M.; Sukhorukov, G. B.; Szleifer, I.; Tsukruk, V. V.; Urban, M.; Winnik, F.; Zauscher, S.; Luzinov, I.; Minko, S., *Nat Mater* **2010,** *9* (2), 101-113.

191. Kumar, A.; Srivastava, A.; Galaev, I. Y.; Mattiasson, B., *Progress in Polymer Science* **2007,** *32* (10), 1205-1237.

192. York, A. W.; Kirkland, S. E.; McCormick, C. L., *Advanced Drug Delivery Reviews* **2008,** *60* (9), 1018-1036.

193. Gil, E. S.; Hudson, S. M., *Progress in Polymer Science* **2004,** *29* (12), 1173-1222.

194. Crespy, D.; Rossi, R. M., *Polymer International* **2007,** *56* (12), 1461-1468.

195. Furyk, S.; Zhang, Y.; Ortiz-Acosta, D.; Cremer, P. S.; Bergbreiter, D. E., *Journal of Polymer Science Part A: Polymer Chemistry* **2006,** *44* (4), 1492-1501.

196. Richard Hoogenboom; Hanneke M. L. Thijs; Mark J. H. C. Jochems; Bart M. van Lankvelt; Fijten, M. W. M.; Schubert, U. S., *The Royal Society of Chemsitry* **2008**, 5758-5760.

197. Lahasky, S. H.; Hu, X.; Zhang, D., *ACS Macro Letters* **2012,** *1* (5), 580-584.

198. Peng, S.; Bhushan, B., *RSC Advances* **2012,** *2* (23), 8557-8578.

199. Li, C.; Gunari, N.; Fischer, K.; Janshoff, A.; Schmidt, M., *Angewandte Chemie International Edition* **2004,** *43* (9), 1101-1104.

200. Zhao, J.; Mountrichas, G.; Zhang, G.; Pispas, S., *Macromolecules* **2010,** *43* (4), 1771-1777.

201. Diehl, C.; Schlaad, H., *Macromolecular Bioscience* **2009,** *9* (2), 157-161.

202. Edwige, C.; Lattes, A.; Laval, J. P.; Mutin, R.; Basset, J. M.; Nouguier, R., *Journal of Molecular Catalysis* **1980,** *8* (1–3), 297-311.

203. Liaw, D.-J.; Tsai, C.-H., *Journal of Molecular Catalysis A: Chemical* **1999,** *147* (1–2), 23-31.

204. Sutthasupa, S.; Sanda, F.; Masuda, T., *Macromolecules* **2009,** *42* (5), 1519-1525.

205. Van Durme, K.; Rahier, H.; Van Mele, B., *Macromolecules* **2005,** *38* (24), 10155-10163.

206. Liu, X.-Y.; Mu, X.-R.; Liu, Y.; Liu, H.-J.; Chen, Y.; Cheng, F.; Jiang, S.-C., *Langmuir* **2012,** *28* (10), 4867-4876.

207. Zhu, W.; Nese, A.; Matyjaszewski, K., *Journal of Polymer Science Part A: Polymer Chemistry* **2011,** *49* (9), 1942-1952.

208. Torchilin, V. P., *Journal of controlled release : official journal of the Controlled Release Society* **2001,** *73* (2-3), 137-172.

209. http://www.esrf.eu/UsersAndScience/Experiments/SoftMatter/ID02/SampleEnvironment/Mettler/mettlermanual.pdf.

210. Vygodskii, Y. S.; Shaplov, A. S.; Lozinskaya, E. I.; Filippov, O. A.; Shubina, E. S.; Bandari, R.; Buchmeiser, M. R., *Macromolecules* **2006,** *39* (23), 7821-7830.

211. Hardy, J.; Allsop, D., *Trends in Pharmacological Sciences* **1991,** *12* (0), 383-388.

212. Mudher, A.; Lovestone, S., *Trends in Neurosciences* **2002,** *25* (1), 22-26.

213. Schild, H. G., *Progress in Polymer Science* **1992,** *17* (2), 163-249.

214. Viegas, T. X.; Bentley, M. D.; Harris, J. M.; Fang, Z.; Yoon, K.; Dizman, B.; Weimer, R.; Mero, A.; Pasut, G.; Veronese, F. M., *Bioconjugate Chemistry* **2011,** *22* (5), 976-986.

Vita

Samuel Henry Lahasky, son of David and Darlene Lahasky, was born in Lafayette, Louisiana. As an undergraduate, he attended Tulane University, where he received a bachelor's degree in the sciences while having a double major in chemistry and Spanish. After college, he worked at Dow Chemicals as a laboratory technician. The year spent at Dow Chemicals sparked an interest in polymer chemistry, an interest that blossomed under the tutelage of Dr. Donghui Zhang. Samuel has spent time at Oak Ridge National Laboratory on the synthesis and characterization of interesting polymeric architectures. During his time at LSU, he has developed into a synthetic polymer chemist that has several peer-reviewed journal articles. He has also presented his research at national and regional conferences.